THE PROCEEDINGS OF
THE PHYSICAL SOCIETY

Section A

VOL. 62, PART 2 1 February 1949 No. 350 A

The Size-Variation of Resistivity for Mercury and Tin

BY E. R. ANDREW
Royal Society Mond Laboratory, Cambridge

Communicated by D. Shoenberg; *MS. received 8th September* 1948

ABSTRACT. Measurements have been made of the low temperature resistivity of mercury wires down to 6 μ diameter and of rolled tin foils down to 3 μ thickness. A continuous increase of resistivity with decrease of diameter and thickness was found, and it is concluded that this was due to a shortening of the mean free path of the conduction electrons by inelastic collision with the boundary surfaces of the metal. The theory of this effect for a wire is examined ; a rigorous theory for a foil already exists (Fuchs 1938). By comparing the experimental results with the theory, values of the product $l\rho$ are found for both metals ; (l is the mean free path and ρ the resistivity for the metal in bulk). These values of $l\rho$ are in satisfactory agreement with those obtained from Pippard's measurements on the anomalous skin effect for the two metals.

§ 1. INTRODUCTION

IN the course of attempts to extend the scope of the investigation on the intermediate state of superconductors (Andrew 1948) to specimens of smaller dimensions, a number of mercury wires down to 6 μ diameter and rolled tin foils down to 3 μ thickness were prepared: in this paper the results of resistance measurements on these specimens in the normal state are described. It had been noticed in the previous work that the normal resistivity increased with decrease of diameter. J. J. Thomson (1901) first suggested that inelastic boundary collisions of conduction electrons in a metal might cause a reduction in mean free path and thus an increase in resistivity; this effect would of course become more pronounced as the dimensions of the conductor are decreased. The effect was found with evaporated metallic films by Hamburger (1931), Lovell (1936) and Appleyard and Lovell (1937), and for wires of small diameter by Eucken and Förster (1934) and Riedel (1937). The lowest temperature used previously was 14° K., but at liquid helium temperatures the bulk resistivity of pure metals such as mercury and tin becomes so small that the mean free path is of order 10^{-2} cm. and thus the size effects should be noticeable for wires and foils of this order of diameter and thickness. By fitting the experimental results to theoretical relations for the size-dependence, values are obtained for the mean free path of the conduction electrons in the bulk metal.

§ 2. EXPERIMENTS WITH MERCURY

2.1. *Experimental Details*

The material used was Hilger 11,023, stated by the makers to contain 1 part in 10^6 of silver as the only measurable impurity. The wires were made by filling glass capillaries of appropriate bore with liquid metal and freezing them, electrical

connections being made to reservoirs at each end of the capillaries. For diameters greater than 20 μ, a pressure difference of one atmosphere sufficed to overcome surface tension effects, and the specimens were those used for measurements on the intermediate state of superconducting mercury which have already been described (Andrew 1948).

For diameters less than 20 μ additional pressure was applied over one of the reservoirs. A pressurizer designed by A. B. Pippard proved useful for this purpose after various modifications and additions had been made; a section of this pressurizer is shown in Figure 1. Pure mercury was held in the distrene cup F

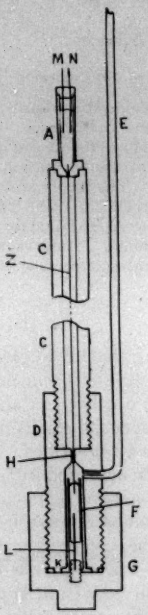

Figure 1.
Section of pressurizer.

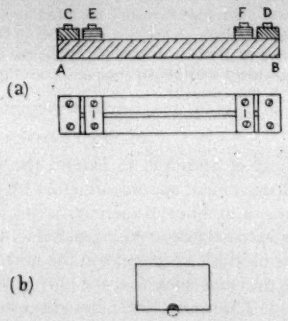

Figure 4.
(*a*) Method of mounting tin foils.
(*b*) Section of potential clamp.

inside the brass pressure chamber G. The capillary Z, 4–5 cm. in length, was sealed into a fine hole H in the top of the chamber with black wax, its lower end dipping into the mercury. This seal, and also the brass rim K, proved an effective seal up to the highest pressure applied (60 atmospheres). The upper end of the capillary was sealed with distrene cement into a hole in the bottom of another distrene cup A containing mercury. This cup was carried by the hollow cylindrical ebonite spacer C, in which longitudinal slots had been cut to enable ready access of liquid helium to the capillary. Compressed air was applied through the fine bore German silver tube E, by which the pressurizer was suspended in the Dewar flask. The two platinum wires M and N served as current and potential leads to

the mercury in the upper vessel. Only one independent electrical connection could conveniently be made to the lower mercury pool, and was made by the platinum wire L, hard-soldered to the brass, current and potential leads being connected to the outside. The resistance of the mercury in the normal state was sufficiently high for the end effect in the brass to be negligible. The specimens were frozen from the top (low pressure) end first, so that the volume reduction on freezing could be taken up by liquid under pressure, without the thread breaking.

Although the capillary of smallest bore tried, 2μ diameter, was successfully filled and the thread frozen, 6μ proved to be the smallest diameter which could be cooled to liquid helium temperatures without the thread breaking. The smaller diameter specimens were annealed for several hours at $-60°$ C. and cooled slowly thereafter. A sensitive indication of strain is given by the breadth of the temperature transition into the superconducting state which, as the data in Table 1 show, became greater as the diameter was reduced below 12μ.

The glass capillaries were drawn down from wider tubes and microscope examination showed that the cross-section maintained its circularity after drawing. As the resistivity of the mercury at room temperature is accurately known, resistance served to give the best estimate of wire diameter, provided of course that the specimen cross-section was uniform. As a check, the inside diameter of the capillaries was also examined by immersing them in a liquid of exactly the same refractive index under a cover glass; the correct liquid was found using the mineralogist's Becke line test and box of graded liquids. The inside diameter could then be measured directly at any point along the length of the capillary with a travelling microscope or a calibrated eyepiece.

Resistance was measured with a potentiometer, using the improvements of Kapitza and Milner (1937). Since mercury becomes superconducting, measurements below 4·17° K. were made in a longitudinal field greater than the critical value. The temperature of the liquid helium bath in which the specimens were immersed was determined from the vapour pressure using the 1932 Leiden scale of temperature.

2.2. *Experimental Results*

The normal resistances of all the wires at 79° K. and at various temperatures in the liquid helium range are given in Table 1, where they are expressed as a fraction of the room temperature (liquid) value. The resistance ratios are plotted in Figures 2 and 3. The full lines are explained in §4. The C series of specimens (Table 1) are those of narrow diameter prepared in the pressurizer, and the B series are those of wider diameter described previously. At 1·05° K. the bulk resistivity was almost entirely independent of temperature and therefore nearly equal to the "residual resistance", while at 4·2° K. it was many times larger and so mostly "ideal resistance". The low value of resistance ratio, $2{\cdot}0 \times 10^{-5}$, for the specimen B6 at 1·05° K. is an indication of the high purity of the material.

Corrections for the magneto-resistance effect and for anisotropy have been made to the measured values before compiling Table 1. For low resistivities such as were obtained with fat specimens at the lowest temperatures, the magneto-resistance effect was quite appreciable, especially as the applied magnetic field required to destroy superconductivity was several hundred gauss; by making measurements over a range of higher fields a fairly accurate extrapolation to zero field could be made.

The resistivity of solid mercury is markedly anisotropic. The ratio of the resistivities parallel and perpendicular to the principal axis is 0·76 (Sckell 1930),

and does not vary appreciably with temperature down to 82° K., the lowest temperature investigated by Sckell. At 79° K., the ratio of the solid resistivity to the room temperature liquid value is $5{\cdot}5 \times 10^{-2}$ for a direction parallel to the principal axis, $7{\cdot}2 \times 10^{-2}$ perpendicular, and $6{\cdot}6 \times 10^{-2}$ for a random polycrystal. It follows from the figures in Table 1 that the thinnest pressurized specimens are probably monocrystalline with the principal axis approximately perpendicular to the wire axis. In fact, for all but three of the fatter specimens (B1, B2 and the second freezing of B4), the ratio lies between 7·0 and $7{\cdot}3 \times 10^{-2}$, suggesting a preference for the crystallites to be oriented with their axes normal to that of the capillary. The three exceptions showed lower ratios, and so presumably had their axes oriented in other directions. Any geometrical effect due to imperfect freezing, such as the formation of cavities, would have produced higher ratios, and hence appears to be absent.

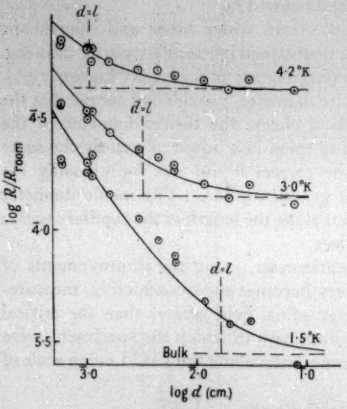

Figure 2.

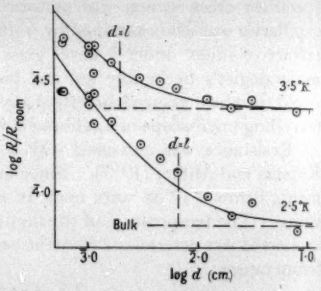

Figure 3.

The resistivity of mercury wires plotted logarithmically against wire diameter d. Figure 2, for 4·2° K., 3·0° K. and 1·5° K. Figure 3, for 3·5° K. and 2·5° K. The full lines are the theoretical curves of Fuchs for diffuse scattering (see § 4).

Since all but the three specimens mentioned have approximately the same crystallographic orientation, a correction should be made to bring these three into line. The correction will, however, be necessarily somewhat uncertain since no data are available for the anisotropy of the ideal or the residual resistance of solid mercury at liquid helium temperatures, and moreover, the effect of anisotropy on the extra resistance due to surface collisions is not known. The mean value of the ratio of the resistance at 79° K. to that at room temperature for all but the three exceptions is $7{\cdot}2 \times 10^{-2}$. For these exceptions the resistances at liquid helium temperatures have been multiplied up in the ratio of $7{\cdot}2 \times 10^{-2}$ to the 79° K. resistance ratio for each specimen. This correction assumes that the anisotropy of resistance is independent of temperature, and in the absence of other information, this is the simplest assumption that can be made. In any case only 3 of the 15 mercury specimens are affected.

The significance of the results is discussed together with those for the thin tin foils in §4.

Table 1. Resistance Ratios for Mercury Wires. The resistance ratios at liquid helium temperatures have been corrected for anisotropy as explained in the text. This correction has *not* been applied at 79° K.

Specimen (1)	Diam. (μ) (2)	(3)	(4) Temperatures (° K.) 79	4·2	4·0	3·5	3·0	2·5	2·0	1·5	1·05
B 6	790	0·013	7·2	4·25	3·60	2·26	1·31	0·67	0·40	0·25	0·20
B 3	310	0·018	7·1	4·70	4·16	2·60	1·61	0·91	0·53	0·40	0·37
B 1	200	0·013	6·2	4·20	3·57	2·34	1·39	0·78	0·52	0·38	0·34
B 2	120	0·013	6·6	4·64	3·98	2·58	1·60	0·96	0·63	0·48	0·42
B 4*	65	0·020	7·1	4·86	4·22	2·90	1·95	1·25	0·91	0·77	0·73
		0·016	5·9	4·90	4·15	2·88	1·85	1·22	0·87	0·72	0·69
C 8	46	0·012	7·3	5·16	4·52	3·10	2·10	1·41	1·06	0·90	0·85
B 5	30	0·020	7·0	5·18	4·52	3·23	2·29	1·62	1·25	1·12	1·08
C 7	16·6	0·020	7·0	5·63	5·00	3·72	2·70	2·04	—	1·45	1·43
C 2	11·6	0·030	7·2	5·60	5·08	3·36	—	2·00	—	1·74	—
C 4	11·8	0·035	7·0	6·44	5·70	4·40	3·37	2·72	2·30	2·16	2·07
C 3*	10·5	0·028	7·3	6·50	5·85	4·42	3·39	2·64	2·22	2·00	1·90
		0·021	7·3	6·38	5·59	4·09	3·10	2·43	1·98	1·80	1·74
C 5	6·0	0·071	7·3	6·68	6·02	4·62	3·56	2·80	2·30	2·06	1·97
C 6	6·1	0·047	7·3	6·99	6·35	4·83	3·65	2·79	2·22	1·97	1·81

(3) Superconducting temperature transition width (° K.) defined as the temperature interval between the 0·1 and 0·9 resistance values.

(4) Resistance expressed as a fraction of room temperature (liquid) value, $\times 10^2$ at 79° K. and $\times 10^4$ for 1·05–4·2° K.

* A second set of measurements was taken on this specimen after melting and refreezing.

§3. EXPERIMENTS WITH TIN

3.1. *The Specimens*

The material used was Johnson and Matthey 2,356, stated by the makers to contain less than 0·004% impurity. The ratio of resistance at 3·8° K. to that at 18° C. for the thickest specimen, $1{\cdot}8 \times 10^{-4}$, appears to be the lowest recorded for tin and indicates that the material is of high purity. Foils were rolled out using an accurately ground and carefully cleaned rolling mill; a range of thickness 3–2,000 μ was covered. The specimens were cut in the form of rectangular strips using a razor blade for the thinner ones and a guillotine for the thicker ones. It was necessary that the width of the strip should be much greater than its thickness in order that the foil should approximate to an infinite plate for the purpose of comparison of the experimental results with the predictions of the theory. For thicknesses of 80 μ or less the foils were 1 mm. wide and 3–5 cm. long. For foils of thickness 0·1–1 mm. the width was increased to 3 mm. The thickest "foil", 2 mm. thick, was made only 4 mm. wide in order to keep the resistance large enough for accurate measurement at liquid helium temperatures. Since the mean free path turned out to be of the order of 70 μ, the size effect for this thickness was almost negligible, so that the insufficient ratio of width to thickness was not important.

The method of mounting is illustrated in Figure 4 (*a*), p. 78. The strips were laid flat on the paxolin board AB, and fastened down at the ends with small brass clamps C and D to which current leads were attached. A few millimetres from the ends, small paxolin clamps pressed on the foil bearing the potential leads. A section of one of these clamps is shown in Figure 4 (*b*). A groove was cut in the base of the clamp parallel to the width of the foil, and a loop of 36 S.W.G. copper wire was fastened along the groove so as to protrude slightly below the plane of the paxolin (dotted line). This protrusion was then ground away until the wire presented a plane surface flush with the paxolin. The force used in tightening the clamp was thus distributed over the whole underside and was not applied to the potential wire alone.

The coefficient of thermal expansion of the paxolin in the direction of the tin strip was about two thirds of the value for tin. For the thinnest foils the small relative contraction of the order 0·005 cm. was easily taken up by the slight lack of tautness in mounting; the thicker and therefore more rigid foils dragged slightly under the clamps which had only been screwed up lightly to avoid biting into the metal, as was indicated by the fact that they bowed out slightly on warming up. The sharpness of the temperature transitions into the superconducting state and of the longitudinal magnetic field transitions from the superconducting state to the normal state for all thicknesses of foil, examples of which are given in the next paper, indicated the absence of appreciable strain.

The thickness of the foils was known roughly from the room temperature resistance, and the mean thickness was found with an accuracy of 1% after the experiment by weighing the portion between the potential points.

3.2. *Experimental Results*

Since the Debye temperature is much higher for tin than for mercury, resistance below 4·2° K. is almost entirely residual, the temperature-dependent part being only about 1%. In order to cover a wide range of bulk resistivities, as was possible with mercury in the liquid helium range alone, it was necessary to make

measurements also in the liquid hydrogen range (14–20° K.). Since, however, at 14° K. the resistivity is already about 16 times its value at 4·2° K., it is unfortunate that the interesting range 4–14° K. was not readily accessible.

The normal resistances of the foils at 3·8° K., 13·9° K. and 20·4° K. are given in Table 2, where they are expressed as a fraction of the resistance at 18° C.; these resistance ratios are plotted in Figures 5 and 6. The full lines are explained in § 4.

Table 2. Resistance Ratios for Tin Foils

Specimen (1)	Thickness (μ) (2)	(3)	(4) Temperatures (° K.) 79	20·4	13·9	3·8
E 7	1,950	11·7	0·203	100·0	30·4	1·80
E 10	915	12·0	0·210	98·7	30·7	2·03
E 9	487	12·1	0·206	100·0	30·3	2·22
E 6	255	12·6	0·207	—	—	2·20
E 8	133	12·2	0·205	102·1	30·7	2·61
E 3	77·7	12·3	0·205	—	—	3·02
E 11	53·5	12·0	0·209	103·1	30·8	2·64
E 12	30·7	12·6	0·207	103·1	31·0	3·10
E 13	15·1	11·9	0·206	104·1	33·7	5·33
E 14	9·9	13·2	0·205	—	—	6·75
E 17	7·46	12·3	0·203	115·0	42·9	10·8
E 4	6·94	12·7	0·208	—	—	10·5
E 15	5·15	13·8	—	—	—	14·4
E 5	4·11	13·4	0·205	—	—	19·0
E 2	3·43	13·5	0·204	—	—	18·6
E 18	3·34	13·7	0·204	128·9	55·2	20·1

(3) Resistivity at 18° C. (microhm cm.).

(4) Resistance expressed as a fraction of value at 291° K. ($\times 10^4$ at 20·4°, 13·9° and 3·8° K.).

Values of the room temperature resistivity are also shown in Table 2. It will be seen that there is a general increase in the resistivity at 18° C. from $11{\cdot}7 \times 10^{-6}$ ohm cm. for the thickest specimen to $13{\cdot}7 \times 10^{-6}$ ohm cm. for the thinnest. Bridgman (1925) has measured the resistivity of single crystals of tin in various directions at 20° C., and found the values 14·3 and $9{\cdot}9 \times 10^{-6}$ ohm cm. for directions parallel and perpendicular to the tetrad axis, so that the value for a random polycrystal is $11{\cdot}1 \times 10^{-6}$ ohm cm. It seems, therefore, that the process of rolling causes the crystal grains of the polycrystalline material to have a preferred orientation of the tetrad axis towards the direction of rolling.

As the figures in Table 2 show, there was no significant difference from one foil to another in the ratios of resistivity at 79° K. and at 291° K.; the small scatter of values is probably due to variations in the temperature of measurement from the nominal 79° K., due to changes of oxygen content in the liquid air. Since the mean free path of the conduction electrons at 79° K. turns out to be less than 10^{-5} cm., no size effect is to be expected, and therefore the constancy of the resistance ratio may be interpreted as a constancy of anisotropy of resistivity from room temperature down to 79° K.

There are some indications from the data in Table 2 that the anisotropy remains much the same down to 14° K.; if it is still constant down to 3·8° K. (which is rather

uncertain since the resistance is residual), then by plotting resistance ratios rather than absolute resistance, the effects of variations in crystal orientation are eliminated. This procedure has been adopted in Figures 5 and 6.

§4. DISCUSSION

The experimental results show that the resistivity increases for both tin and mercury as the specimen size is decreased, but the possibility must be considered that the effects are due to strain or impurity. The mercury is unlikely to have been appreciably contaminated in handling, particularly in a systematic manner, but strain was indicated by the superconducting properties for wires of diameter less than 12 μ. The increase in resistivity on the other hand was quite appreciable for diameters as large as 100 μ. For tin the superconducting properties in dica ted no

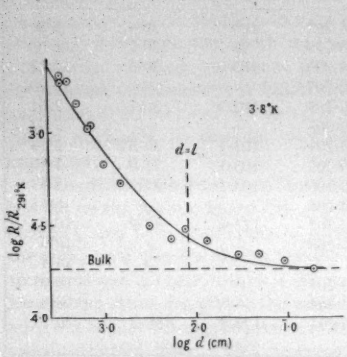

Figure 5.

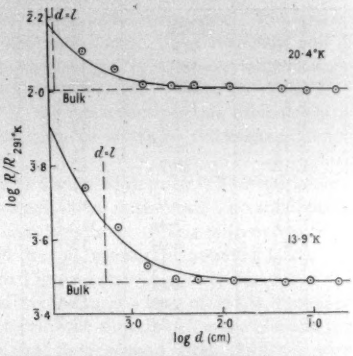

Figure 6.

The resistivity of tin foils plotted logarithmically against foil thickness.
Figure 5, for 3·8° K. Figure 6, for 13·9° K. and 20·4° K.
The full lines are the theoretical curve of Fuchs for diffuse scattering ($\epsilon=0$).

appreciable strain, so that only impurity need be seriously considered. While it is true that the thinner foils are likely to pick up more impurity in rolling than the thicker ones, the amount is unlikely to account for the factor of ten increase in resistivity found with the thinnest foils.

A test that may be applied to the hypothesis that the increase in resistivity is due to strain or impurity is to see whether Matthiessen's rule is obeyed. As the temperature approaches 0° K., the ideal resistance tends to zero roughly as the fourth power of the temperature (actually a 4·2 power law fits the mercury results best). By plotting resistance as a function of temperature, the temperature-independent resistance may be readily found from the experimental results of Table 1, and is in fact very little lower than the value at 1·05° K. If there is no effect due to electron collisions with the boundaries, then this temperature-independent resistance is the residual value due to strain and impurity alone. Subtraction from the actual resistance at each temperature then gives the ideal resistance as a function of temperature, and if the observed increase of resistance were due to impurity or strain, this ideal resistance should be independent of specimen diameter. The curves obtained after this subtraction are shown in Figure 7 for four mercury

specimens, and it is seen that there is a size variation of this apparent ideal resistance; the increased resistance cannot therefore be explained away as due to strain if Matthiessen's rule is valid, although strain may make a contribution. For the tin foils also, the application of Matthiessen's rule to the data in Table 2 for the foils investigated at the lowest three temperatures, leads to values of apparent ideal resistance which are greater for the thinner foils; the increased resistance cannot therefore be explained away as due to impurity for tin either, although additional impurity may make a contribution. The theory of the increase of resistivity due to inelastic scattering of the conduction electrons at the metal surface does however lead to a size-variation of the apparent ideal resistance in the manner found experimentally.

The variation of the resistivity of thin films due to inelastic scattering at the film boundaries has been the subject of theoretical investigation by Thomson (1901)

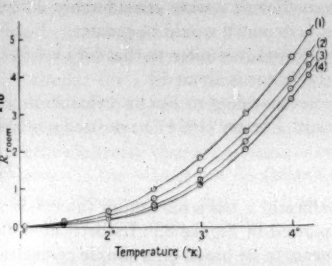

Figure 7. The temperature dependence of the apparent "ideal" resistance of mercury for four wire diameters: (1) 6 μ, (2) 10·5 μ, (3) 46 μ, (4) 790 μ.

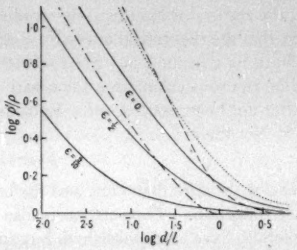

Figure 8. The theoretical variation of resistivity with size of conductor.
l=mean free path in bulk metal,
d=plate thickness or wire diameter,
ϵ=proportion of electrons scattered elastically.
———— plate, Fuchs (1938).
—·—·—·— plate, Lovell (1936), $\epsilon=0$.
— — — — wire, using Lovell's assumptions, $\epsilon=0$.
..... wire, Nordheim's relation, $\epsilon=0$.

who first suggested the possibility, by Lovell (1936) and by Fuchs (1938). Making certain simplifying assumptions, Lovell obtained the following relation between the resistivity ρ' of the thin film and that of the bulk material ρ:

$$\rho/\rho' = (d/l)[1 + \ln l/d], \qquad \ldots\ldots(1)$$

where d is the film thickness and l is the mean free path of the conduction electrons in the bulk metal. Relation (1) is plotted logarithmically in Figure 8. Fuchs made a more rigorous calculation and solved the problem for the general case when a proportion ϵ of the electrons is scattered elastically at the surface (Lovell had assumed $\epsilon=0$). Curves of Fuchs' solution for $\epsilon=0$, $\frac{1}{2}$, 9/10 are also shown in Figure 8.

For the tin foils these theoretical relations of Fuchs should be directly applicable, and the curve for $\epsilon=0$ (diffuse scattering) has been fitted as well as possible to the experimental data from Table 2. In the absence of other information the simplest value to assume for ϵ is zero. The process of fitting yields

values at each temperature of the bulk mean free path l and of the ratio of the bulk resistivity ρ to the room temperature value. The product of these two quantities should be independent of temperature if ϵ is independent of temperature. The curves for the three temperatures using a constant product $l\rho = 2{\cdot}0 \times 10^{-11}$ ohm cm^2 are shown as the full lines in Figures 5 and 6, and indicate a satisfactory agreement between theory and experiment. The scatter of points is most noticeable at 3·8° K. for the fatter specimens, but since the scale is logarithmic this corresponds to only small differences in (residual) resistivity of the order usually found between various samples of the same material. If the bulk residual resistivity is isotropic, rather than having the same anisotropy as the ideal resistivity as is assumed by the method of plotting, the effect would be to cause the points for the thinnest foils to lie slightly above the theoretical curve in Figure 5.

The accuracy of the product $l\rho$ for tin is estimated to be about 25% from the scatter of the points. If the scattering coefficient ϵ were considerably different from the zero value assumed, the product $l\rho$ deduced would be greater. Figure 8 shows that the theoretical curve for $\epsilon = \frac{1}{2}$ is roughly similar to that for $\epsilon = 0$ but is displaced by a factor 2·5. For $\epsilon = 9/10$ the factor is about 14.

The rigorous calculation for a wire corresponding to Fuchs' calculation for a film has not been carried out. Eucken and Förster (1934) have used a relation due to Nordheim:

$$\rho'/\rho = 1 + \alpha(l/d), \qquad \ldots\ldots(2)$$

where d is the wire diameter, and the coefficient α has a maximum value $8/3\pi$ for diffuse reflection. The relation is also plotted in Figure 8. Its derivation does not seem to have been published, but appears to be based on a simple geometrical argument involving the assumption that collisions with the boundary may be described by an appropriate relaxation time for the process as for lattice collisions; the validity of this assumption seems doubtful. From the form of relation (2), if α is independent of temperature, the additional resistance should appear as an increased residual resistance, since $l\rho$ is independent of temperature; this is not in agreement with the results for mercury illustrated in Figure 7, or the corresponding results for tin. Thus it seems that Nordheim's relation is inadequate. The solution for a wire using Lovell's assumptions has been worked out, as is shown in Figure 8; an outline of the calculation is given in the Appendix.

It will be seen from Figure 8 that the curves for a plate and for a wire, using Lovell's assumptions, are very similar, being laterally displaced along the $\log d/l$ axis by a roughly constant amount which corresponds to a ratio of about 3 in d/l for the ρ'/ρ values dealt with here. Pending the availability of a rigorous solution of the problem for a wire, it therefore seems reasonable to assume that it would yield curves similar to those of Fuchs a for plate, but laterally displaced by the same ratio. Although such a mathematical guess should be treated with caution, it is unlikely to be in error by more than a factor of two. Comparison of the results for the tin foils using Fuchs' curves, which are directly applicable to this case, with some scanty data for tin wires suggests that the ratio 3 is quite reasonable. *

The curve of Fuchs for $\epsilon = 0$ has accordingly been fitted as well as possible to the experimental data for mercury from Table 1; the curves for the various temperatures using a constant product $l\rho = 1{\cdot}5 \times 10^{-11}$ ohm cm^2 are shown as the full lines in Figures 2 and 3. In view of the uncertainty associated with the factor

* The thinnest tin wires were made using the pressurizer described in § 2 suitably modified for use in a furnace.

3 which has been applied, an accuracy of better than 50% in $l\rho$ cannot be assumed.

Values of $l\rho$ for mercury and tin have been calculated by Pippard from his 1,200-Mc/s. high frequency measurements (1947), using the theoretical treatment of the anomalous skin effect by Reuter and Sondheimer (1948). For mercury he finds the values of the product to be 2·0 and $3{\cdot}9\times10^{-11}$ ohm cm² for diffuse and elastic scattering respectively, while for tin the values are 1·0 and $1{\cdot}5\times10^{-11}$ ohm cm², each with an estimated accuracy of 50%. The coefficient of elastic scattering ϵ in the D.C. case is not necessarily the same as that for the high-frequency case, since in the latter case only electrons moving in directions almost parallel to the surface contribute to the current, while in the D.C. case electrons moving in all directions contribute. Bearing this in mind, and also the limited accuracy of both determinations of the product $l\rho$, the agreement is satisfactory, and leaves little doubt that the size-variation of D.C. resistivity is due to inelastic scattering of the conduction electrons at the metal surface; the correlation with the high-frequency measurements suggests that a low value of ϵ characterizes the scattering.

Although no theoretical value of the product $l\rho$ is available for tin or mercury, the formulae for a free electron metal may be used to check that the order of magnitude of the experimental values is correct. Simple considerations show that the resistivity of a free electron metal is given by $\rho=\boldsymbol{m}v/n\boldsymbol{e}^2l$, where $\boldsymbol{e}$ and $\boldsymbol{m}$ are the electronic charge and mass, n is the effective number of free electrons per cm³ and v is the velocity of the electrons at the top of the Fermi distribution. Quantum theory shows that $v=(\boldsymbol{h}/\boldsymbol{m})(3n/8\pi)^{\frac{1}{3}}$, where $\boldsymbol{h}$ is Planck's constant. Hence the product $l\rho$ is given by

$$l\rho=(\boldsymbol{h}/2\boldsymbol{e}^2)(3/\pi n^2)^{\frac{1}{3}}, \qquad \ldots\ldots(3)$$

and rough values of n may be found by substituting in (3) the values of $l\rho$ deduced from the present experiments. The values of n thus obtained correspond to 0·43 electrons per atom for tin and 0·57 electrons per atom for mercury. Such values are quite reasonable, and imply that the experimentally determined values of $l\rho$ are of the right order of magnitude.

ACKNOWLEDGMENTS

I wish to thank Dr. D. Shoenberg, Mr. A. B. Pippard and Mr. R. G. Chambers for useful discussions, Mr. A. B. Pippard for putting his pressurizer at my disposal, and Dr. G. J. van den Berg for drawing my attention to the earlier German work.

APPENDIX

The assumptions made by Lovell (1936) in calculating the resistivity of thin films will also be made here for a wire. The diameter of the wire d is considered sufficiently less than the bulk mean free path l for all free paths to be taken as starting from the wire surface. The collisions with the surface are considered inelastic, so that there is a uniform density of electrons in all inward directions from the surface.

Consider one point on the wire surface. Path directions from this point will be designated by the polar coordinates θ, ϕ; ϕ determines the azimuth in a plane normal to the wire axis through the point, and θ is the angle of elevation of the path above the plane. The fraction of paths from the point lying within the element of solid angle defined by θ, $\theta+d\theta$ and ϕ, $\phi+d\phi$ is $\cos\theta\,d\theta\,d\phi/2\pi$. The distance r

along any path to the next intersection with the wire boundary is $d\cos\phi\sec\theta$. Again, following Lovell, it is assumed that for $r<l$ the free path is r, while for $r>l$ the free path is l. Hence the modified mean free path l' is given by

$$l' = \frac{2}{\pi}\int_0^{\pi/2}\left[\int_0^{\cos^{-1}(a\cos\varphi)} d\cos\phi\, d\theta + \int_{\cos^{-1}(a\cos\varphi)}^{\pi/2} l\cos\theta\, d\theta\right] d\phi,$$

where $a=d/l$. Hence for $a\leqslant 1$

$$\frac{\rho}{\rho'} = \frac{l'}{l} = 1 + a - \frac{2}{\pi}\{E(a) + a^2 B(a)\},$$

and for $a\geqslant 1$

$$\frac{\rho}{\rho'} = \frac{l'}{l} = 1 + a - \frac{2}{\pi}\left\{aE\left(\frac{1}{a}\right) + \frac{1}{a}B\left(\frac{1}{a}\right)\right\},$$

where E and B are complete elliptic integrals.

The case $a>1$ is considered in order to complete the curve although the assumption made above that all paths commence on the wire surface no longer holds. The integrals have been computed graphically for the purpose of drawing the curve in Figure 8.

REFERENCES

ANDREW, E. R., 1948, *Proc. Roy. Soc.* A, **194,** 80 ; 1949, *Proc. Phys. Soc.* A, **62,** 88.
APPLEYARD, E. T. S., and LOVELL, A. C. B., 1937, *Proc. Roy, Soc.* A, **158,** 718.
BRIDGMAN, P. W., 1925, *Proc. Amer. Acad. Sci.*, **60,** 305.
EUCKEN, A., and FÖRSTER, F., 1934, *Göttingen Nachrichten*, **1,** 43, 129.
FUCHS, K., 1938, *Proc. Camb. Phil. Soc.*, **34,** 100.
HAMBURGER, L., 1931, *Ann. Phys., Lpz.*, **10,** 789.
KAPITZA, P., and MILNER, C. J., 1937, *J. Sci. Instrum.*, **14,** 165.
LOVELL, A. C. B., 1936, *Proc. Roy. Soc.* A, **157,** 311.
PIPPARD, A. B., 1947, *Proc. Roy. Soc.* A, **191,** 385.
REUTER, G. E. H., and SONDHEIMER, E. H., 1948, *Proc. Roy. Soc.* A, in the press.
RIEDEL, L., 1937, *Ann. Phys., Lpz.*, **28,** 603.
SCKELL, O., 1930, *Ann. Phys., Lpz.*, **6,** 932.
THOMSON, J. J., 1901, *Proc. Camb. Phil. Soc.*, **11,** 120.

Critical Field Measurements on Superconducting Tin Foils

BY E. R. ANDREW
Royal Society Mond Laboratory, Cambridge

Communicated by D. Shoenberg ; MS. received 8th September 1948

ABSTRACT. The critical fields of superconducting tin foils have been determined from resistance measurements in a longitudinal magnetic field. Pomeranchuk's relation, $H_f=H_c(1+\lambda'/d)$, between the foil critical field H_f and the foil thickness d was verified, and values of the length λ' were found as a function of temperature ; at 0° K. the value of λ' was estimated to be $1{\cdot}2\times10^{-5}$ cm., rising rapidly close to the transition temperature. It is noticed that λ' is approximately twice the penetration depth λ for tin at all temperatures. Assuming the validity of Ginsburg's interpretation of λ' as the sum of λ and the surface energy parameter β, it is seen that λ and β are approximately equal.

§1. INTRODUCTION

It was found by Pontius (1937) that the critical field of thin superconducting lead wires is greater than the value H_c for the metal in bulk. A more complete investigation of the size-variation of critical field for mercury in the form of evaporated films has been made by Appleyard, Bristow, London and Misener (1939). The present paper describes the results of a similar investigation for tin using thin rolled foils. Since, however, the thinnest foil was much thicker than the penetration depth λ of a magnetic field, the information derived was necessarily less comprehensive than that for mercury obtained by Appleyard *et al.*, who used films of thickness of the order λ. Experiments were also carried out using the thin pressurized mercury wires described in the previous paper (Andrew 1949), but no useful results were obtained since the small changes of critical field were masked by effects due to strain.

Pomeranchuk (1938) has shown that if there is a difference in surface energy $\lambda' H_c^2/8\pi$ between a plate in the normal and the superconducting states, the critical field for the plate is given by

$$H_f = H_c(1+\lambda'/d), \qquad \ldots\ldots(1)$$

where d is the plate thickness, provided that $d \gg \lambda'$. Ginsburg (1945) has shown that if the penetration laws of F. and H. London are assumed valid, and the penetration depth is assumed independent of field strength, then $\lambda' = \lambda + \beta$, where $\beta = 8\pi(\alpha_n - \alpha_s)/H_c^2$ and α_n, α_s are the surface energies per unit area between the normal metal and an insulator, and the superconducting metal and an insulator respectively.

The experiments described here show that the relation between H_f and d has in fact the form of equation (1); values of λ' as a function of temperature are deduced, and their interpretation is discussed.

§2. EXPERIMENTAL DETAILS

2.1. *The Specimens*

The material used was Johnson and Matthey tin No. 2,356. The report of the maker's spectrographic analysis indicated less than 0·004% impurity. The foils were rolled out using an accurately ground and carefully cleaned rolling mill. The specimens were cut with a razor blade in the form of rectangular strips 1 mm. wide and 3–5 cm. long. The method of mounting is described in the previous paper (Andrew 1949). The sharpness of the temperature transitions, and of the longitudinal magnetic field transitions, for all foil thicknesses, indicated the absence of appreciable strain, as did also the residual resistance measurements given in the previous paper.

The specimens were mounted vertically in the appendage of a Dewar flask at the centre of a Helmholtz pair of coils whose field was uniform within 0·1% over the length of the foil. Resistance was measured by a potentiometer method, using the improvements of Kapitza and Milner (1937). A measuring current of 1 ma. was used for foils 3–4 μ thickness, while for the thicker foils the measuring current was increased roughly in proportion to the thickness. The magnetic field due to this measuring current could be neglected since it was found that close to the transition temperature, where its effect should be greatest, a current three times as large caused an apparent reduction in critical field of only 0·1 gauss. The thickness of the foils was known roughly from the room temperature resistance, and

the mean thickness was found with an accuracy of about 1% after the experiment by weighing the portion between the potential points.

The temperatures of the specimens were deduced from the vapour pressure of the liquid helium in which they were immersed, using the 1932 Leiden scale of temperature.

2.2. *Special Precautions*

For the thinnest foil (3 μ) the change in critical field that has to be measured ranges from about 1 gauss when H_c is 3 gauss to about 8 gauss when H_c is 240 gauss. While such a change may be readily observed, a reasonable accuracy in the determination of λ' calls for critical field measurements with an accuracy of a few tenths of a gauss, and hence involves a number of precautions. It was not necessary of course to have an absolute accuracy of this order, and in fact one could work entirely in terms of the currents passed through the Helmholtz coils. Since the slope of the threshold curve is about 150 gauss/°K. at the transition temperature, falling off to about 75 gauss/°K. at 1·6° K., very careful temperature control was essential in order to achieve the desired accuracy, and this was conveniently obtained using the automatic device described elsewhere (Andrew 1948b); the error in critical field measurement due to temperature drift was not more than 0·1 gauss except at the lowest temperature, 1·66° K., where an error of 0·3 gauss was possible.

It was important that the applied field should be accurately parallel to the plane of the foil. The field coils were mounted so that they could be rotated through $\pm 5°$ about any horizontal axis. The position of the plane of the foil was known within a few degrees beforehand. Longitudinal resistance transitions were measured for several coil directions a few degrees on either side of the position which had been guessed as correct. From the transition at the highest field strengths the correct position of the coils could be found within $\frac{1}{2}°$. An error of $\pm 1°$ caused the transition to be displaced to field values about 0·2% lower, and of $\pm 2°$ to field values about 0·8% lower.

Since the transition temperatures T_c for various specimens are never quite the same, a correction for the differences is necessary. Such a correction involves some assumption concerning the functional form of the threshold field curves. For instance, it may be assumed that H_c is a function of $(T_c - T)$, or of T/T_c. The former implies that the threshold field curves are geometrically similar for different specimens, but subject to small shifts along the temperature axis, while the latter assumes that the values of critical field become equal at 0° K. Near the transition temperature, however, all likely assumptions will lead to the same correction, while at lower temperatures H_c is much larger and dH_c/dT is smaller, so that the fractional correction is in any case small. For practical purposes the former assumption was therefore made, and in order to avoid as far as possible the application of a numerical correction to the experimental results, measurements were made at temperatures T such that $\Delta T (= T_c - T)$ took certain predetermined values. The small remaining correction that had to be applied, due to the fact that the ΔT values were not quite equal to the predetermined values, amounted to only a few tenths of a gauss.

The experimental procedure was therefore as follows: (*a*) the temperature transition was measured (i.e. resistance against temperature in zero field);

(*b*) the coil system was exactly aligned at $\Delta T = 0{\cdot}53°$ K.; (*c*) the specimen was allowed to warm up above the transition temperature; (*d*) systematic measurements were made of resistance as a function of field at various ΔT.

For the measurements of the temperature transition, the earth's vertical field was compensated, but it was uncompensated in the critical field determinations and, therefore, its value, 0·4 gauss, had to be added to the applied fields. The earth's horizontal field (about 0·15 gauss) was not compensated in any of the measurements; its direction was almost in the plane of the specimen, so that no serious error is likely to result from its neglect.

2.3. *Determination of the Critical Fields*

The value of the applied longitudinal field which was taken as the critical field, was the value which restored half the normal resistance. This requires some justification since previous workers have sometimes taken the field which produces the first trace of resistance (e.g. Pontius 1937). It is well known that unstrained single crystals of tin give sharp temperature and longitudinal field transitions, whilst those for polycrystalline material are usually about 0·02° K. and 3 gauss broad respectively. Since strain is known to affect the temperature and field transitions (Sizoo, de Haas and Onnes 1925), it may be supposed that the crystal grains of which the polycrystalline material is composed are each under stress at low temperatures, due to the anisotropy of thermal expansion coefficient for tin and an inability to anneal at such temperatures. If one assumes a Gaussian distribution of stresses for the crystal grains, then one has a Gaussian distribution of transition temperatures and critical fields, since the effects of stress, being small, may be taken as linear. This information alone, however, does not suffice to determine the shape of the resistance transitions as the geometrical arrangement of the crystal grains is also of importance. If, however, we first consider the fictitious one-dimensional case of a metallic line consisting of a random distribution of elements, some superconducting and some normal, then it is obvious that the fractional resistance will be proportional to the fractional length of normal metal. If the transition temperature and the critical field have a Gaussian distribution, then the fraction α of normal resistance restored either at a temperature T in a temperature transition or at a field h in a field transition will have the form

$$\alpha = \frac{1}{\sqrt{\pi}} \int_{-\infty}^{x} \exp(-t^2)\, dt, \qquad \ldots\ldots(2)$$

where, for a temperature transition, $x = (T - T_c)/\sqrt{2}T_0$ and for a longitudinal field transition $x = (h - H_c)/\sqrt{2}H_0$, ($T_c$ is the critical temperature, H_c the critical field, and T_0 and H_0 are the standard deviations of the two Gaussian distributions).

Temperature transitions for the four foils, of thickness 3–20 μ, are shown in Figure 1 and equation (2) has been fitted to them as well as possible (broken lines). It will be seen that the theoretical form for the fictitious one-dimensional model fits the results fairly well. Etching showed that the crystal grains varied in size from 0·1 to 1 mm.: thus for all the foils there was generally not more than one single crystal extending through the thickness of the foil, but there were generally two or three grains across the width. For one foil (6·94 μ) there were many large crystal grains, several of which extended over the whole width of the foil (1 mm.). It is satisfactory that for this foil equation (2) fits particularly well (Curve (2),

Figure 1), confirming that it is a good approximation to the one-dimensional model. The slight deviations from equation (2) for the more usual case in which there are several grains across any width may be accounted for qualitatively by simple arguments.

Since the crystal grains extend right through the foil, each affords entry and exit for lines of force in a magnetic field, so that approximately the longitudinal magnetic field transitions should be geometrically similar to the temperature transition. This is in fact the case, as is illustrated for the 4·11 μ foil in Figure 2 close to the transition temperature, and continues to be the case with roughly the same width (or slightly narrower) at lower temperatures. The transitions were about 3 gauss wide for all specimens and temperatures.

There will be a family of critical field–temperature curves corresponding to the various values of T_c and H_c in the Gaussian distributions. Any member of the family near the mean will serve our purpose since, when plotted as a function of ΔT, they will all coincide. The half-resistance point on the resistance–field curves has been chosen to determine the critical field values because this critical field is very close to the mean of the Gaussian distribution, and also because the field value can be determined most precisely at this point since the curves are steepest there.

§ 3. EXPERIMENTAL RESULTS AND DISCUSSION

The foils used had thicknesses 3·43, 4·11, 6·94 and 19·4 μ. In order to obtain, in addition, critical field values close to the bulk values, a wire of diameter 0·26 mm. was used rather than a thick foil. A foil of this thickness would have a demagnetization coefficient n of 0·005, causing an apparent lowering of the critical field by a fraction of this order; the value of n for the 19·4 μ foil, the thickest used for these measurements, was 4×10^{-4}, the effect of which was negligible. For the wire of diameter 0·26 mm. and length 5 cm., the value of n was $1{\cdot}3 \times 10^{-4}$, and hence its effect also was negligible. The wire was cast in a thin-walled capillary and the glass cracked off; potential leads of pure tin were fixed on with a pinhole flame.

The values of the foil critical fields H_c are shown in Table 1, and were plotted against the reciprocal of the thickness d,* as is shown for three values of ΔT in Figure 3; the fact that the relations are linear is a confirmation of (1). The slope $\lambda' H_c$, the intercept H_c, and their probable errors were calculated by the method of least squares. From these quantities λ' was obtained as a function of ΔT; the values are shown in Table 1 and are plotted in Figure 4, the vertical lines indicating the calculated probable errors. The smooth curve that has been drawn through the points indicates that λ', like the penetration depth λ, tends to infinity at T_c and becomes independent of temperature at low temperatures. The calculated values of H_c are also shown in Table 1, and are in good agreement with other published values (de Haas and Engelkes 1937, Daunt and Mendelssohn 1937, Andrew 1948).

Unfortunately absolute values of λ are not available for comparison with the present values of λ', but Pippard (1947) has obtained relative values $(\lambda - \lambda_{2{\cdot}3^\circ\mathrm{K}})$. Using the relation $\lambda^2_{0^\circ\mathrm{K}}/\lambda^2 = 1 - (T/T_c)^4$, which fits the data for mercury well (Daunt, Miller, Pippard and Shoenberg 1948), Pippard's results lead to the value $\lambda_{2{\cdot}3^\circ\mathrm{K}} = (0{\cdot}6 \pm 0{\cdot}1) \times 10^{-5}$ cm. The measurements of Laurmann and Shoenberg (see Shoenberg 1948) are in good agreement with this estimate. The absolute values of λ thus deduced are shown in Figure 4 (broken line). If Ginsburg's

* In the case of the wire, the appropriate value is twice the reciprocal of the diameter, as a cylinder has twice the surface area/volume ratio of a plate.

interpretation of λ' is correct, the differences $\lambda' - \lambda$ give the values of β, and these also are shown in Figure 4 (chain line). Smoothed values of λ', together with values of λ and β, are given in Table 2.

The interesting feature which emerges, and which is shown clearly by Figure 4, is the near equality of λ and β at all temperatures. The same feature was found for mercury also by Ginsburg (1945), who calculated values of λ and β from the mercury

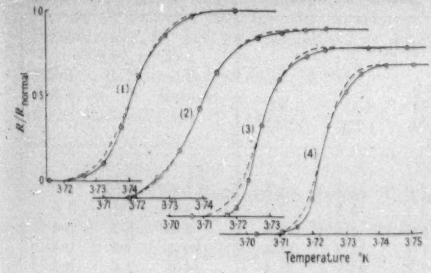

Figure 1. Temperature transitions of four tin foils; thickness (1) 3·43 μ, (2) 6·94 μ, (3) 4·11 μ, (4) 19·4 μ. The broken lines are given by equation (2).

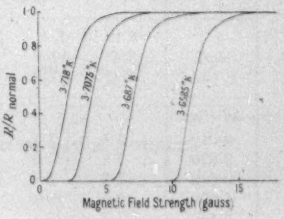

Figure 2. Resistance curves in a longitudinal field for the 4·11 μ foil. Measuring current 1 ma.; $T_c = 3{\cdot}728°$ K. The vertical component of the earth's field (0·4 gauss) opposes the applied field.

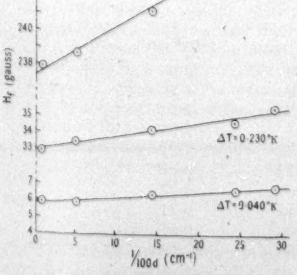

Figure 3. Critical field values H_f of the foils for three values of ΔT, plotted against the reciprocal of the thickness d.

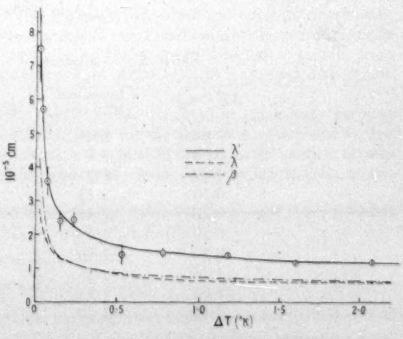

Figure 4. The values of λ' deduced from the experiments, plotted against $\Delta T\,(=T_c - T)$, together with the values of the penetration depth λ, and of β (defined as $\lambda' - \lambda$).

film results of Appleyard *et al.* (1939). The result of this calculation is, however, at variance with that of Désirant and Shoenberg (1948 a), who combined the results of their absolute determination of λ for mercury (obtained from susceptibility measurements on colloidal spheres and on thin wires) with the critical field measurements of Appleyard *et al.* Doubt has however been cast on the reliability of the thin wire results (Shoenberg 1948); the discrepancy may therefore prove

unfounded. In any case the interpretation of λ' as $\lambda+\beta$ assumes, as Ginsburg pointed out, that λ is independent of magnetic field strength; this is an assumption which may well be untrue. The correct interpretation of λ' therefore awaits a more complete theory. It is of interest to note, however, that if Ginsburg's interpretation is adopted, the values of β which have been derived here for tin are

Table 1. Values of H_f, H_c and λ'

	Values of H_f (gauss)					H_c (gauss)	λ' *	P.E. in λ' *
$d(\mu)$	E 16 260	E 1 19·4	E 4 6·94	E 5 4·11	E 2 3·43			
T_c (° K.)	3·715	3·724	3·739	3·728	3·742			
ΔT (° K.)								
0·010	1·4	1·5	2·0	1·8	2·1	1·4	15·0	3·9
0·020	3·1	3·0	3·4	3·5	3·7	3·0	7·5	1·0
0·040	5·9	5·9	6·4	6·6	6·8	5·8	5·7	0·4
0·070	10·4	10·4	11·1	11·2	11·4	10·4	3·6	0·4
0·150	21·7	22·4	22·8	23·1	23·4	21·9	2·4	0·3
0·230	32·9	33·5	34·2	34·6	35·5	33·0	2·45	0·20
0·530	73·2	74·9	76·0	76·0	76·7	73·9	1·38	0·26
0·780	105·6	—	108·3	109·2	110·2	105·7	1·47	0·12
1·180	153·1	153·2	155·8	157·4	159·1	152·6	1·40	0·08
1·600	197·1	—	200·4	202·7	203·5	197·0	1·16	0·04
2·080	237·8	238·7	241·2	244·5	245·7	237·4	1·20	0·03

* λ' in 10^{-5} cm.

Table 2. Values of λ', λ and β for Tin

ΔT (° K.)	λ'(smoothed) (10^{-5} cm.)	λ (10^{-5} cm.)	β (10^{-5} cm.)
0·02	8·0	3·0	5·0
0·04	5·4	2·2	3·2
0·07	3·8	1·7	2·1
0·10	3·15	1·5	1·65
0·20	2·40	1·18	1·22
0·50	1·69	0·82	0·87
0·80	1·46	0·69	0·77
1·20	1·33	0·62	0·71
1·60	1·25	0·60	0·65
2·10	1·20	0·58	0·62

of the same order of magnitude as the values of Δ obtained from experiments on tin cylinders in the intermediate state (Désirant and Shoenberg 1948 b, Andrew 1948 a), where $\Delta = 8\pi\alpha_{ns}/H_c^2$ and α_{ns} is the surface energy per unit area at the boundary between normal and superconducting domains of metal. This means that α_{ns} and $(\alpha_n - \alpha_s)$ are of the same order, as one might expect.

REFERENCES

ANDREW, E. R., 1948 a, *Proc. Roy. Soc.* A, **194**, 80; 1948 b, *J. Sci. Instrum.* (in the press); 1949, *Proc. Phys. Soc.* A, **62**, 77.

APPLEYARD, E. T. S., BRISTOW, J. R., LONDON, H., and MISENER, A. D., 1939, *Proc. Roy. Soc.* A, **172**, 540.

DAUNT, J. G., and MENDELSSOHN, K., 1937, *Proc. Roy. Soc.* A, **160**, 127.
DAUNT, J. G., MILLER, A. R., PIPPARD, A. B., and SHOENBERG, D., 1948, *Phys. Rev.* **74**, 842.
DÉSIRANT, M., and SHOENBERG, D., 1948 a, *Proc. Phys. Soc.*, **60**, 413 ; 1948 b, *Proc. Roy. Soc.* A, **194**, 63.
GINSBURG, V., 1945, *J. Phys. U.S.S.R.*, **9**, 305.
DE HAAS, W. J., and ENGELKES, A. D., 1937, *Physica*, **4**, 325.
KAPITZA, P., and MILNER, C. J., 1937, *J. Sci. Instrum.*, **14**, 165.
LONDON, F. and H., 1935, *Proc. Roy. Soc.* A, **149**, 71.
PIPPARD, A. B., 1947, *Proc. Roy. Soc.* A, **191**, 370.
POMERANCHUK, I., 1938, see *Superconductivity*, by D. Shoenberg (Cambridge : University Press), p. 98.
PONTIUS, R. B., 1937, *Phil. Mag.*, **24**, 787.
SHOENBERG, D., 1948, *Amsterdam Conference on Metals.*
SIZOO, C. J., DE HAAS, W. J., and ONNES, H. K., 1925, *Leiden Comm.*, 180 c, d.

On the Radiation from Transient Light Sources

BY F. BOOTH
H. H. Wills Physical Laboratory, University of Bristol

MS. received 2*nd February* 1948, *in amended form* 14*th August* 1948

ABSTRACT. A theoretical treatment is given of the problem of analysing the radiation from transient light sources in the form of clouds of incandescent particles. Recently a method of correlating this radiation with various physical parameters has been suggested by E. F. Caldin. In the present paper a critical examination of this method is made, and exact formulae derived for special models.

Expressions for the radiation emitted by a cloud of incandescent particles, all at the same temperature, are obtained for the following cases : (i) a uniform spherical distribution of equal, perfectly emitting and absorbing particles; (ii) a uniform distribution of particles which are not perfect absorbers, but in which (*a*) radiation is reflected specularly from the particle surface, and (*b*) the particles reflect light diffusely; (iii) a uniform distribution of particles in a thin spherical shell.

It is shown that the condition for the radiation from a cloud of black body particles to be equal in intensity to that from a black body of the same size and shape is that $R^3 a \rho_0 \ll M$, where R is the radius of the cloud, a the particle radius, ρ_0 the particle density and M the total mass of the cloud. The cooling of clouds by radiation transfer is also examined theoretically.

The bearing of the results on Caldin's method is discussed, and more exact methods of analysing the cooling of this form of light source sketched.

§1. INTRODUCTION

THE following paper is a theoretical investigation of some problems suggested by an analysis due to Caldin (1946) of the radiation from transient light sources. The light sources Caldin considers are all of the same general type. A metal is ignited either in oxygen, or in the presence of an oxidizing agent; owing to the large amount of heat liberated, the temperature of the reactants becomes very high and part of the energy is radiated as light. All the sources show the same type of light intensity–time curve—a rapid rise to the maximum intensity, followed by a slower fall in intensity.

A general theory of transient light sources of this kind would be very complicated since three distinct problems would have to be solved: (*a*) determination of the behaviour with time of the pressure, temperature and velocity of various parts of the system as the reaction proceeds; (*b*) some knowledge of the kinetics of the

oxidation would be required so that the proportion of metal oxidized at any time and the temperature of the products could be found; (*c*) evaluation of the radiation reaching an external point from the source.

For practical purposes all we need to know is the quantity and quality of the luminous radiation as found by (*c*). But although problem (*c*) is quite distinct from problems (*a*) and (*b*), these must first be solved to find the radiation emitted. Unfortunately the two problems cannot be solved independently. For example, the dynamical behaviour will depend upon the reaction kinetics, and the rate of oxidation upon the pressure and temperature of the material of the light source, that is, upon variables determined by (*a*). At the present stage an exact solution of the whole behaviour seems out of the question; drastic assumptions must be made about the first two problems (*a*) and (*b*) and attention concentrated upon the remaining problem (*c*). This is the procedure proposed by Caldin (1946 a, b).

In Caldin's first paper (1946 a) the cooling of a body by radiation from the surface is considered. It is assumed that initially, and during the subsequent cooling, the body is of uniform temperature. By equating the rate of energy loss from the surface to the rate of reduction of the internal energy, expressions are derived for the total intensity of radiation, brightness and temperature as a function of the time. In the second paper (1946 b) the spectral distribution of the energy is found as a function of the time, and, by integration, the total amount of energy radiated at a given wavelength is obtained as a function of the initial temperature. All the expressions obtained hold only for a "Planckian radiator"—that is, for a radiator whose emissivity is independent of the wavelength and temperature.

Now consider the transient light sources. Suppose that at the maximum intensity of the light emission the chemical reaction is complete, and that the material is of uniform temperature and at rest. Then if we assume that the material behaves as a "Planckian radiator" of uniform temperature, the theory can be used to analyse the decay of the light intensity. For example, from the total energy liberated at any particular wavelength, the initial temperature can be found. The validity of the method rests, however, on whether or not the radiating material can be treated as a uniform temperature "Planckian radiator". From observations on the spectrum and temperature it seems probable that the light radiated after the maximum intensity is due to temperature radiation from incandescent solid particles—very probably oxide particles. If we assume that there is little radial motion, problem (*c*) is resolved into the determination of the radiation from a roughly spherical cloud of fine particles, each cooling by radiation. The temperature and density are not, in general, uniform. If the problem of cooling is solved by Caldin's method two basic assumptions are implied: (1) the temperature throughout the cloud is initially uniform, and remains so as it cools; (2) the radiation from the cloud is the same as it would be from a solid surface consisting of the radiating material and coincident with the boundary between the outer layers of the cloud and surrounding space.

The second assumption may be restated as two rather simpler assumptions: (2′) if each solid particle in the cloud is a perfect absorber and emitter then the radiation from the cloud is that of a solid black body at the same temperature; (2″) if the surface emissivity of each particle is ϵ then the radiation from the cloud is that of a solid black body at the same temperature multiplied by ϵ.

In the following account, we shall find the conditions which these assumptions impose on the physical properties of the material in the light source.

§ 2. EXAMINATION OF ASSUMPTION (2)

2.1. *Radiation from a Cloud of black-body Particles* (*Assumption* (2'))

We first consider assumption (2'), assuming (1) to be valid. Let R be the radius of a spherical cloud composed of spherical particles of radius a, density ρ_0, and at temperature T; the density distribution is assumed to be spherically symmetrical. If $N(r)$ is the number of particles per cm³ in a small region round a point P, distant r from the centre of the cloud, then N_0, the total number of particles in the cloud is given by

$$N_0 = 4\pi \int_0^R N(r) r^2 \, dr = 3M/4\pi\rho_0 a^3, \qquad \ldots\ldots(2.1)$$

where M is the total mass of solid material in the cloud. To examine assumption (2') we require the total amount of light radiated from a cloud of this form in unit time. It is first necessary to derive the fundamental equation for the transfer of radiation.

Let I denote the total intensity of radiation of all wavelengths at a point P, in direction $\mathbf{s}$. Then if dA is a small area element at P in a plane perpendicular to $\mathbf{s}$, the amount of radiation which crosses dA in unit time and spreads into a small solid angle $d\omega$ containing direction $\mathbf{s}$ is $I(\mathrm{P}, \mathbf{s})\, d\omega\, dA$. Let P' be a point distant ds from P along direction $\mathbf{s}$. In traversing PP', part of the radiation is lost by absorption, but there is also a gain from the radiation emitted by the particles. Assuming that $(dA)^{\frac{1}{2}}$ and ds are large compared with a,* the number of particles within the cylinder formed by dA and ds will be $N dA\, ds$.

Since each particle is a perfect absorber the amount of light absorbed in unit time by the particles from the light in direction $d\omega$ will be $I(\mathrm{P}, \mathbf{s})\pi a^2 N(r)\, dA\, ds\, d\omega$. The radiation emitted into $d\omega$ per second will be $4\pi a^2 N(r)\, dA\, ds B(T)\, d\omega/4\pi$, where $B(T)$ is the total energy liberated by unit area of the surface of a black body in unit time at temperature T. From radiation theory

$$B(T) = \sigma T^4, \qquad \ldots\ldots(2.2)$$

where σ is Stefan's constant.

Hence

$$[I(\mathrm{P}', \mathbf{s}) - I(\mathrm{P}, \mathbf{s})]\, dA\, d\omega = \pi a^2 N(\mathrm{P})\, dA\, ds\, d\omega[(\sigma T^4/\pi) - I(\mathrm{P}, \mathbf{s})],$$

or

$$(\mathrm{P}, \mathbf{s})\, dI/ds = \pi a^2 N(r)[(\sigma T^4/\pi) - I(\mathrm{P}, \mathbf{s})]. \qquad \ldots\ldots(2.3)$$

Now $dI/ds = \partial I/\partial s + \partial I/c\partial t$, where c is the velocity of light. Since we assume the cloud at rest and T constant, $\partial I/\partial t = 0$, and (2.3) can be written

$$\partial I/\partial \tau = \sigma T^4/\pi - I, \qquad \ldots\ldots(2.4)$$

where

$$\tau = \pi a^2 \int^s N \, ds. \qquad \ldots\ldots(2.5)$$

Integrating the equation along direction $\mathbf{s}$ from P_1 ($s = s_1$ or $\tau = \tau_1$) to P_2 ($s = s_2$ or $\tau = \tau_2$), we get

$$I(\tau_1, \mathbf{s}) \exp \tau_1 - I(\tau_2, \mathbf{s}) \exp \tau_2 = (\sigma T^4/\pi)(\exp \tau_1 - \exp \tau_2). \qquad \ldots\ldots(2.6)$$

Now apply this equation to determine the radiation from the cloud. We first take $N(\mathrm{P})$ uniform, but this restriction will be removed later. Thus $\tau = \alpha s$ where $\alpha = \pi a^2 N_0$. Let PQ denote a small cylindrical volume element of the sphere,

* The only essential limitation this condition imposes, is that $a \ll R$. This is a fairly obvious restriction, for it would seem absurd to analyse the radiation transfer in the manner we intend, if all the material in the flash were concentrated in a few pieces. It transpires, however, that even in this case, the *results* of the method are correct.

whose axis is parallel to **s** and whose normal cross section is dA (Figure 1). The total light emitted from the end surface at Q in $d\omega$ about direction **s** is $I(\mathrm{Q},\mathbf{s})\,dA\,d\omega$. From (2.6),

$$I(\mathrm{P},\mathbf{s})-I(\mathrm{Q},\mathbf{s})\exp(\alpha\mathrm{PQ})=(\sigma T^4/\pi)\{1-\exp(\alpha\mathrm{PQ})\}. \quad \ldots\ldots(2.7)$$

Clearly $I(\mathrm{P},\mathbf{s})=0$ since we assume no light reaches the sphere from outside, and so

$$I(\mathrm{Q},\mathbf{s})=(\sigma T^4/\pi)\{1-\exp(-\alpha\mathrm{PQ})\}. \quad \ldots\ldots(2.8)$$

If z is the distance of the axis of PQ from O, the centre of the sphere, $dA=z\,dz\,d\theta$ where θ is the angle between the normal to PQ from O, and a reference line in the plane through O perpendicular to **s**. Hence from (2.8) the total radiation emitted into $d\omega$ is

$$H=d\omega(\sigma T^4/\pi)\int_0^R\int_0^{2\pi} z(1-\exp\{-2\alpha\sqrt{(R^2-z^2)}\})\,dz\,d\theta, \quad \ldots\ldots(2.9)$$

which integrates to

$$d\omega\sigma T^4R^2\left[1-\frac{1}{2R^2\alpha^2}+\exp(-2R\alpha)\left(\frac{1}{R\alpha}+\frac{1}{2R^2\alpha^2}\right)\right]. \quad \ldots\ldots(2.10)$$

Integrating over $d\omega$, the total radiation emitted becomes

$$H=4\pi R^2\sigma T^4\left[1-\frac{1}{2R^2\alpha^2}+e^{-2R\alpha}\left(\frac{1}{R\alpha}+\frac{1}{2R^2\alpha^2}\right)\right]$$
$$=H^*E(R\alpha), \quad \ldots\ldots(2.11)$$

where
$$H^*=4\pi R^2\sigma T^4, \quad \ldots\ldots(2.12)$$

that is, the radiation from a solid black body sphere of radius R, and $E(x)$ is given by

$$E(x)=1-\frac{1}{2x^2}+e^{-2x}\left(\frac{1}{x}+\frac{1}{2x^2}\right). \quad \ldots\ldots(2.13)$$

Clearly we may call $E(x)$ the "effective emissivity" of the cloud.

Consider the behaviour of $E(x)$ as x varies: (i) as $x\to\infty$, $E(x)\to 1$; (ii) as $x\to 0$, $E(x)\to 4x/3$; (iii) $dE(x)/dx=x^{-3}[1-e^{-2x}(2x^2+2x+1)]$. Since x is always positive $e^{2x}>1+2x+2x^2$ and so $dE(x)/dx>0$. Hence $E(x)$ is always positive and increases steadily from $4x/3$ to 1 as x moves from small to large values. Therefore the condition that $H=H^*$ or that assumption (2′) is fulfilled, is that $R\alpha\gg 1$, or from (2.1),

$$R^2a\rho_0\ll 9M/16\pi. \quad \ldots\ldots(2.14)$$

On the other hand, for $R\alpha$ small or when

$$R^2a\rho_0\gg 9M/16\pi, \quad \ldots\ldots(2.15)$$

$$H=4R\alpha H^*/3=4\pi a^2N_0\sigma T^4. \quad \ldots\ldots(2.16)$$

The radiation is then simply the sum of the radiations emitted by each particle and none is absorbed.

In subsequent work we shall frequently refer to (2.14) and (2.15) as E and E′ respectively. For brevity, when a cloud satisfies inequality E, we shall say it is an "E" state, when inequality E′, in an "E′" state.

Now let us consider how the results of the analysis are modified if we remove the restriction that $N(r)$ is constant. Equation (2.9) then becomes

$$H=4\sigma T^4\int_0^R\int_0^{2\pi} z(1-\exp\{-\tau(\mathrm{PQ})\})\,dz\,d\theta, \quad \ldots\ldots(2.17)$$

where

$$\tau(\mathrm{PQ}) = \pi a^2 \int_{\mathrm{P}}^{\mathrm{Q}} N(r)\, d(\mathrm{PQ}). \qquad \ldots\ldots (2.18)$$

To evaluate H accurately, the exact form of $N(r)$ is required. But it seems very likely that condition (2.14) still applies for assumption (2′) to be valid, for it is easily derived for the case of a thin cloud in the form of a spherical shell, which is a probable density distribution for practical cases. Suppose the material is concentrated in a thin spherical shell of thickness Δ. Then H may be written

$$H = 4\sigma T^4 \int_0^{2\pi} \left[\int_0^{R-\Delta} z(1 - \exp\{-\tau(\mathrm{PQ})\})\, dz + \int_{R-\Delta}^{R} z(1 - \exp\{-\tau(\mathrm{PQ})\})\, dz \right] d\theta. \qquad \ldots\ldots (2.19)$$

Since $\Delta \ll R$, the second term is small compared with the first and we have very nearly

$$H = 4\sigma T^4 \int_0^{R-\Delta} \int_0^{2\pi} z(1 - \exp\{-\tau(\mathrm{PQ})\})\, dz\, d\theta. \qquad \ldots \quad (2.20)$$

For $H = H^*$ then, we must have, for all possible values of PQ, $\exp\{-\tau(\mathrm{PQ})\} \ll 1$ or

$$\tau(\mathrm{PQ}) \gg 1. \qquad \ldots\ldots (2.21)$$

Now in the range of integration 0 to $R-\Delta$, $\tau(\mathrm{PQ})$ has its minimum value when PQ lies along the diameter in the direction **s**. Hence (2.21) is satisfied if

$$2\pi a^2 \int_{R-\Delta}^{R} N\, dr \gg 1. \qquad \ldots\ldots (2.22)$$

Since $4\pi R^2 \int_{R-\Delta}^{R} N\, dr = N_0$, (2.22) gives $R^2 a \rho_0 \ll 3M/8\pi$ which is equivalent to E.

When $\tau(\mathrm{PQ}) \ll 1$, it is easy to show that we can derive expression (2.16) for the total radiation emitted for in this case

$$H = 4\sigma T^4 \pi a^2 \int_0^{R} \int_0^{2\pi} \int_{\mathrm{P}}^{\mathrm{Q}} N(r) z\, dz\, d\theta\, d(\mathrm{PQ}) = 4\pi a^2 \sigma T^4 N_0.$$

Summarizing these results, we see that for a spherical shell of radiating particles we may write

$$H = H^* E_s(\tau_0), \qquad \ldots\ldots (2.23)$$

where

$$\tau_0 = \pi a^2 \int_{R-\Delta}^{R} N(r)\, dr \qquad \ldots\ldots (2.24)$$

and $E_s(x) \simeq E(x)$ for both large and small x.

Hence the main conclusions reached for the case of a uniform distribution still hold for a spherical shell.

2.2. *Radiation from a Cloud in which the Particles are not Perfect Absorbers or Perfect Emitters (Assumption (2″))*

We shall now examine assumption (2″). Suppose the absorption coefficient of the surface of the particle is independent of the wavelength. Then, by Kirchhoff's law, the absorption coefficient equals the emissivity ϵ, where ϵ is defined as the ratio of the total energy radiated by unit area of the surface in unit time to the energy radiated by a unit area of black body surface in unit time. To evaluate the radiation from the cloud, it is now necessary to take into account scattering of

radiation by the particles. For, consider a single particle, in the path of a parallel beam. If I is the intensity of the beam in direction $\mathbf{s}$ in $d\omega$, the total amount of light received from the beam in unit time is clearly $I\pi a^2 d\omega$. But the radiation absorbed in unit time is $\epsilon I\pi a^2 d\omega$. Hence the amount scattered out of the beam by the particle is $(1-\epsilon)I\pi a^2 d\omega$. Let a fraction

$$\gamma(\mathrm{P}, \mathbf{s}', \mathbf{s})\, d\omega'/4\pi \qquad \ldots\ldots(2.25)$$

of the total light scattered by a particle be scattered into directions within solid angle $d\omega'$ about the direction $\mathbf{s}'$. It follows that

$$\int \gamma(\mathrm{P}, \mathbf{s}', \mathbf{s})\, d\omega' = 4\pi, \qquad \ldots\ldots(2.26)$$

where integration is over all directions $\mathbf{s}'$. The more general form of equation (2.3), in which account is taken of scattering is

$$\frac{\partial I(\mathrm{P}, \mathbf{s})}{\partial s} = \pi a^2 N\left[\frac{\epsilon\sigma T^4}{\pi} - I(\mathrm{P}, \mathbf{s}) + \frac{(1-\epsilon)}{4\pi}\int I(\mathrm{P}, \mathbf{s})'\gamma(\mathrm{P}, \mathbf{s}', \mathbf{s})\, d\omega'\right]. \qquad \ldots\ldots(2.27)$$

The first term of the right-hand side represents radiation gained by emission, the second, radiation lost by absorption and scattering, and the third, the contribution due to radiation scattered *into* direction $\mathbf{s}$. The integration in the third term is again over all directions $\mathbf{s}'$.

If we neglect the light scattered into $d\omega'$ equation (2.27) becomes

$$\frac{\partial I(\mathrm{P}, \mathbf{s})}{\partial s} = \pi a^2 N\left[\frac{\epsilon\sigma T^4}{\pi} - I(\mathrm{P}, \mathbf{s})\right], \qquad \ldots\ldots(2.28)$$

which is equivalent to (2.3) with σ replaced by $\epsilon\sigma$. Hence if (2.28) were satisfied, together with the condition E, assumption (2″) would be correct. But it is clearly illegitimate to reject the light scattered *into* $d\omega$ and retain the light scattered *out* in the derivation of (2.27). Hence (2″) is incorrect and gives too small a value for the emitted radiation.

On the other hand, even if E is satisfied the radiation is *less* than it would be from a solid sphere emitting black-body radiation. For, suppose the cloud is placed in a black-body enclosure whose walls are at temperature T. Let H_m be the radiation emitted by the material of the cloud which traverses the outer surface in unit time. Then the total radiation received by the enclosure from the particles is $H_1 = H_m + H_s$ where H_s represents the part of the energy from the walls of the enclosure which is scattered back to the walls by the cloud. But H_1 represents the energy emitted by a cloud of black-body material since in this case $H_s = 0$. Thus for $\epsilon < 1$, $H_m < H^*$. Hence it follows that the total energy radiated per second is

$$H = 4\pi R^3 \epsilon' \sigma T^4, \qquad \ldots\ldots(2.29)$$

where $\epsilon < \epsilon' < 1$. To determine ϵ', which we may again call the "effective emissivity" it is first necessary to determine $\gamma(\mathrm{P}, \mathbf{s}', \mathbf{s})$. This is, strictly, a matter for experiment. But $\gamma(\mathrm{P}, \mathbf{s}', \mathbf{s})$ can be calculated for simple cases. For example, if the light scattered is reflected specularly from the particle surface

$$\gamma(\mathrm{P}, \mathbf{s}', \mathbf{s}) = 1. \qquad \ldots\ldots(2.30)$$

For diffuse reflection

$$\gamma(\mathrm{P}, \mathbf{s}', \mathbf{s}) = (8/3\pi)(\sin\phi - \phi\cos\phi), \qquad \ldots\ldots(2.31)$$

where ϕ is the angle between **s** and **s'**. Another law which might be considered is that for "Rayleigh scattering", which is given by

$$\gamma(\mathrm{P}, \mathbf{s}', \mathbf{s}) = 3(1+\cos^2\phi)/4. \qquad \ldots\ldots(2.32)$$

But for this law to hold, a would have to be small compared with the light wavelength and it is unlikely that the particles in the light sources we are considering are so small. The evaluation of the expressions (2.30) and (2.31) is given in Appendix I.

It now remains to calculate ϵ' by substituting expressions (2.30) or (2.31) in equation (2.27) and solving for I. Unfortunately, owing to the last term of equation (2.27), the total radiation from the sphere cannot be evaluated in the same manner as in the case of (2.11). We can, however, give an approximate calculation, the results of which agree quite well with (2.11) in the case of $\epsilon = 1$.

Let the angle between the radius vector drawn to any point in the cloud and the direction **s** be θ. Then

$$\frac{\partial I}{\partial s} = \cos\theta \frac{\partial I}{\partial r} - \frac{\sin\theta}{r}\frac{\partial I}{\partial \theta}. \qquad \ldots\ldots(2.33)$$

If we again assume N is constant and write

$$\tau = \pi a^2 N(r), \qquad \ldots\ldots(2.34)$$

then equation (2.27) becomes

$$\cos\theta \frac{\partial I}{\partial \tau} - \frac{\sin\theta}{\tau}\frac{\partial I}{\partial \theta} = \frac{\epsilon\sigma T^4}{\pi} + \frac{(1-\epsilon)}{4\pi}\int I(\tau,\theta')\gamma(\tau,\theta',\theta)\,d\omega' - I. \qquad \ldots\ldots(2.35)$$

Let J denote the total intensity of radiation and F the total flux of radiation in the direction of increasing τ, then

$$J(\tau) = \int I\,d\omega = 2\pi\int_0^\pi I(\tau,\theta)\sin\theta\,d\theta, \qquad \ldots\ldots(2.36)$$

$$F(\tau) = \int I\cos\theta\,d\omega = 2\pi\int_0^\pi I(\tau,\theta)\sin\theta\cos\theta\,d\theta. \qquad \ldots\ldots(2.37)$$

We also define a quantity K by the relation

$$K(\tau) = \int I\cos^2\theta\,d\omega = 2\pi\int_0^\pi I(\tau,\theta)\sin\theta\cos^2\theta\,d\theta. \qquad \ldots\ldots(2.38)$$

Multiplying equation (2.35) by $d\omega$ and integrating over all directions, we have

$$\frac{dF}{d\tau} - \frac{1}{\tau}\int\frac{\partial I}{\partial\theta}\sin\theta\,d\omega = 4\epsilon\sigma T^4 + \frac{(1-\epsilon)}{4\pi}\int d\omega\int I(\tau,\theta')\gamma(\tau,\theta',\theta)\,d\omega' - J. \qquad \ldots\ldots(2.39)$$

Using (2.26)

$$\int d\omega\int I(\tau,\theta')\gamma(\tau,\theta',\theta)\,d\omega' = \int I(\tau,\theta')\,d\omega'\int\gamma(\tau,\theta',\theta)\,d\omega = 4\pi J. \qquad \ldots\ldots(2.40)$$

Also

$$\int\frac{\partial I}{\partial\theta}\sin\theta\,d\omega = 2\pi\int_0^\pi\frac{\partial I}{\partial\theta}\sin^2\theta\,d\theta - 2\pi\left[I\sin^2\theta\Big|_0^\pi - 2\int_0^\pi I\sin\theta\cos\theta\,d\theta\right] = -2F. \qquad \ldots\ldots(2.41)$$

Hence (2.39) becomes

$$dF/d\tau + 2F/\tau = \epsilon(4\sigma T^4 - J). \qquad \ldots\ldots(2.42)$$

Multiplying equation (2.35) by $\cos\theta\, d\omega$ and integrating again, we get

$$\frac{dK}{d\tau} - \frac{1}{\tau}\int \frac{\partial I}{\partial \theta}\sin\theta\cos\theta\, d\omega = \frac{(1-\epsilon)}{4\pi}\int \cos\theta\, d\omega \int I(\tau,\theta')\gamma(\tau,\theta',\theta)\, d\omega' - F. \quad \ldots\ldots(2.43)$$

Reversing the order of integration, we find

$$\int \cos\theta\, d\omega \int I(\tau,\theta')\gamma(\tau,\theta',\theta)\, d\omega' = \int I(\tau,\theta')\, d\omega' \int \gamma(\tau,\theta',\theta)\cos\theta\, d\omega. \quad \ldots\ldots(2.44)$$

Let ϕ denote the angle between $\mathbf{s}$ and $\mathbf{s}'$, and ψ the angle between the plane containing directions $\mathbf{s}'$ and $\mathbf{s}$ and the plane containing direction $\mathbf{s}'$ and the radius vector. Then we can put $d\omega = \sin\phi\, d\phi\, d\psi$, and since

$$\cos\theta = \cos\phi\cos\theta' + \sin\phi\sin\theta'\cos\psi,$$

we have

$$\begin{aligned}\int \gamma(\tau,\theta',\theta)\cos\theta\, d\omega &= \int_0^{\pi}\int_0^{2\pi} \gamma(\phi)(\cos\phi\cos\theta' + \sin\theta'\sin\phi\cos\psi)\sin\phi\, d\phi\, d\psi \\ &= -4\pi X\cos\theta', \quad \ldots\ldots(2.45)\end{aligned}$$

where X is a constant. $\gamma(\phi)$ is given by one of the relations (2.30), (2.31) or (2.32).

Integrating (2.45) we find $X=0$ for regular reflection or Rayleigh scattering, and $X=4/9$ for diffuse reflection.

We also have

$$\begin{aligned}\int \frac{\partial I}{\partial \theta}\sin\theta\cos\theta\, d\omega &= 2\pi\int_0^{\pi}\frac{\partial I}{\partial\theta}\sin^2\theta\cos\theta\, d\theta \\ &= 2\pi\left[I\sin^2\theta\cos\theta\Big|_0^{\pi} - \int_0^{\pi} I(3\sin\theta\cos^2\theta - \sin\theta)\, d\theta\right] = J - 3K. \quad \ldots\ldots(2.46)\end{aligned}$$

Now the mean value of $\cos^2\theta$ over the unit sphere is $\frac{1}{3}$. Hence we have, approximately,

$$K = \int I\cos^2\theta\, d\omega \simeq \overline{\cos^2\theta}\int I\, d\omega = \tfrac{1}{3}J. \quad \ldots\ldots(2.47)$$

This approximation is exact if I could be expanded in odd powers of $\cos\theta$. It is a well-known approximation (Eddington 1930) in the theory of radiative equilibrium. Hence (2.43) becomes

$$dK/d\tau = -F[X(1-\epsilon)+1]. \quad \ldots\ldots(2.48)$$

From (2.42), (2.47) and (2.48) we have a single differential equation for J, namely

$$\frac{d^2J}{d\tau^2} + \frac{2}{\tau}\frac{dJ}{d\tau} = 3\epsilon[X(1-\epsilon)+1][J - 4\sigma T^4]$$

or

$$d^2(J\tau)/d\tau^2 = \beta^2\tau(J - 4\sigma T^4), \quad \ldots\ldots(2.49)$$

if

$$\beta = \sqrt{\{3\epsilon[X(1-\epsilon)+1]\}}. \quad \ldots\ldots(2.50)$$

The solution is

$$J(\tau) = 4\sigma T^4 + \tau^{-1}(A\, e^{-\beta\tau}\beta\tau + B\, e^{-\beta\tau}\beta\tau), \quad \ldots\ldots(2.51)$$

where A and B are constants of integration.

Since J must remain finite near $\tau=0$ we must have

$$A + B = 0. \quad \ldots\ldots(2.52)$$

To find A, we observe that, at the boundary $I(\alpha R, \theta)=0$ for $\theta>\pi/2$. Hence

$$F(\alpha R)=2\pi\int_0^{\pi/2} I(\alpha R,\theta)\sin\theta\cos\theta\,d\theta, \qquad J(\alpha R)=2\pi\int_0^{\pi/2} I(\alpha R,\theta)\sin\theta\,d\theta.$$

Replacing $\cos\theta$ in the first integral by its mean value from 0 to $\pi/2$, we find

$$J(\alpha R)=2F(\alpha R). \qquad \ldots\ldots(2.53)$$

But from (2.48)

$$F(\alpha R)=-\frac{\epsilon}{\beta^2}\frac{dJ}{d\tau}\bigg|_{\tau=\alpha R}. \qquad \ldots\ldots(2.54)$$

Hence from (2.51), (2.53) and (2.54),

$$A=\frac{2\alpha RT^4}{\left[\frac{\epsilon}{\beta^2\alpha R}-\frac{\epsilon}{\beta}-\frac{1}{2}\right]\exp(\alpha\beta R)-\left[\frac{\epsilon}{\beta^2\alpha R}+\frac{\epsilon}{\beta}-\frac{1}{2}\right]\exp(-\alpha\beta R)}, \qquad \ldots\ldots(2.55)$$

and for the surface flux $F(\alpha R)=\sigma T^4 E_e(\alpha R)$ where

$$E_e(\alpha R)=\frac{4\epsilon\left[\left(1-\frac{1}{\beta\alpha R}\right)+\left(1+\frac{1}{\beta\alpha R}\right)\exp(-2\beta\alpha R)\right]}{\left[\beta+2\epsilon\left(1-\frac{1}{\beta\alpha R}\right)-\left(\beta-2\epsilon\left[1+\frac{1}{\beta\alpha R}\right]\right)\exp(-2\beta\alpha R)\right]}. \qquad \ldots\ldots(2.56)$$

Since the surface flux would be σT^4 if the boundary were replaced by a black body, $E_e(\alpha R)$ represents the effective emissivity. It is clearly a generalization of the formula (2.11) for $E(\alpha R)$ to the case when $\epsilon<1$.

Consider the value of $E_e(\alpha R)$ for $\epsilon=1$ and αR large, i.e. condition E satisfied. We find

$$E_e(\infty)=4\epsilon/(\beta+2\epsilon). \qquad \ldots\ldots(2.57)$$

Since $\beta=\sqrt{(3\epsilon)}$ it follows that $E_1(\infty)=1{\cdot}072$; the correct value is, of course, 1. This shows that our approximation is quite close, and suggests that we write, for the effective emissivity, ϵ_e'

$$\epsilon_e'(\alpha R)=0{\cdot}93E_e(\alpha R), \qquad \ldots\ldots(2.58)$$

instead of the quantity $E_e(\alpha R)$ defined by equation (2.56).

The following special cases of formula (2.56) are of interest.

1. For $\epsilon=1$ we should have, from formulae (2.58) and (2.57) $\epsilon_1'(\alpha R)=E(\alpha R)$. In Figure 2, curves 1 and 2 show how these quantities compare. Curve 1 is, of course, exact, and the two curves differ because of the approximations (2.47) and (2.53) which have been introduced to obtain expression (2.56). It will be seen that curve 2 lies just below 1 for most of the range. If $E_e(\alpha R)$ were plotted it would almost lie on curve 1 except near the origin. The curves show that the approximation (2.58) is only a few per cent out.

2. Suppose E is satisfied, that is αR is large. Then for uniform and Rayleigh scattering

$$\epsilon_e'(\infty)=3{\cdot}72\sqrt{\epsilon}/(2\sqrt{\epsilon}+\sqrt{3}). \qquad \ldots\ldots(2.59)$$

For diffuse reflection

$$\epsilon_e'(\infty)=\frac{3{\cdot}72\sqrt{\epsilon}}{2\sqrt{\epsilon}+\sqrt{\{(13-4\epsilon)/3\}}}. \qquad \ldots\ldots(2.60)$$

Figure 3 shows how these expressions depend upon ϵ.

When E is satisfied, higher degrees of approximation are possible and $\epsilon_e'(\infty)$ is better expressed by

$$\epsilon_e'(\infty)=1-\frac{2(1-\epsilon)}{2\epsilon+\sqrt{(3\epsilon)}}\left[1-\frac{\ln\{1+\sqrt{(3\epsilon)}\}}{\sqrt{(3\epsilon)}}\right]. \quad \ldots\ldots(2.61)$$

This approximation gives $\epsilon'=1$ when $\epsilon=1$; it is almost indistinguishable from (2.59) in Figure 3. This expression is derived in Appendix II.

3. When αR is small, that is, the cloud is in state "E′", $E_e(\alpha R)=4\epsilon\alpha R/3$ and

$$H=4\pi a^2 N_0 \epsilon\sigma T^4. \quad \ldots\ldots(2.62)$$

As we should expect physically, the radiation is simply the total radiation emitted by each of the particles.

The dependence of ϵ' upon a for a cloud of given size and mass is seen in Figure 2, which is plotted for a cloud of aluminium oxide particles. The curves show several points of interest. There is not very much difference between the curves for diffuse and uniform scattering—the latter lying slightly above the former. For different values of ϵ, the curves are of the same general shape, but reduced in scale along both the y and x directions. From the shape it will be seen that the radiation is sensitive to a, the particle size, over a fairly restricted range. For $\epsilon=1$ this range is approximately 10^{-3} to 6×10^{-3} cm. When $\epsilon=0{\cdot}1$ and $0{\cdot}01$ the corresponding ranges are 5×10^{-4} to 2×10^{-3} cm. and 10^{-3} to 3×10^{-4} cm. respectively.

2.3. *Radiation from a Cloud of Particles in the Form of a Spherical Shell*

Suppose now that N is constant within the spherical shell of bounding radii R' and R but that there is no matter within the sphere of radius R'. The whole of the analysis of the radiation within the uniform sphere given above applies to the radiation within the shell, except the boundary condition (2.52). This is replaced by a boundary condition at $r=R'$. Since there is no matter inside the sphere of radius R', there can be no net flow of radiation outwards across the surface. Hence, by symmetry,

$$F(\alpha R')=0. \quad \ldots\ldots(2.63)$$

The formulae for the effective emissivity corresponding to equation (2.56) is

$$\begin{aligned}\epsilon_e'(\alpha,R,R')=1{\cdot}86\Bigg[1-\beta\Bigg\{&\beta+2\epsilon\left[1-\frac{1}{\alpha\beta R}\right]\\&+[\exp\{-2\alpha\beta(R-R')\}]\left[\frac{\alpha\beta R'-1}{\alpha\beta R'+1}\right]\left[\beta-2\epsilon\left(1+\frac{1}{\alpha\beta R}\right)\right]\Bigg\}^{-1}\\&-\beta\Bigg\{\beta-2\epsilon\left[1+\frac{1}{\alpha\beta R}\right]\\&+[\exp\{2\alpha\beta(R-R')\}]\left[\frac{\alpha\beta R'+1}{\alpha\beta R'-1}\right]\left[\beta+2\epsilon\left(1-\frac{1}{\alpha\beta R}\right)\right]\Bigg\}^{-1}\Bigg].\end{aligned}$$

$\ldots\ldots(2.64)$

When $R'=0$, it is easy to verify that (2.64) gives formula (2.58).

Suppose $\alpha(R-R')$ is large. Then *a fortiori* αR is large and we find (2.64) gives (2.59) or (2.60) for the effective emissivity. For αR small we again obtain formula (2.62). If α is fixed, as $R'\to R$, $\epsilon_e'(\alpha,R,R')\to0$. But suppose we fix a and the total mass of material in the cloud but vary R'. As R' increases, the

material is compressed more and more into a thin shell between radii R' and R. In fact, if α_0 is the value of α when $R=0$ the value of α in the general case is

$$\alpha=\alpha_0 R^3/(R^3-R'^3). \qquad \ldots\ldots(2.65)$$

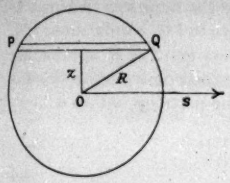

Figure 1.

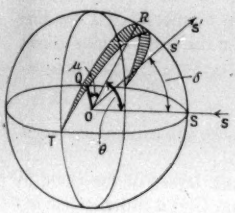

Figure 5.

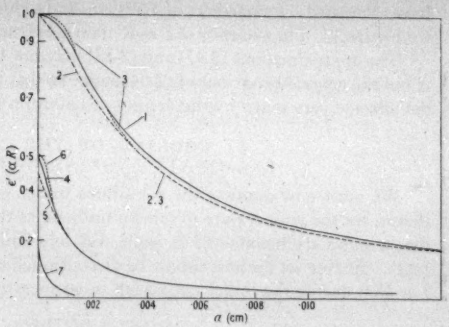

Figure 2. Variation of effective emissivity with particle radius. $M=3{\cdot}7$ gm. $R=1$ ft. 1, $\epsilon=1$, exact formula (2.13); 2, $\epsilon=1$, approximate formula (2.58); 3, $\epsilon=1$, uniform scattering, uniform distribution in thin spherical shell, formula (2.66); 4, $\epsilon=0{\cdot}1$, uniform scattering, formula (2.58); 5, $\epsilon=0{\cdot}1$, diffuse scattering (2.58); 6, $\epsilon=0{\cdot}1$, uniform scattering, thin shell (2.66); 7, $\epsilon=0{\cdot}01$, uniform scattering (2.58).

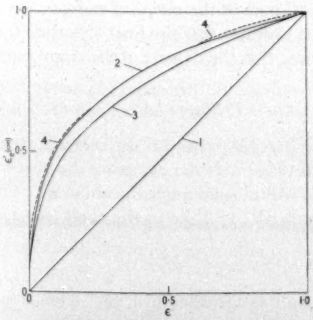

Figure 3. Variation of effective emissivity ϵ' with ϵ (clouds in E state). 1, $\epsilon=\epsilon$; 2, uniform scattering, first approximation (2.59); 3, diffuse scattering, first approximation (2.60); 4, uniform scattering, second approximation (2.61).

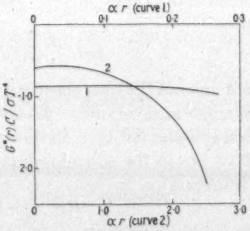

Figure 4. Dependence upon αR of temperature distribution when cloud is cooling. Curve 1, $\alpha R=0{\cdot}3$. Curve 2, $\alpha R=3$.

In the limiting case $R'\to R$ we find $\alpha\beta R=\alpha\beta R'\to\infty$; $\exp\{-2\alpha\beta(R-R')\}\to\exp\{-2\alpha_0\beta R/3\}$. Hence the effective emissivity of a thin spherical shell is given by

$$\epsilon_e'(\alpha,R,R')=\frac{3{\cdot}72\epsilon(1-\exp\{-2\alpha_0\beta R/3\})}{\beta+2\epsilon+(\beta-2\epsilon)\exp\{-2\alpha_0\beta R/3\}}. \qquad \ldots\ldots(2.66)$$

In Figure 2 we have plotted this expression against the particle size for $\epsilon = 1$ and 0·1 and regular scattering. The emissivity is not markedly different from that of the uniform spherical distribution. This rather surprising indifference of ϵ' to the distribution law is also shown by calculating $\epsilon_1'(\alpha, R, R')$ as a function of R'. We have calculated ϵ' for particles of 0·004 cm. and a cloud of the same size and mass as for Figure 2. The variation of ϵ' as R' increases from zero to 1 ft. is only about 1%.

The approximations (2.47) and (2.53) may not be very good as R' approaches R but the general behaviour of (2.64) suggests that the radiation from the cloud is not affected very much by the density distribution of the particles within it.

§3. COOLING OF THE CLOUD. EXAMINATION OF ASSUMPTION (1)

We must now examine the conditions under which assumption (1) is valid; that is, for the temperature to remain uniform as the cloud cools. Suppose that the particles are maintained in some way at a uniform temperature T for time $t<t'$. At $t=t'$ let the heat supply be discontinued so that the cloud begins to cool. Let $G(r)$ denote the initial rate of fall in temperature.

$$G(r) = -\partial T(r)/\partial t|_{t'}. \qquad \ldots\ldots(3.1)$$

The condition that the temperature remains uniform in the subsequent cooling is, clearly, that $G(r)$ is independent of r.

Heat may be transferred from the inner to the outer layers of the cloud by radiation, conduction or convection. The condition that $G(r)$ is independent of r will, in each of the three cases, impose restrictions on the physical quantities involved. We first consider the transfer of heat by radiation.

The total loss of heat from a spherical part of the cloud of radius r equals the amount of heat emitted from the portion radius r, less the heat absorbed from the outer shell of thickness $(R-r)$. Assuming that the density of the cloud is uniform this gives

$$4\pi C\int_0^r G(r)r^2\,dr = 4\pi r^2\sigma T^4 E(\alpha r) - A, \qquad \ldots\ldots(3.2)$$

where A denotes the heat absorbed from part $(R-r)$ and C the thermal capacity of the cloud per unit volume. To estimate A we consider as before the heat transfer in a thin cylinder SP′Q′T, in directions within solid angle $d\omega$ about **s**. The portion P′Q′ lies in the sphere radius r, and SP′, Q′T lie in the shell $(R-r)$. We have from (2.6)

$$I(\mathrm{P}', \mathbf{s}) = (\sigma T^4/\pi)\{1-\exp(-\alpha \mathrm{SP}')\}. \qquad \ldots\ldots(3.3)$$

A fraction $1-\exp(-\alpha \mathrm{P}'\mathrm{Q}')$ of this light is absorbed in P′Q′. Hence the total amount of light absorbed by the inner sphere from the outer shell is

$$A = 8\pi\sigma T^4\int_0^R [1-\exp(-\alpha \mathrm{SP}')][1-\exp(-\alpha \mathrm{P}'\mathrm{Q}')]z\,dz, \qquad \ldots\ldots(3.4)$$

where z is the distance of P′Q′ from the axis. The integral cannot be evaluated, but the maximum value of SP is $(R^2-r^2)^{\frac{1}{2}}$ and the minimum value is $(R-r)$. Hence it follows that the heat absorbed lies between the quantities

$$8\pi\sigma T^4[1-\exp\{-\alpha(R-r)\}]\int_0^r z[1-\exp\{-2\alpha(r^2-z^2)^{\frac{1}{2}}\}]\,dz$$

and

$$8\pi\sigma T^4[1-\exp\{-\alpha(R^2-r^2)^{\frac{1}{2}}\}]\int_0^r z[1-\exp\{-2\alpha(r^2-z^2)^{\frac{1}{2}}\}]\,dz$$

or

$$4\pi\sigma T^4 r^2 E(\alpha r)[1-\exp\{-\alpha(R-r)\}] < A < 4\pi\sigma T^4 r^2 E(\alpha r)[1-\exp\{-\alpha(R^2-r^2)^{\frac{1}{2}}\}]. \quad \ldots\ldots(3.5)$$

Substituting the value of A given by equation (3.2) we find

$$r^2 E(\alpha r)\exp\{-\alpha(R^2-r^2)^{\frac{1}{2}}\} < \frac{CG}{\sigma T^4}\int_0^r G(r) r^2\, dr < r^2 E(\alpha r)\exp\{-\alpha(R-r)\}. \quad \ldots\ldots(3.6)$$

If $G(r)=G$, where G is independent of r, we must have, for all values of r,

$$r^{-1}E(\alpha r)\exp\{-\alpha(R^2-r^2)^{\frac{1}{2}}\} < CG/3\sigma T^4 < r^{-1}E(\alpha r)\exp\{-\alpha(R-r)\}. \quad \ldots\ldots(3.7)$$

The two outer limits $r\to 0$ and $r\to R$ must converge, hence the condition that $G(r)$ is independent of r is

$$\operatorname*{Lt}_{r\to 0} r^{-1}E(\alpha r)\exp\{-\alpha(R-r)\} = \operatorname*{Lt}_{r\to R} r^{-1}E(\alpha r)\exp\{-\alpha(R-r)\}. \quad \ldots\ldots(3.8)$$

From (2.13) $\operatorname*{Lt}_{r\to 0} r^{-1}E(\alpha r) = 4\alpha/3$. Hence (3.8) becomes

$$4\alpha R/3 = \exp(\alpha R)E(\alpha R). \quad \ldots\ldots(3.9)$$

Now from equation (2.13) for $E(x)$ we have

$$4\alpha R/3 - \exp(\alpha R)E(\alpha R) = -\sum_2^\infty a_n(\alpha R)^n, \quad \ldots\ldots(3.10)$$

where $a_n=[(n+3)(n+1)]/(n+2)!$, n odd, and $a_n=n/(n+1)!$, n even. Hence, since all the coefficients a_n are greater than 0, condition (3.10) is only satisfied if

$$\alpha R \ll 1, \quad \ldots\ldots(3.11)$$

that is, if condition E′ holds. This is the reverse of E, the condition found for the radiation to be equivalent to that of a solid back-body radiator.

Unfortunately relation (3.6) cannot tell us much about the behaviour of $G(r)$ since it does not follow that

$$\frac{d}{dr}[r^2 E(\alpha r)\exp\{-\alpha(R^2-r^2)^{\frac{1}{2}}\}] < \frac{Cr^2}{\sigma T^4}G(r) < \frac{d}{dr}[r^2 E(\alpha r)\exp\{-\alpha(R-r)\}]. \quad \ldots\ldots(3.12)$$

In view of equation (3.6), however, and the fact that the above relation is certainly true near $r=0$, it seems reasonable to suppose that the quantity

$$G^*(r) = \frac{\sigma T^4}{2Cr^2}\frac{d}{dr}r^2 E(\alpha r)[\exp\{-\alpha(R-r)\}+\exp\{-\alpha(R^2-r^2)^{\frac{1}{2}}\}], \quad \ldots\ldots(3.13)$$

gives a good approximation to the behaviour of $G(r)$.

In Figure 4, $G^*(r)$ is plotted as a function of r for the two cases $\alpha R=0{\cdot}3$ and $\alpha R=3$. It will be seen that in the first case G^* is very nearly uniform but this is by no means correct for $\alpha R=3$. It is easy to visualize the physical mechanism in cases $\alpha R\gg 1$. Strictly each part of the material radiates the same amount of energy but most of the energy is re-absorbed except near the surface where it can escape into outer space. Hence the temperature of the outer part is lower than that of the interior. The same general considerations will obviously apply to particles for which ϵ is less than 1.

We must now examine the possibility of the temperature being maintained uniform in state E by conduction of heat. Suppose heat is lost from the surface

of the cloud by radiation only, whereas inside it is transferred by conduction only. Let k be the thermal conductivity of the gas occupying the space between the particles. If H is the energy radiated by the cloud in unit time

$$H = -4\pi kR^2(\partial T/\partial r)|_R. \qquad \ldots\ldots(3.14)$$

But

$$H = -4\pi \int_0^R C\frac{\partial T}{\partial t} r^2\, dr. \qquad \ldots\ldots(3.15)$$

If the temperature is nearly uniform, we may replace the second integral by

$$4\pi C\frac{\overline{\partial T}}{\partial t}\int_0^R r^2\, dr = \frac{4\pi R^3}{3} C\frac{\overline{\partial T}}{\partial t}, \qquad \ldots\ldots(3.16)$$

where $\overline{\partial T/\partial t}$ represents the mean value of $\partial T/\partial t$. But we also have

$$kr^2\frac{\partial T}{\partial r} = \int_0^r C\frac{\partial T}{\partial t} r^2\, dr \quad \text{or} \quad k\frac{\partial T}{\partial r} = C\frac{\overline{\partial T}}{\partial t}\frac{r}{3}. \qquad \ldots\ldots(3.17)$$

Integrating, we find

$$T(R) - T(0) = (CR^2/6k)(\overline{\partial T/\partial t}) = H/8\pi kR. \qquad \ldots\ldots(3.18)$$

For $R = 1$ ft. and $T = 2700°$ K. and a temperature difference of 100° C. between the centre and surface of the cloud we should require $k \simeq 1$ C.G.S. units.

At $T \sim 2700°$ K., k for air is about 4×10^{-4} C.G.S. unit; thus it appears that the thermal conductivity is much too low to maintain uniform temperature.

There remains transport of heat by convection or turbulence; this is difficult to deal with quantitatively. But it seems possible that this factor is quite important in view of the high temperatures involved.

Hence we conclude that E′ is a necessary condition for the temperature of the cloud to remain uniform if it were so initially, unless the temperature is maintained uniform by convection.

§4. DISCUSSION

Summarizing our results, we find:

(i) If the transfer of heat by convection may be ignored, uniform temperature during cooling requires condition E′. When this condition is not satisfied, the cloud is cooler near the surface than in the interior.

(ii) When the temperature is uniform and $\epsilon = 1$, the cloud is equivalent to a solid black body if E holds. Whether or not E is satisfied for ϵ less than 1 the total radiation lies between the value it would have if ϵ equalled 1, and this value multiplied by ϵ. In other words, if ϵ' is the effective emissivity $\epsilon < \epsilon' < 1$.

Now let us consider the bearing of these results on Caldin's theory. If transfer of heat by convection is important it follows that this method is legitimate provided that the appropriate expression for the effective emissivity is employed. On the other hand, if transfer of heat takes place through radiation only, it would seem at first sight that our results show that it would be impossible to apply Caldin's theory to transient light sources, for this theory assumes uniform temperatures—which requires condition E′—and yet assumes E and that $\epsilon = \epsilon'$ in the determination of the heat radiated. But one or the other of E and E′ may be satisfied, not both simultaneously. This is a little too drastic however; for if E′ is satisfied, the theory is still valid provided that for the effective emissivity ϵ' of the radiator we use *not* the ordinary solid surface emissivity ϵ, but the expression

$$\epsilon' = 3M\epsilon/4\pi R^3 a\rho_0. \qquad \ldots\ldots(4.1)$$

This follows from equation (2.16).

Condition E′ imposes a lower limit on the particle size—for example, with a cloud of radius one foot containing 4 grammes of magnesium oxide we require $a \gg 2{\cdot}0 \times 10^{-3}$ cm. Magnesium metal burning in air gives small cubic crystals of the oxide with side lengths from 10^{-5} to 10^{-4} cm., so that in this case E′ is apparently not satisfied. But experimental evidence must decide the state of the cloud in each particular case.

It is of interest, however, to consider some of the consequences if, both in the formation of the cloud and its subsequent cooling, the cloud is cooler near the surface than in the interior. A necessary condition for this state of affairs would be the non-fulfilment of condition E′. The amount of radiation given off is determined mainly by the temperature of the surface layers. For, owing to absorption, the fraction of the emitted radiation which escapes to outer space decreases as we move from surface to centre; defining the effective temperature T_e of the cloud by the equation

$$F(0) = \sigma T_e^4, \qquad \ldots\ldots(4.2)$$

then $T_e < \overline{T}$.

In certain cases it is possible to find the effective temperature in terms of the temperatures in the interior and at the surface. For, assume E and that $\epsilon = 1$; then equation (2.3) gives the intensity. Suppose the temperature, instead of being constant is given by

$$T^4(\tau) = T_0^4[1 - \mu \exp(-\tau/\tau_0)]. \qquad \ldots\ldots(4.3)$$

This would represent a temperature distribution like that of Figure 4, curve 2, in general shape—nearly uniform temperature in the interior surrounded by a cooler layer. τ_0 is a rough measure of the thickness of this layer. The surface temperature will be

$$T_s = T_0(1-\mu)^{\frac{1}{4}} \qquad \ldots\ldots(4.4)$$

if T_0 is the temperature of the interior. The equation for I is

$$\cos\theta\, \partial I(\tau,\theta)/\partial\tau = I(\tau,\theta) - (\sigma T_0^4/\pi)[1 - \mu\exp(-\tau/\tau_0)]. \qquad \ldots\ldots(4.5)$$

Integrating, for $\theta < \pi/2$,

$$I(0,\theta) = (\sigma T_0^4/\pi)[1 - \mu\tau_0/(\tau_0 + \cos\theta)]. \qquad \ldots\ldots(4.6)$$

Hence

$$F(0) = \sigma T_e^4 = 2\pi \int_0^{\pi/2} I(0,\theta)\sin\theta\cos\theta\, d\theta,$$

$$= \sigma T_0^4[1 - 2\mu\tau_0\{1 - \tau_0 \ln(1+\tau_0)/\tau_0\}]. \qquad \ldots\ldots(4.7)$$

For $\tau_0 \gg 1$, that is for large optical depth of the cool layer, $T_e = T_s$, and for $\tau_0 \ll 1$, or for small optical depth of the cool layer, $T_e = T_0$. From Figure 4, curve 2, we should expect in practice $\tau_0 \sim 1$, i.e. from (4.7)

$$T_e^4 \simeq 0{\cdot}39\, T_0^4 + 0{\cdot}61\, T_s^4. \qquad \ldots\ldots(4.8)$$

This result still holds even if the cool layer is so thin, compared with the radius of the cloud, that the mean temperature is effectively T_0.

Conditions E and E′ have a bearing upon the efficiency of transient light sources. Consider two clouds initially at the same uniform temperature, and of the same thermal capacity, one of which, S, satisfies E, the other, S′, E′. Let us also

assume that in S convection is not sufficient to maintain uniform temperature. After a long time both will have ultimately lost all their heat to the surroundings. But whereas S′ cools with uniform temperature, S has a cool outer layer and so its radiation escapes more slowly, and at a lower effective temperature than S. In the temperature range which we are concerned, the ratio of the quantity of light energy to total energy in the black body spectrum increases as the temperature increases. Hence, although S and S′ ultimately lose the same amount of energy, a greater fraction escapes as light in S′ than in S. Thus the efficiency of a cloud as a source of light increases as we pass from state E to state E′.

Another consequence of the cool outer layer is that the emergent radiation will not be black-body radiation for states E. When E is satisfied the intensity of radiation of wavelength λ emerging at θ is

$$I_\lambda(0,\theta)=\frac{2hc^2}{\lambda^5}\int_0^\infty \frac{\exp(-\tau\sec\theta)}{\exp(hc/\lambda kT)-1}\sec\theta\,d\tau. \qquad \ldots\ldots(4.9)$$

This will not necessarily correspond to the Planck distribution at temperature T_e since T in the integrand is a function of τ. The energy distribution of (4.9) for *radiative equilibrium* has been studied by Milne (1900). In this case the spectrum of the total flux corresponds to a temperature 4% higher than T_e. The spectral distribution is slightly bluer than black-body radiation for the effective temperature T_e. The deviation from the Planck formula is so slight that it is of little importance in astrophysics. It seems reasonable to conclude that the same applies to light sources.

§ 5. EXACT THEORY OF COOLING

In view of the limitation on Caldin's method it is natural to enquire if a more exact theory is possible in which account is taken of variations of temperature in the light source. The above analysis suggests various possible approximations; for example we might use equation (4.8) to give the radiation lost in unit time assuming $T_s=0$. It is quite easy, however, to set up an exact formal theory of cooling but the equation must eventually be solved numerically.

Consider how the fundamental equation (2.27) is modified, if, instead of being maintained at constant temperature the material cools by radiation. The only change in the equation is that T, instead of being constant, is a function of r. We have, also, an additional equation determining the rate of change of temperature at any point.

For a single particle the total radiation absorbed from a beam of intensity I in directions within solid angle $d\omega$ about directions $\mathbf{s}$ in unit time is $\epsilon\pi a^2 I d\omega$. Integrating over all directions this becomes $\epsilon\pi a^2 J$. The amount of energy radiated if T is the temperature is $4\pi a^2\epsilon\sigma T^4$, hence the equation to determine T is

$$\frac{4\pi a^3\rho_0 h}{3}\frac{\partial T}{\partial t}=\epsilon\pi a^2 J-4\pi a^2\epsilon\sigma T^4 \quad \text{or} \quad \frac{4a\rho_0 h}{3}\frac{\partial T}{\partial t}=\epsilon(J-4\sigma T^4), \qquad \ldots\ldots(5.1)$$

where h is the specific heat of the solid material.

If we assume a uniform density distribution, (2.27) becomes (2.35). The temperature and radiation intensity are determined for all t and r from equations (5.1) and (2.35) provided the initial and boundary conditions are known. (5.1) and (2.35) cannot be solved exactly. The only feasible method seems to be to retain (2.35) unmodified, but to replace (5.1) by a difference equation.

Suppose we know T as a function of r at $t=0$. Then, solving (2.35) we can determine I and so J at $t=0$. Suppose Δt is a small time interval, so small that J and T are not changed very much at the end of it. Then if ΔT denotes the small change in T in intervals Δt, we have from (5.1)

$$\Delta T=(J-4\sigma T^4)3\Delta t/4a\pi\rho_0 h. \qquad \ldots\ldots(5.2)$$

Hence T is known at $t=\Delta t$ and, from (2.35), I and J. From (5.1) we can find T at $2\Delta t$ and so on. Any desired degree of accuracy is obtainable by making the interval Δt sufficiently small, but the process becomes more tedious with smaller intervals.

It only remains to express the solution of (2.35) in a suitable form, when T is given as an arbitrary function of τ. Using the method of §2, (2.35) becomes

$$d^2(J\tau)/d\tau^2=\beta\tau^2(J-4\sigma T^4), \qquad \ldots\ldots(5.3)$$

since equation (2.49) is still true if T is an arbitrary function of τ.

Writing
$$J(\tau)=\beta\exp(\beta\tau)\int_0^\tau L\,d\tau, \qquad \ldots\ldots(5.4)$$

(5.3) becomes
$$(dL/d\tau)+2\beta L+4\beta\sigma T^4\tau\exp(-\beta\tau)=0. \qquad \ldots\ldots(5.5)$$

Integration gives

$$L(\tau)=L(0)\exp(-2\beta\tau)-4\beta\sigma\exp(-2\beta\tau)\int_0^\tau xT^4(x)\exp(\beta x)\,dx, \qquad \ldots\ldots(5.6)$$

and for J

$$J(\tau)=A\exp(\beta\tau)+B\exp(-\beta\tau)-4\beta\sigma\exp(\beta\tau)\int_0^\tau\exp(-2\beta z)\,dz\int_0^z xT^4(x)\exp(\beta x)\,dx. \qquad \ldots\ldots(5.7)$$

A and B are determined by the boundary condition at $r=0$ and $r=R$, namely $F=0$ when $\tau=0$, $F=2J$ when $\tau=\pi a^2NR$. The total radiation from the sphere is

$$H=8\pi R^2J(R). \qquad \ldots\ldots(5.8)$$

There is no point in making any calculations by the above method until more is known about the size of the particles.

APPENDIX I

(a) *Law of scattering for particles with a perfectly reflecting surface*

Let the angle the radius vector to any point on the surface makes with **s** be θ. The particle is placed in the path of a parallel beam and we require the amount of light scattered into $d\omega$ about **s** when the surface scatters light according to the law of reflection. Clearly all the light which meets the surface between radii whose angles θ lie between $\phi/2$ and $\phi/2+d\phi/2$ is scattered into directions **s** between angles ϕ and $\phi+d\phi$.

Hence, using the definition (2.25) of $\gamma(\mathrm{P},\mathbf{s}',\mathbf{s})$, we have

$$(1/4\pi)\gamma(\mathrm{P},\mathbf{s}',\mathbf{s})2\pi\sin\phi\,d\phi=(\sin^2(\phi+d\phi)/2-\sin^2\phi/2). \qquad \ldots\ldots(6.1)$$

Hence
$$\gamma(\mathrm{P},\mathbf{s}',\mathbf{s})=1, \qquad \ldots\ldots(6.2)$$

and the scattering is uniform.

(b) *Law of scattering for particles with a diffusely reflecting surface*

Let OT (Figure 5) be normal to the plane containing **s** and **s**′. OR lies in the plane containing **s**, **s**′ and OQ lies in the plane containing OT and OR.

All the points T, Q and R lie on the surface. Put $\angle ROS=\theta$, $\angle SOS=\delta$, $\angle ROQ=\mu$. Let ψ_1, ψ_2 be the angles between the normal at Q and the directions **s** and **s'**. Now the element of area at Q is $a^2\cos\mu\,d\mu\,d\theta$.

If I is the intensity of the incident light in directions in $d\omega$ about **s**, the amount of light falling on this area at Q is $I\cos\psi_1\,d\omega a^2\cos\mu\,d\mu\,d\theta$. By Lambert's law of diffuse reflection, the amount of light scattered into directions $d\omega'$ about **s'** is

$$\pi^{-1}d\omega'\cos\psi_2 I\cos\psi_1\,d\omega a^2\cos\mu\,d\mu\,d\theta.$$

But $\cos\psi_1=\cos\mu\cos\theta$, $\cos\psi_2=\cos\mu\cos(\theta-\delta)$. Hence the above expression becomes $\pi^{-1}\,d\omega\,d\omega' a^2 I\cos^3\mu\cos\theta\cos(\theta-\delta)\,d\mu\,d\theta$. Hence

$$\frac{1}{4\pi}\gamma(\mathrm{P},\mathbf{s}',\mathbf{s})=\frac{1}{\pi^2}\int_{\varphi-\pi/2}^{\pi/2}\int_{-\pi/2}^{\pi/2}\cos^3\mu\cos\theta\cos(\theta-\delta)\,d\theta\,d\mu$$

$$=\frac{2}{3\pi^2}[(\pi-\delta)\cos\delta+\sin\delta]. \qquad \ldots\ldots(6.3)$$

If we put ϕ equal to the angel between directions **s** and **s**, i.e. $\phi=\pi-\delta$, then we have finally from (6.3)

$$\gamma(\mathrm{P},\mathbf{s}',\mathbf{s})=(8/3\pi)(\sin\phi-\phi\cos\phi). \qquad \ldots\ldots(6.4)$$

APPENDIX II

Calculation of the higher approximation to ϵ for the case when E *is satisfied*

When $\epsilon=1$ we have from (2.8)

$$I(\mathrm{S},\mathbf{s})=(\sigma T^4/\pi)[1-\exp(-\alpha\mathrm{PS})] \qquad \ldots\ldots(7.1)$$

if P is the point where direction $-\mathbf{s}$ through S cuts the surface of the envelope of the cloud. If condition E holds, αPS is large except when PS$\ll R$. Hence I is uniform and of magnitude $\sigma T^4/\pi$ except in a thin layer near the surface of the sphere. At the surface I cannot be uniform; for when $\theta>\pi/2$, $I=0$. As the thickness of this layer is reduced, conditions near the surface clearly approximate more and more to those of a plane surface. Hence with E satisfied, the second term of (2.33) is small compared with the first and

$$\partial I/\partial s=\cos\theta(\partial I/\partial r). \qquad \ldots\ldots(7.2)$$

The same kind of behaviour is to be expected for the case $\epsilon<1$. Hence (2.27) becomes

$$\cos\theta\frac{\partial I(r,\theta)}{\partial r}=\pi a^2 N\left[\frac{\epsilon\sigma T^4}{\pi}-I(r,\theta)+\frac{(1-\epsilon)}{4\pi}\int I(r,\theta')\gamma(r,\theta',\theta)\,d\omega\right], \qquad \ldots\ldots(7.3)$$

or if

$$\tau=\pi a^2\int_R N\,dr, \qquad \ldots\ldots(7.4)$$

$$\cos\theta\frac{\partial I(\tau,\theta)}{\partial\tau}=I(\tau,\theta)-\frac{(1-\epsilon)}{4\pi}\int I(\tau,\theta')\gamma(\tau,\theta',\theta)\,d\omega'-\frac{\epsilon\sigma T^4}{\pi}. \qquad \ldots\ldots(7.5)$$

When $\tau=0$, $r=R$ and from (7.4), τ is large for points in the interior of the cloud not near the surface.

An *exact* solution of (7.5) is possible only for the case $\gamma(r,\theta',\theta)=1$, that is, for scattering by specular reflection. Equation (7.5) can then be transformed into an integral equation which is very similar to the fundamental integral equation of

the theory of radiative equilibrium developed by Schwarzschild and others for astrophysical purposes (Milne 1928, Titchmarsh 1937). The solution is complicated, however, and requires extensive computations (Lindblad 1923).

The method of § 2 can, however, be applied (with only slight modifications) to obtain a first approximation for ϵ'. From this approximation it is possible to calculate a second approximation in the case $\gamma = 1$. The method cannot be applied to the more general equation (2.35). For J, the first approximation is

$$J(\tau) = 4\sigma T^4 + B\exp(-\beta\tau), \qquad \ldots\ldots(7.6)$$

where β is given by (2.50) and

$$B = -4\sigma T^4/(1 + 2\epsilon/\beta). \qquad \ldots\ldots(7.7)$$

Substituting expression (7.6) for J in (7.5) the equation for I is

$$\cos\theta\frac{\partial I}{\partial\tau} = I - \frac{\sigma T^4}{\pi} - B\frac{(1-\epsilon)}{4\pi}\exp(-\beta\tau). \qquad \ldots\ldots(7.8)$$

Integrating with respect to τ from 0 to ∞,

$$I(0,\theta) = \frac{\sigma T^4}{\pi} + \frac{B(1-\epsilon)}{4\pi(1+\beta\cos\theta)} \quad \text{if } \theta < \pi/2. \qquad \ldots\ldots(7.9)$$

Hence

$$F(0) = 2\pi\int_0^{\pi/2} I(0,\theta)\sin\theta\cos\theta\, d\theta = \sigma T^4\left[1 - \frac{2(1-\epsilon)}{\beta+2\epsilon}\left\{1 - \frac{\ln(1+\beta)}{\beta}\right\}\right]. \qquad \ldots\ldots(7.10)$$

It follows that if we denote the second approximation to ϵ' by $[\epsilon_0'(\tau)]_{II}$

$$[\epsilon_0'(\infty)]_{II} = 1 - \frac{2(1-\epsilon)}{2\epsilon + \sqrt{(3\epsilon)}}\left[1 - \frac{\ln\{1+\sqrt{(3\epsilon)}\}}{\sqrt{(3\epsilon)}}\right]. \qquad \ldots\ldots(7.11)$$

For $\epsilon = 1$ we find $[\epsilon_1'(\infty)]_{II} = 1$.

In Figure 2 the first and second approximations are plotted. It will be seen that there is very close agreement between the two, suggesting that (2.59) and (2.60) are very near to the correct values. For diffuse scattering the method fails unless further approximations are introduced. It is interesting to note that a more sophisticated method of obtaining successive approximations to the solution of the fundamental equation of radiative equilibrium, which has been developed recently by Chandrasekhar (1944), could also be applied to equation (7.5). Since, however, it is not our aim to obtain very exact estimates of ϵ we shall not pursue the matter further.

ACKNOWLEDGMENT

The calculations given above are based upon work done in the Theoretical Research Section of the Armament Research Department, Ministry of Supply. The writer wishes to thank the Chief Scientist, Ministry of Supply, for permission to publish this paper.

REFERENCES

Caldin, E. F., 1946a, *Proc. Phys. Soc.*, **58**, 342; 1946b, *Ibid.*, **58**, 350.
Chandrasekhar, S., 1944, *Astrophys. J.*, **99**, 180; **100**, 76, 117.
Eddington, A. S., 1930, *The Internal Constitution of the Stars* (Cambridge: University Press), p. 322.
Lindblad, B., 1923, *Nova Acta R. Soc. Upsala*, Ser. 4, **6**, No. 1.
Milne, E. A., 1928, *Handbuch der Astrophysik*, Band III/1, Chapter 2, p. 111, equation (63).
Titchmarsh, E. C., 1937, *Theory of Fourier Integrals* (Oxford: Clarendon Press), p. 344.

On the Schumann-Runge O_2 Bands emitted at Atmospheric Pressure

By M. W. FEAST

Imperial College of Science and Technology, London

MS. received 26*th May* 1948

ABSTRACT. The Schumann-Runge bands of O_2, previously analysed in the region 3100–4200 A. and photographed below 3100 A. under small dispersion, with only a tentative analysis, have been obtained from 2000 A. to 5000 A. on sufficient dispersion for the vibrational analysis to be extended and for the rotational structure to be clearly resolved. Conditions for their emission are discussed and the probable process, involving dissociation followed by recombination, is outlined. On this basis the results obtained in discharges, ozonizers and high-voltage arcs are explained. Flory's suggestion of predissociation in the upper state is reviewed and the experimental evidence found to be against it. The conclusions reached are applied to considerations regarding the spectrum of the night sky.

§1. INTRODUCTION

CONSIDERABLE interest is now being taken by spectroscopists in the spectra of the aurorae and the night sky, since from these a great deal of information may be obtained about processes occurring in the upper atmosphere. In connection with this work it is necessary to study the spectra emitted by the atmospheric gases in the laboratory. The present paper describes some new experiments on the emission spectrum of O_2, and it is convenient to begin with a brief summary of previous investigations.

(*a*) In the red and infra-red regions of the spectrum absorption bands corresponding to the transition $A^1\Sigma_g^+ \leftarrow X^3\Sigma_g^-$ have been observed. Near these bands others are found resulting from the transition $^1\Delta_g \leftarrow X^3\Sigma_g^-$. Recently Kaplan (1947) has obtained some of these bands in emission from an oxygen afterglow.

(*b*) Absorption bands found by Hopfield and others in the far ultraviolet region have been shown to be due to transitions from the O_2 ground state to various O_2^+ states, forming a Rydberg series of bands.

(*c*) Hopfield (1930) discovered a number of emission bands near 2000 A. forming a single v'' progression. They are produced in a condensed discharge in a O_2–He mixture and are attributed to O_2 on experimental evidence only.

(*d*) Herzberg's ultraviolet absorption system ($^3\Sigma_u^+ \leftarrow X^3\Sigma_g^-$) is forbidden and has not yet been obtained in emission in the laboratory, though some strong night-sky bands are thought to belong to this system.

(*e*) The most readily observed absorption in O_2 is that found by Schumann, which sets the limit to observations in the ultraviolet region with air-filled spectrographs. These bands result from the transition $^3\Sigma_u^- \leftarrow X^3\Sigma_g^-$ and bands observed by Runge in a high voltage arc in the region 4200–3100 A. are known to be part of the same system in emission.

(*f*) At very high pressures new absorption bands appear in the oxygen spectrum, and these are thought to be due to the molecule O_4. Further absorption bands are obtained in solid and liquid oxygen, most of which have been analysed into four systems.

The present paper gives extended data on Runge's bands and discusses the processes involved in their emission. The new results are not consistent with the suggested predissociation of the $^3\Sigma_u^+$ state at $v' = 2$, and, therefore, all the relevant experimental evidence is examined in order to settle this question definitely. Finally the conclusions reached in this investigation are reviewed in relation to the work on the night-sky spectrum.

§2. EXPERIMENTAL

The discovery of the Schumann-Runge bands in emission was published by Runge (1921), and various workers measured and analysed the plates he obtained, the most complete analysis being given by Lochte-Holtgreven and Dieke (1929). This work was confined to the region 3100 A. to 4200 A., and no spectra were published. In his experiments Runge used a high voltage D.C. arc in flowing oxygen. Whilst investigating the oxonizer discharge, Wulf and Melvin (1939) compared its spectrum when filled with cylinder oxygen with that given by a high voltage, low current A.C. arc in the same oxygen. They published a small dispersion spectrogram of the two sources; that of the arc showing Schumann-Runge bands extended from 4000 A. to 2500 A., whereas that of the ozonizer shows only N_2 Second Positive bands. Millon and Herman (1944) have carried out experiments with discharges in extremely pure oxygen and also report the appearance of some of the bands; this work will be considered in a latter section.

In the present investigation a high voltage, low current A.C. arc was used. A two-litre Pyrex flask contained the source, which consisted of an arc running between two thin (0·03 in. diameter) platinum–rhodium wires. The Pt–Rh wires were supported on the ends of tungsten wires sealed into ground-glass joints which fitted into the flask, so that easy adjustment of the electrodes was possible. A Hyvac pump and a McLeod gauge were provided and the gas was supplied from a cylinder. Pressures between 0·05 mm. and 1 atmosphere were employed. The discharge is a true arc, the electrodes becoming red- or white-hot and presumably maintaining the arc by thermionic emission. Various electrodes were tried, the difficulty being to find a material which can remain red-hot in oxygen without oxidizing. Platinum has been found to work reasonably well, but it is an advantage to use a platinum–rhodium alloy as the melting point is then raised.

The voltage in such a source is determined mainly by the separation of the electrodes, whilst the current can be varied by means of variable resistances in the primary circuit of the transformer used. Usually the arc ran at about 1000 v. and 0·1 amp. These figures are, however, only of qualitative significance since the voltage characteristic is far from sinusoidal. Current and voltage wave-forms were investigated with a Cossor double-beam oscilloscope and showed the form predicted for A.C. arc (Simon 1905, Loeb 1939, figure 286); the current is practically sinusoidal, whereas the voltage shows a sharp breakdown peak at the start of each half-cycle, followed by a period of constant voltage. Higher intensities could presumably be obtained by using higher currents, but the source is convenient in its present form, runnning extremely steadily and giving sufficient intensity for photographs to be obtained on a Quartz Littrow (Hilger E.1) spectrograph with exposures of about ½ hour in the more intense regions.

Commercial cylinder oxygen was used and, although this contains various impurities, especially nitrogen, no bands of molecules other than O_2 appeared on the plates taken at 1 atmosphere pressure. The bands are in fact quite strongly

excited in air at atmospheric pressure so long as a continuous flow is maintained to remove the NO_2 which is formed and which has strong absorption bands in the visible and ultraviolet regions. This should be contrasted with the behaviour of impure oxygen in a normal low pressure discharge, when only impurity bands are readily emitted. The only necessary precaution is the complete drying of the gas with P_2O_5, otherwise the OH bands appear. Experiments showed that as the pressure is reduced from 1 atmosphere the intensity of the bands falls rapidly and that at about $\frac{1}{2}$ atmosphere they become difficult to photograph, especially as the bands of NO and N_2 are readily excited at the lower pressures. In consequence of this the reproductions are all from spectra taken at atmospheric pressure. With the Quartz Littrow the region 2000 A. to 5000 A. has been investigated, and from 4500 A. to 9000 A. spectra have been taken on a prism-grating instrument.

§3. DESCRIPTION OF THE SPECTRUM

The present investigation shows the Schumann-Runge bands extending from 2000 A. to 4800 A. The bands fall into no well-marked sequences, the system having a wide Condon parabola. The heads are weak since the bands are strongly degraded towards the red and the rotational temperature is high ($\simeq$2000 K.). The region 4200 A. to 3100 A. has been measured in detail by Lochte-Holtgreven and Dieke (1929). Their work shows that the transition is $^3\Sigma_u^- \rightarrow {}^3\Sigma_g^-$ and each band has six main branches, three P and three R. On the dispersion used here the spin splitting is unresolved, and hence each band appears simply as consisting of a single P and R branch. In some bands the structure is further simplified by the R and P branches being unresolved from each other.

Identification of new bands cannot conveniently be made from head data since the band heads are very weak. However, extension of the analysis was achieved by calculating from the measurements of Lochte-Holtgreven and Dieke the wavelengths of several of the lines of each band in the $v'=0, 1, 2$ progressions. It was found best to calculate P(17), R(21) and P(27), R(31), and these four lines appear, in the majority of cases, as two doublets separated by four other doublets, and hence the rest of the bands may be readily identified. In the plate, in order to avoid the confusion which would result if every line identified were marked, only a few lines of each band are indicated. It is not possible to calculate accurately in this way the rotational structure of bands with $v'>2$; these were found by inspection. At the short wavelength end of the spectrum it was necessary to use plates with rather large grains, and hence the resolving power was slightly reduced, also (see §5 (i)) the band lines in this region which correspond to higher v' values than in the near ultraviolet were somewhat broadened. The far ultraviolet region is not, as yet, very completely analysed, though it seems safe to assume that it consists of bands with $v'>2$.

The only atomic lines occurring in the ultraviolet spectrum are due to platinum and rhodium. As will be seen from the plate, these are not of sufficient number or intensity to cause trouble. In the infra-red region a few lines appear, and these have been identified, from the list of Edlén (1943), as due to O I:

8446 A.: $(^4S)3s\,^3S_1 - (^4S)3p\,^3P_{0,1,2}$;
7774 A.: $(^4S)3s\,^5S_2 - (^4S)3p\,^5P_{1,2,3}$;
7950 A.: $(^2D)3s\,^3D_{1,2,3} - (^2D)3p\,^3F_{2,3,4}$.

These are the strongest lines in Edlén's list, the rest being too weak to be observed in the present work.

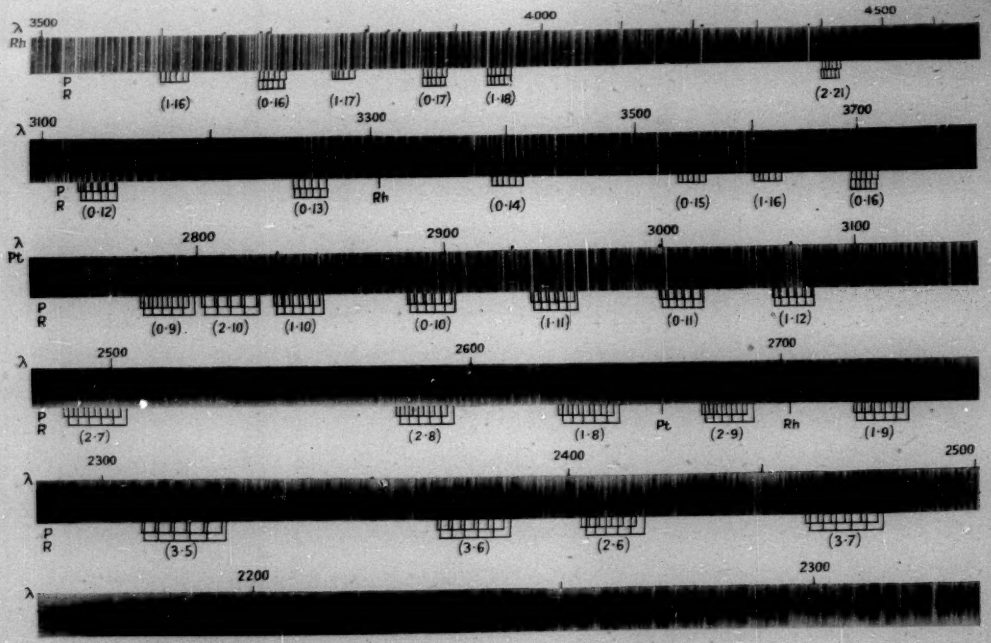

The spectra are reproduced from E.1 spectrograms of a high voltage arc in O_2 between Pt–Rh electrodes. A part of the rotational structure of each band found is marked and the vibrational quantum numbers shown. Lines marked with dots are of Pt or Rh (the chemical symbol is given on the left of each strip). An approximate wavelength scale is included.

To face page 116

§4. THE EMISSION PROCESS.

The present experiments show that the intensity of the band system falls rapidly with decrease of pressure in the discharge, so that at $\frac{1}{2}$ atmosphere it is exceedingly weak. This behaviour is completely different from that of many other gases (for example N_2) which emit best in a discharge at low pressure. Hence it becomes necessary to attempt an explanation of this result. The reason for this behaviour may best be discussed in conjunction with the figure, which shows the potential curves of the upper and lower states of the Schumann-Runge system. These curves are drawn to agree with the experimental evidence, absorption, emission and photochemical. As is well known (e.g. Mott and Massey 1933), a collision of an electron with a molecule leading to electronic excitation may be treated according to the Franck-Condon principle. Thus it follows from the

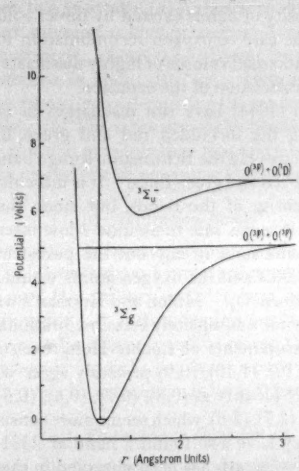

figure that the excitation of O_2 molecules in the ground state will most frequently result in dissociation in the upper state. The experiments of Ladenburg and Van Voorhis (1933) on the absorption coefficient of oxygen in the vacuum ultraviolet region show that the transition of maximum probability (equal instantaneous internuclear distance in the upper and lower stat s) gives an average kinetic energy of about 1·7 ev. per atom after dissociation. The action of a discharge on oxygen will thus be to start dissociating it, and various authors have pointed out that atomic oxygen is very reactive, readily combining with gaseous or solid impurities. However, in the high pressure experiments here described there is a much greater probability than in the low pressure discharge that the atoms will recombine again to the upper state of the Schumann-Runge system. This would probably take place by a three-body process, and the molecule would then return to the ground state by emitting the Schumann-Runge bands. It should be noted that the dissociation leads to a normal $O(^3P)$ atom and an excited $O(^1D)$ atom. But since the ^1D level is metastable (mean life 100 sec. (Condon 1934)), it will not easily revert to the ground state by radiation, and so prevent the recombination taking place. Furthermore, recent experiments (Vegard and Kvifte 1947) have shown that the

de-activation of metastable oxygen atoms by collisions with other oxygen atoms or molecules has a very low probability. The high rotational temperature of the bands is consistent with these views of the emission process, since the recombination of atoms with high kinetic energy will obviously lead to the formation of molecules of high rotational energy.

It is of interest to apply the above reasoning to the results obtained by Wulf and Melvin (1939) with an ozonizer discharge in commercial cylinder oxygen. At 1 atmosphere pressure they obtained no oxygen bands but only N_2 impurity bands. Here the dissociation phenomenon gives an explanation, since, although in the ozonizer the volume of gas in which excitation takes place is much larger than in the case of the high voltage arc, the amount of energy dissipated may not be very different (Wulf and Melvin used the same transformer for both). Hence to a first approximation the intensity of bands excited by direct collisions in each case will be the same. But in the case of oxygen recombination followed by emission is favoured in the arc with its small volume of highly dissociated gas rather than in the uniformly distributed dissociation of the ozonizer.

Millon and Herman (1944) have run discharges in extremely pure oxygen during investigations on the forbidden red and green lines of oxygen. At a pressure of a few centimetres Hg the Schumann-Runge bands occur with intensity comparable to that of the red and green lines. It is difficult to tell from their short paper the absolute intensity of the bands, but since the lines simultaneously observed are forbidden it seems safe to assume a low intensity. This then falls into line with other results since in any but the purest oxygen impurity bands would obscure the O_2 bands and the oxygen atoms would tend to react with the impurities rather than reform O_2. Millon and Herman's wavelengths of heads are not of sufficient accuracy for a completely certain vibrational analysis of the bands, but apart from the measurements of Lochte-Holtgreven and Dieke, the assignments (0,11), (1,11), (0,10), (1,10), (0,9) probably agree with the present work. However, the bands they identify as (0,8), (0,7), (0,6), (0,5) are possibly the ones taken here as (2,9), (2,8), (2,7), (2,6), which seems more consistent with the expected Condon parabola. They have also found a band at 2331 A. which they take as (6,4); no band at this wavelength has been observed in the present investigation. It is hoped that a complete rotational analysis will settle any doubts about the vibrational scheme.

When the major part of this paper had been written a note by Lalji Lal (1948) appeared. He has observed bands from 2450 A. to 4490 A. in a high frequency discharge in pure oxygen. Twenty-six heads have been measured on small dispersion, and these bands have been assigned to the Schumann-Runge system. The analysis he gives is quite different from that given here, and no bands at his wavelengths can be found on the present spectra. The two results have been briefly compared by the author (Feast 1948), and further data on Lalji Lal's bands, especially a photograph, are needed before the matter is completely discussed.

§5. PREDISSOCIATION

Flory (1936) has suggested that the behaviour of oxygen can only be successfully explained by assuming that the upper state of the Schumann-Runge system is predissociated by a repulsive $^3\Pi_u$ state at $v'=2$ of the $^3\Sigma_u^-$ state, this leading to the formation of two normal oxygen atoms. This would mean that bands with $v'>2$ would not be observed in emission. However, according to the analysis proposed

here, bands with $v' = 3$ are found, and it seems difficult to find any other interpretation for the unanalysed region at the short wavelength end of the spectrum than that it is due to bands with $v' > 2$. It is therefore important to re-examine Flory's arguments to see if all oxygen phenomena can be explained without assuming predissociation.

(i) *Emission Bands*

Flory suggests that from Lochte-Holtgreven and Dieke's results a Condon parabola may be deduced which indicates that the bands (3,15), (3,16), (3,20), (3,21), (3,22) should have appeared on Runge's plates: in fact these bands are not found. He maintains that collision quenching could not have prevented observation of the bands since he assumes Runge's pressure as less than 0·01 atmosphere. This can be criticized on two grounds: (*a*) As has been shown earlier, the bands are only produced with high intensity at high pressures; Runge's pressure would thus probably be near atmospheric, where the collision frequency is about 10^{10} sec., while the radiative lifetime is about 10^{-8} sec. Hence collision broadening is very important at these pressures and explains the tendency to broadening in the short wavelength bands. (*b*) The intensity of the bands, on the plates published here, indicates a wider Condon parabola than that taken by Flory, so that the bands quoted above do not lie on the line of maximum intensities.

(ii) *Absorption Bands*

Analysis of the absorption Schumann-Runge bands has been carried out by Curry and Herzberg (1934) working at 1 atmosphere pressure and by Knauss and Ballard (1935) at 5–15 mm. Hg. Curry and Herzberg's photograph is thought by Flory to show broadening for $v' > 2$, thus bearing out the predissociation theory. The effect must in any case have been small to escape the experimenters, and the fact that in the lower pressure work the bands are clearly resolved, with no trace of diffuseness, suggests that any broadening may be put down to collision quenching.

(iii) *Fluorescence Experiments*

Rasetti (1929) found O_2 fluorescence at atmospheric pressure but none at 8 mm. Hg. This is explainable on a theory of predissociation, but it may also be understood if collision quenching does not fall off more rapidly than the number of molecules excited by fluorescence when the pressure is reduced.

(iv) *Photochemical Experiments*

The pressure decrease when oxygen is exposed to radiation of $\lambda < 1751$ A. is due to the reaction of the atoms formed by absorption of the Schumann-Runge continuum with wall impurities (Neujmin and Popov 1934). Flory and Johnston (1935) used 1 cm. of air as a filter and claim that the small pressure decrease, still noted, is due to a predissociation following absorption of radiation of $\lambda > 1751$ A. However, since the observed effect is small, there are some other factors worth considering: (*a*) 1 cm. of air may still allow transmission of a small amount of radiation with $\lambda < 1751$ A., thus forming atoms in the normal way; (*b*) though, as Flory states, the effect of dissociation by a bimolecular collision of an excited and a normal molecule will be small, it may not be completely negligible; (*c*) absorption of radiation in the region of the Herzberg system continuum is a possible mechanism for dissociation at wavelengths greater than 1751 A.

(v) *Conclusion*

From the above discussion, and from the results on the emission bands, it appears that the experimental evidence is against the predissociation theory. In certain cases the results previously quoted in support of the predissociation are found to have other possible causes.

§6. APPLICATION TO THE NIGHT-SKY SPECTRUM

Since oxygen is abundant in the upper atmosphere, its presence or absence in the spectrum of the night sky is of great importance. At present there seems a good deal of agreement amongst astrophysicists that the Herzberg oxygen bands occur in emission. The presence of the Schumann-Runge bands is somewhat doubtful, though various authors claim to have identified them. The Herzberg emission bands are calculated from the absorption measurements and from the ground-state differences of the Schumann-Runge bands ($\Delta v''$). At present the $\Delta v''$ values required have to be extrapolated from the measurements of Lochte-Holtgreven and Dieke. The work described here was started with the object of extending the data on the Schumann-Runge bands so that the Herzberg bands could be calculated without the uncertainty of an extrapolation. Since it appears that the heads are too weak for direct measurement, the necessary information will only be obtained by a complete rotational analysis, and it is hoped to publish this shortly. Various workers (e.g. Pearse 1943) have calculated the wavelengths of bands corresponding to bands of the Schumann-Runge system with $v' = -1$ and -2 and have noted some good coincidences with night-sky bands. This has led to some speculation as to whether the accepted v' values are correct. None of these bands can be found on the present spectra, and hence it must be assumed that the v' assignment is correct. The most conclusive test would be a study of the isotope shifts.

We know that above 100 km. the oxygen is almost completely dissociated by solar radiation during the day (Wulf and Deming 1938). Thus it seems possible that a three-body recombination to the upper state of the Schumann-Runge bands will take place at night, though this would yield low intensities.

Swings (1947) and Nicolet (1948) have advocated that night-sky bands should be identified by first computing the low temperature profiles of the bands. In this connection it should be noted that if the Schumann-Runge bands do occur due to the process outlined above then their rotational temperature may be considerably higher than the accepted night-sky value, and the profile computing method would break down.

Finally, since the pressure is low in the upper atmosphere, collision quenching will not be important and higher v' values should be expected.

ACKNOWLEDGMENTS

This work was suggested by Assistant Professor R. W. B. Pearse, and the author is deeply indebted to him for many helpful discussions during its progress. The work was made possible by the award of a D.S.I.R. maintenance grant.

REFERENCES

Condon, E. U., 1934, *Astrophys. J.*, **79**, 217.
Curry, J., and Herzberg, G., 1934, *Ann. Phys., Lpz.*, **19**, 800.
Edlén, B., 1943, *Kungl. Svenska VetenskAkad. Handl.*, **20**, No. 10.
Feast, M. W., 1948, *Nature, Lond.*, **162**, 214.

FLORY, P. J., 1936, *J. Chem. Phys.*, **4**, 23.
FLORY, P. J., and JOHNSTON, H. L., 1935, *J. Amer. Chem. Soc.*, **57**, 2641.
HOPFIELD, J. J., 1930, *Phys. Rev.*, **36**, 789.
KAPLAN, J., 1947, *Nature, Lond.*, **159**, 673.
KNAUSS, H. P., and BALLARD, S. S., 1935, *Phys. Rev.*, **48**, 796.
LADENBURG, R., and VAN VOORHIS, C. C., 1933, *Phys. Rev.*, **43**, 315.
LALJI LAL, 1948, *Nature, Lond.*, **161**, 477.
LOCHTE-HOLTGREVEN, W., and DIEKE, G. H., 1929, *Ann. Phys., Lpz.*, **3**, 937.
LOEB, L. B., 1939, *Fundamental Processes of the Electrical Discharge in Gases* (New York : John Wiley).
MILLON, J., and HERMAN, L., 1944, *C.R. Acad. Sci., Paris*, **218**, 152.
MOTT, N. F., and MASSEY, H. S. W., 1933, *Theory of Atomic Collisions* (Oxford : Clarendon Press).
NEUJMIN, H., and POPOV, B., 1934, *Z. phys. Chem.* B, **27**, 15.
NICOLET, M., 1948, Conference on *The Emission Spectra of the Night Sky and Aurorae* (Report from Gassiot Committee) (London : Physical Society), p. 105.
PEARSE, R. W. B., 1943, *Rep. Prog. Phys.*, **9**, 42.
RASETTI, F., 1929, *Proc. Nat. Acad. Sci.*, **15**, 411.
RUNGE, C., 1921, *Physica*, **1**, 254.
SIMON, H. T., 1905, *Phys. Z.*, **6**, 297.
SWINGS, P., 1947, *Report on the Night Sky and the Aurorae to the Conference on Planetary Atmospheres* (Yerkes Observatory).
VEGARD, L., and KVIFTE, G., 1947, *Geofys. Publ., Oslo*, No. 1.
WULF, O. R., and DEMING, L. S., 1938, *Terr. Magn. Atmos. Elect.*, **42**, 283.
WULF, O. R., and MELVIN, E. H., 1939, *Phys. Rev.*, **55**, 687.

The CN Tail Bands emitted by the Carbon Arc in Air

BY M. W. FEAST

Imperial College of Science and Technology, London

MS. received 16*th July* 1948

ABSTRACT. Wavelengths and intensities of twenty-one CN tail bands, observed in the carbon arc spectrum, are listed and v', v'' values assigned. Nine of the bands have been previously reported as occurring in the nitrogen afterglow excitation. The intensities of the tail bands are shown to be in accordance with the accepted potential curves for this system.

§ 1. INTRODUCTION

As is well known, the CN violet band system ($^2\Sigma - {}^2\Sigma$) occurs readily in many laboratory and astrophysical light sources. The system consists of several strong sequences degraded to the shorter wavelengths, together with some weaker bands degraded in the opposite direction and known as the tail bands. The principal sources used by investigators of this system have been the carbon arc in air and the nitrogen afterglow with carbon compounds present. In active nitrogen both the main bands (Jevons 1926) and the tail bands (Jenkins 1928) have been studied. Extensive rotational structure measurements of the main bands as obtained in the arc have also been made (see Jevons (1926) for references). However, there seem to be no data available on the arc excitation of the tail bands. Such data are of importance both for laboratory identification of the bands, the carbon arc being used extensively in analysis, and for identification of astrophysical spectra. The present communication gives wavelengths and

intensities of twenty-one tail bands observed in the arc spectrum: nine of these are bands which have been reported in the afterglow spectrum, whilst the rest correspond to previously unreported transitions. The band intensities are in qualitative agreement with the Condon parabola deduced from the accepted potential curves.

§2. MEASUREMENTS AND ANALYSIS

The measurements of the band heads were made from Hilger E.1 spectrograms of a 110 v. 5 amp. carbon (graphite) arc in air. To obtain the tail bands with sufficient intensity it was necessary to have the main CN bands considerably over-exposed.

The new data are given in the table.

v', v''	λ_c (A.)	I_c	λ_n (A.)	ν_c (cm^{-1})	ν_0 (cm^{-1})	$\nu_c - \nu_0$
15, 15	a		4078·72			
14, 14	4028·38 e	6 ?	4029·33	24817	24779 m	38
13, 13	3984·52 e	9	3984·62	25090	25049 m	41
12, 12	3944·52 e	9	3944·66	25345	25288 m	57
11, 11	3909·90 e	10	b	25569	25498 m	71
10, 10	a		b			
12, 11	a		b			
11, 10	3657·66 e	5	3658·13	27332	27275 m	57
10, 9	3628·53 e	7	b	27552	27477 m	75
9, 8	3602·63 e	7	b	27750	27642 m	108
13, 11	a		b			
12, 10	3465·33	6	b	28849	28818 m	31
11, 9	3432·92	6	3433·00	29126	29080 m	46
10, 8	3404·84	7		29362	29302	60
9, 7	3380·29	6		29575	29494	81
8, 6	3359·06	4		29762	29651	111
7, 5	3340·56	4		29926	29776	150
6, 4	3322·29	4		30091	29868	223
5, 3	3296·29	3		30328	29932	396
10, 7	3203·46	4		31207	31154	53
9, 6	3180·22	4		31436	31371	65
8, 5	3159·89	4		31637	31556	81
7, 4	3142·57	4		31812	31708	104
6, 3	3127·56	3		31964	31827	137
5, 2	3114·34	2		32101	31929	182

v', v'', vibrational quantum numbers; λ_c, I_c, wave length, intensity, of band head in arc; λ_n, wavelength of band head in afterglow spectrum (see text); ν_c, wave number corresponding to λ_c; ν_0, the wave number of origin ("m" denotes measured values); "a", band obscured by main bands; "b", band, but not head, observed in afterglow; "e", measurement of band made difficult by strong overlapping main bands.

In calculating ν_0, the combined data of Jevons and Jenkins have been used; where the experimental values are available they are indicated by "m". For the majority of the bands reported here the values of B' and B'' are not known with sufficient accuracy for the positions of the band heads to be reliably calculated and compared with the experimental values. However, the values of $\nu_c - \nu_0$ given in the table are all of the correct order and vary from band to band in the expected manner.

The column λ_n in the table gives the wavelengths of heads measured by Jenkins in the afterglow spectrum and it will be noted that in several cases there is a considerable difference between this value and λ_c. This is partly due to the fact that in the arc many of the tail bands are badly confused with the main CN bands

(those most affected are marked "e" in the table). A second reason for this discrepancy is that λ_n is the wavelength of the last rotational line in the R branch, as measured by Jenkins, the rotational temperature being such that no lines on the returning part of the branch are observed. A consideration of Jenkins' measurements shows that the line taken as forming the band head may be 0·5 cm^{-1} or more to the long wavelength side of the true head.

§3. DISTRIBUTION OF VIBRATIONAL INTENSITIES

The figure shows the distribution of the intensities in the CN main and tail bands as excited in the arc. The band intensities are head estimates, and since $\nu_c - \nu_0$ is not constant from band to band, these values are not reliable for the overall intensity of the band though they may be used for a qualitative investigation. The main band intensities were obtained by microphotometry of Hilger E.1 spectrograms (Tawde 1936). No attempt has been made to put the two parts of the system on a common intensity scale as the difference of intensities between the main and tail bands is too great to be estimated by eye. The tail band intensities are eye estimates.

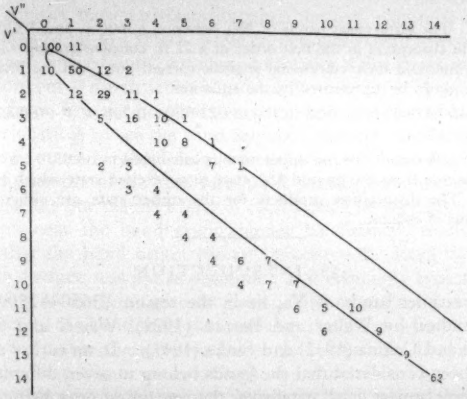

The Condon parabola in the figure is drawn from the potential curves calculated by Herzberg (1939, figure 177) and is practically the same as that obtained from the Morse and Rydberg potential curves given by Tawde. It is seen that it fits quite closely to the experimental line of maxima. Bands near the parabola, in the (1, 0) sequence from $v' = 4$ to 8 and in the (0, 0) sequence from $v' = 5$ to 10, are not observed since these bands are either headless or fall in regions where the main bands are very strong.

The vibrational intensity distribution in the afterglow (Jenkins 1928) is similar to that given here except that bands with the head far from the origin appear relatively weaker, due to the low intensity of high J value lines.

§4. NOTE ON THE (4,4) MAIN BAND

The wavelength of the (4, 4) band is 3850·95 A.; this measurement does not appear to have been recorded previously.

ACKNOWLEDGMENTS

The author wishes to express his thanks to Dr. R. W. B. Pearse, who suggested this investigation, for his interest and advice. The work was made possible by a D.S.I.R. grant.

REFERENCES

HERZBERG, G., 1939, *Molecular Spectra and Molecular Structure*, Vol. I (New York: Prentice-Hall).
JENKINS, F. A., 1928, *Phys. Rev.*, **31**, 539.
JEVONS, W., 1926, *Proc. Roy. Soc.* A, **112**, 407.
TAWDE, N. R., 1936, *Proc. Indian Acad. Sci.*, 3A, 140.

Ultra-Violet Bands of Na_2

BY S. P. SINHA
Science College, Patna, India *

MS. received 27th July 1948

ABSTRACT. The ultra-violet bands of Na_2 between λ 3600 A. and λ 3200 A. have been photographed in absorption in the first order of a 21 ft. concave grating with a dispersion of about 1·3 A/mm. and their vibrational analysis carried out. All the bands belong to a single system and can be represented by the equation

$$\nu = 29342 + 119{\cdot}33\,(u') - 0{\cdot}53\,(u')^2 - 159{\cdot}23\,(u'') + 0{\cdot}726\,(u'')^2 + 0{\cdot}0027\,(u'')^3,$$

where $u = v + \frac{1}{2}$.

The heat of dissociation for the upper state is calculated to be 6510 cm^{-2}. The bands are due to transition from the ground $^1\Sigma_g^+$ state to an excited state which is probably $^1\Sigma_u^+$ in character. The dissociation products for the upper state are either $3\,^2S + 4\,^2P$ or $3\,^2S + 3\,^2D$ atoms of sodium.

§ 1. INTRODUCTION

THE ultra-violet bands of Na_2 lie in the region λ3650–λ2500 A. and have been studied by Walter and Barratt (1928), Weizel and Kulp (1930), Kimura and Uchida (1932) and Sinha (1947). In an earlier report (Sinha 1947), it has been considered that the bands belong to seven different systems of which only three appear at all extensive, the remaining ones being merely fragmentary. Two of these systems, reported there as system 1 and system 3, have been found to be strong while system 2 is comparatively weak. The analysis proposed suffers from the defect that the vibrational differences are not quite satisfactory. It was, therefore, considered necessary to photograph the bands at higher dispersion and determine the molecular constants more accurately. This has, however, been done only for the bands lying between λ3500 and 3200 A., corresponding to the first ultra-violet system mentioned above.

§ 2. EXPERIMENTAL

The bands have been studied in absorption. The details of the absorption tube used have been described elsewhere (Sinha 1948). Sodium, freed from the oil in which it was stored, was placed at the centre of the tube and was heated electrically from outside. To prevent rapid distillation of the metal to cooler

* The work described in the present paper was done at Imperial College, London.

parts some nitrogen was introduced inside the chamber. The bands were found to appear most satisfactorily when the temperature inside the tube was about 750° C. and the pressure of nitrogen was 5 to 10 cm. of mercury. A hydrogen discharge tube of the type described by Hunter and Pearse (1936) was used as a source of continuum and the bands were photographed in the first order of a 21-ft. concave grating with a dispersion of about 1·3 A. per mm.

§3. APPEARANCE OF THE SPECTRUM AND MEASUREMENT

The Na_2 ultra-violet bands first appear at about 700° C. when the pressure of nitrogen inside the chamber is about 5 cm. of mercury and lie between λ3450 and λ3250 A. As the temperature is raised they become stronger and extend up to λ3600 A. on the long wavelength side and λ3200 A. on the short wavelength side. With temperature higher than 850° C., the absorption in this region becomes almost continuous and quite strong bands begin to appear at wavelengths lower than about λ3000 A. At still higher temperature (1000 to 1100° C. or more), the entire region from λ3600 to λ2800 A. is completely absorbed except for a narrow region at about λ3100 A. which still continues to be transparent.

The λ3600–λ3200 A. system of bands which forms the subject of the present investigation appears most satisfactorily when the temperature is about 750° C. The strong bands lie up to λ3550 A. while fainter ones extend to even longer than λ3600 A. Closely spaced lines pertaining to rotational fine structure appear over the entire region, but as the structure of one band overlaps that of the neighbouring band in most cases, it is not possible to separate the structure of each individual band, nor is it possible to see the band origins. A rough calculation with values of B's of the two states involved reveals that the head is formed by as low as the third or fourth member of the head forming R branch, and since both B' and B'' are so small that the low member lines of each branch lie very close together, the individual lines near the band origin cannot be distinctly resolved, with the consequence that the band origin cannot be observed. Even the band head, although quite distinct, was not as prominent as is ordinarily expected in view of the close spacing of the lines near the head. The reason for this is that in the rotational structure of a band there is an intensity maximum which lies at a J value that is higher the higher the temperature or the smaller B. In the present case B is low and the temperature used was high, and therefore the higher members of the branch were stronger than the lower members which formed the heads. The difficulty could probably be overcome by working at a lower temperature and a correspondingly longer absorption path.

Measurements are given in Table 1. The iron arc was used for comparison spectra. The values of λ's given here differ from those published before (Sinha 1947). Since the heads are formed from relatively weak lines there is difficulty in correctly locating the position of the band-heads in both cases, but since the present measurements are from a plate of much higher dispersion and since the bands were more satisfactorily developed it is considered that the present measurements are definitely the more accurate.

The bands were all degraded to the red and appeared to have single heads suggesting $^1\Sigma$–$^1\Sigma$ transition. It may, however, be noted that even if the bands had more than one head, it may not always be possible, under the circumstances described above, to see the different heads distinctly and the band may appear to have just a single head.

Table 1. Na_2 Bands between λ3600 and λ3200 A.

λ_{air} (A.)	Int.	v', v''	$\nu_{obs}-\nu_{calc}$	λ_{air} (A.)	Int.	v', v''	$\nu_{obs}-\nu_{calc}$
3595·2	1	2, 12	2	3400·4	8	3, 2	0
86·7	1	—	—	3395·9	5	2, 1	0
80·2	1	3, 12	2	92·0	4	1, 0	0
77·0	1	2, 11	3	87·1	5	4, 2	0
70·5	1	0, 9	3	82·4	6	3, 1	0
65·4	2	4, 12	2	77·8	4	2, 0	0
62·3	3	3, 11	2	74·1	5	5, 2	0
59·0	2	2, 10	2	69·2	10	4, 1	1
55·5	3	1, 9	4	64·6	4	3, 0	−1
52·0	2	0, 8	2	61·4	5	6, 2	0
47·7	3	4, 11	2	56·5	8	5, 1	−1
44·3	3	3, 10	2	51·5	7	4, 0	0
40·8	3	2, 9	4	48·7	5	7, 2	0
37·3	2	1, 8	2	43·7	6	6, 1	0
33·5	2	0, 7	3	38·8	10	5, 0	−1
30·1	2	4, 10	1	31·4	5	7, 1	−1
26·3	3	3, 9	3	26·3	10	6, 0	−1
22·6	3	2, 8	2	19·2	5	8, 1	−1
19·0	3	1, 7	2	14·0	10	7, 0	−2
15·0	3	0, 6	3	07·3	5	9, 1	−2
12·1	3	4, 9	3	3295·5	5	10, 1	−3
08·3	3	3, 8	1	90·0	9	9, 0	−2
04·5	3	2, 7	3	83·9	5	11, 1	−3
00·6	3	1, 6	2	78·4	8	10, 0	−3
3496·6	3	0, 5	2	72·3	4	12, 1	−2
94·2	3	4, 8	2	66·8	7	11, 0	−2
90·2	3	3, 7	3	66·2	5	14, 2	1
86·3	4	2, 6	2	60·8	4	13, 1	0
82·2	3	1, 5	3	55·5	7	12, 0	−2
78·2	3	0, 4	2			15, 2	−2
72·2	3	3, 6	2	50·2	6	17, 3	−2
68·1	5	2, 5	2	49·6	3	14, 1	0
64·0	3	1, 4	1	44·5	3	16, 2	−2
60·0	3	0, 3	0	39·8	5	18, 3	−3
50·0	7	2, 4	2	38·7	3	15, 1	0
46·0	4	1, 3	0	34·1	3	17, 2	−1
41·6	4	0, 2	0	33·2	5	14, 0	−1
32·2	7	2, 3	0	29·5	5	19, 3	−2
27·7	5	1, 2	0	28·2	3	16, 1	−1
23·2	4	0, 1	0	23·6	3	18, 2	−1
18·5	4	3, 3	−1	19·3	4	20, 3	−3
14·0	5	2, 2	0	17·6	4	17, 1	−2
09·4	4	1, 1	0	13·4	3	19, 2	−2
03·8	5	0, 0	0	09·2	2	21, 3	−2
		3, 4	−1	03·3	2	20, 2	−3

Table 2. Deslandres' Scheme for Na_2 Bands

Table 2. Deslandres' Scheme for Na_2 Bands

v'' / v'	0	1	2	3	4	5	6	7	8	9	10	11	12	Mean diff.
0	29362	29204	29048	28893	28742	28591	28441	28292	28145	27999				
	158 118	158 118	156 118	155 118	151 118	151 118	150 117	147 117	146 117	146 118				117·7
1	29480	29322	29166	29011	28860	28709	28558	28409	28262	28117				
	158 117	158 117	156 117	155 117	151 117	151 117	150 118	147 118	147 118	145 117				117·3
2	29597	29439	29283	29128	28977	28826	28676	28527	28380	28234	28090	27948	27807	
	157 116	158 117	156 117	155 116	151 117	151 117	150 116	149 116	147 116	146 116	144 116	142 116	141 116	116·2
3	29713	29556	29400	29244			28792	28643	28496	28350	28206	28064	27923	
	157 116	156 116	156 115	156 118			149 116	147 115	146 115	146 115	144 114	142 115	141 116	115·6
4	29829	29672	29515	29362					28611	28465	28320	28179	28039	
	157 113	157 112	155 114	153										113·0
5	29942	29784	29629											
	158 113	157 114	156 113											113·3
6	30055	29898	29742											
	157 111	157 111	155 112											111·3
7	30166	30009	29854											
	157 110													110·0
8	*	30119												
	158 109													109·0
9	30386	30228												
	158 108	158 108												108·0
10	30494	30336												
	159 108	157 107												107·5
11	30602	30443												
	158 107	158 108												107·5
12	30709	30551												
		157 107												107·0
13		30658												
	156 106	156												106·0
14	30920	30764	30608											
		158 103	156 101											102·0
15		30867	30709											
		157 101	156 102											101·5
16		30968	30811											
		156 101	156 102	155										101·5
17		31069	30913	30758										
			156 100	156 99										99·5
18			31013	30857										
			155 98	155 99										98·5
19			31111	30956										
			155 98	155 98										98·0
20			31209	31054										
				155 97										97·0
21				31151										
Mean diff.	157·6	156·2	155·0	151·0	151·0	150·3	149·0	147·0	145·8	144·3	141·7	140·7		
From Loomis and Nusbaum	158·0	156·0	155·0	153·5	151·0	150·5	149·0	146·5	146·0	144·0	143·0	140·0		

§ 4. VIBRATIONAL ANALYSIS AND MOLECULAR CONSTANTS

The vibrational quantum numbers assigned to the bands are given in column 3 of Table 1. Table 2 gives their wave-numbers in vacuum in the usual v', v'' square array. The asterisk denotes the position of the Na_2 band that was overlapped by the λ 3303 A. line of Na. The mean differences between the vibrational levels for the ground state from the work of Loomis and Nusbaum (1932) are given at the foot of Table 2.

Nearly all the bands measured can be represented by the equation

$$\nu = 29342 + 119{\cdot}33(u') - 0{\cdot}53(u')^2 - 159{\cdot}23(u'') + 0{\cdot}726(u'')^2 + 0{\cdot}0027(u'')^3,$$

where $u = v + \frac{1}{2}$. The terms in u'' correspond to those given by Loomis (1928). The values for $\nu_{obs} - \nu_{calc}$ given in column 4 of Table 1 have been calculated from the above equation. Although there is not much discrepancy between the observed and the calculated values there seems to be rather a systematic difference for large values of both the quantum numbers v' and v''. The discrepancy for large values of v'' seems to be due to fact that the constants in v'' used in the above formula do not refer to the band heads but to the magnetic rotation lines which very nearly represent the band origins, whereas the measurements included in Table 1 refer to the band heads. The difference between ν_{head} and ν_{origin} for bands degraded to the red becomes larger for higher values of the vibrational quantum numbers of the lower state (Jevons 1932), and since for such bands $\nu_{head} - \nu_{origin}$ is positive, $\nu_{obs} - \nu_{calc}$ should also be positive. This agrees with the present observation. The discrepancy for large values of v' suggests that higher terms in v' should be included in the above equation. It further indicates, as is often seen with the excited states of such molecules, that the levels are tending to converge more rapidly than is demanded by the linear relationship between ω_v and v. However, the discrepancies are nowhere too large and the arrangement seems satisfactory.

Vibrational constants for the four states of Na_2 are given in Table 3. The heat of dissociation for the upper state of the present system has been calculated by the method of extrapolation due to Birge and Sponer and would probably be a little higher than the true value. The constants ν_e, ω_e, $\omega_e x_e$, $\omega_e y_e$ are given in cm^{-1} and are those in the usual expansion $\nu(v) = \nu_e + \omega_e u - \omega_e x_e u^2 + \omega_e y_e u^3$, where $u = v + \frac{1}{2}$.

Table 3. Vibrational Constants for the Ground and the Excited States of Na_2

State	ν_e	ω_e	$\omega_e \lambda_e$	$\omega_e y_e$	D	Dissociation Products
$^1\Sigma_g^+$	0	159·23	0·726	−0·0027	6150	3 ^{2}S 3 ^{2}S
$^1\Sigma_u^+$	14680·4	117·6	0·38	—	8100	3 ^{2}S 3 ^{2}P
$^1\Pi_u$	20318·9	123·79	0·63	−0·0094	2840	3 ^{2}S 3 ^{2}P
$^1\Sigma_u^+$ (?)	29342	119·33	0·53	—	6510	3 ^{2}S 3 ^{2}D or 3 ^{2}S 4 ^{2}P

§ 5. DISSOCIATION PRODUCTS

The energy possessed by the dissociated atoms in the upper state of the system can be calculated from the equation $\nu_{atom} = \nu_{0,0} + D' - D''$, where the terms used have the usual significance. Since, $\nu_{0,0} = 29360\,cm^{-1}$, $D' = 6510\,cm^{-1}$ and $D'' = 6150\,cm^{-1}$, we have $\nu_{atom} = 29720\,cm^{-1}$. Also from the line spectra data it is

known that for sodium $3\,^2S-3\,^2D=29170\,cm^{-1}$ and $3\,^2S-4\,^2P=30270\,cm^{-1}$. The above are the nearest atomic states to the calculated ν_{atom}, other states being still farther apart. Since, however, the energy possessed by the dissociated atoms is midway between that corresponding to $3\,^2S-3\,^2D$ and $3\,^2S-4\,^2P$, it is difficult to decide between these two sets of dissociation products. Of the three terms used in calculating ν_{atom}, D'', the heat of dissociation for the ground state, is known correct up to $\pm 175\,cm^{-1}$ due to the work of Loomis and Nusbaum (1932). Table 2 giving the $v'-v''$ scheme indicates that the value of $\nu_{0,0}$ can be taken to be quite reliable. Hence the only uncertainty lies in the value of D' employed in the above calculation. D' has been calculated by Birge and Sponer's extrapolation method. This method is applicable to an electronic state for which the relationship between ω_v and v is linear and has been found to yield fairly satisfactory results for the ground states of non-polar molecules. At any rate, the smaller the range of extrapolation employed the more certain one can be of the calculated value of the heat of dissociation. For the excited states the values calculated by this method are often too high. A critical discussion on the suitability of this method has been provided by Gaydon (1946). Although in the case of the present system of bands, over the range investigated the relationship between ω_v and v seems fairly linear, it is difficult to predict how it would behave for higher values of v'. Judging from experience of other states of such molecules it can be concluded that, possibly, the true D' and hence ν_{atom} may be smaller than the value given above. This would lead to the conclusion that the dissociation products are $3\,^2S+3\,^2D$ atoms rather than $3\,^2S+4\,^2P$ atoms, but a definite decision should not be based on this consideration alone.

§6. DISCUSSION

The ground state of Na_2 is a stable $^1\Sigma_g^+$ state formed from two atoms of sodium each in the unexcited $3\,^2S$ state. The other state formed from these two atoms is a $^3\Sigma_u^+$ state which is regarded as a repulsive one. Since in absorption, transition is to take place from the ground $^1\Sigma_g^+$ state, the only excited states that matter are those of the type $^1\Sigma_u^+$ and $^1\Pi_u$. The excited states are obtained by considering one of the sodium atoms to be raised from the ground $3\,^2S$ state to higher and higher excited states like the $3\,^2P$, $4\,^2S$, $3\,^2D$, $4\,^2P$ etc. If we consider states resulting from $3\,^2S$ and $3\,^2P$ atoms, there will be as many as eight of them of which only one will be $^1\Sigma_u^+$ and only one $^1\Pi_u$. There should thus be two systems of bands $^1\Sigma_u^+ \leftarrow {}^1\Sigma_g^+$ and $^1\Pi_u \leftarrow {}^1\Sigma_g^+$ whose upper state should dissociate into $3\,^2S$ and $3\,^2P$ atoms of sodium. These correspond respectively to the red system studied notably by Fredrickson and Watson (1927) and Fredrickson and Stannard (1933), and to the green system studied notably by Loomis (1931) and Loomis and Nusbaum (1932).

Let us now consider that one of the sodium atoms is raised to the next excited state i.e. the $4\,^2S$ state. The $3\,^2S+4\,^2S$ atoms of sodium will give four states, out of which there will be one $^1\Sigma_u^+$ and no $^1\Pi_u$ state. The transition from the ground state to this $^1\Sigma_u^+$ state should give rise to a system of bands whose origin should lie at about $\lambda\,3900$ A., if we assume that the excited state has nearly the same dissociation energy as the ground state, or at longer or shorter wavelengths according as D' is greater or smaller than D''. Experiment does not reveal any band due to Na_2 near $\lambda\,3900$ A. The bands at longer wavelengths are the green system of Na_2 bands which are definitely known to be due to $3\,^2S+3\,^2P$ atoms. The bands at shorter wavelengths are the bands under present investigation and

lie between λ3600 and λ3200 A. If we wish to associate this system of bands with Na 3^2S+4^2S, D' for the upper state should be about 2500 cm^{-1}. Although this is not an improbable value, the results of analysis do not suggest that D' could be as low as that. Further from analogy with the known Σ states of Na_2, K_2 and NaK, it is expected that this state should also be fairly deep. This might lead one to conclude that the $^1\Sigma_u^+(3^2S+2^2S)\leftarrow{}^1\Sigma_g^+$ system of bands is not observed.

The next excited states should result from consideration of an unexcited 3^2S and an excited 3^2D atom of sodium. This gives twelve molecular states, with only two possible transitions, viz. $^1\Sigma_u^+$ and $^1\Pi_u$ from the ground state. Consequently two systems of bands should be obtained whose upper states will dissociate into 3^2S+3^2D atoms. Again, just as two systems of bands are observed due to transitions from the ground state to the excited states resulting from 3^2S+3^2P atoms of sodium, similarly two systems should be observed due to $^1\Sigma_u^+\leftarrow{}^1\Sigma_g^+$ and $^1\Pi_u\rightarrow{}^1\Sigma_g^+$ transitions whose upper states will dissociate into 3^2S+4^2P atoms. We should thus have four systems of bands, two associated with 3^2D atoms and two with 4^2P atoms, all of which should lie close together. Actually, however, only three systems of bands are observed in the corresponding region including the present system (Sinha 1947). Study of the absorption spectrum of K_2 has also revealed only three systems of bands in the corresponding region (Sinha 1948). Work is in progress to explain this discrepancy and also to understand the absence of bands associated with 3^2S+4^2S atoms.

ACKNOWLEDGMENTS

The author wishes to acknowledge his indebtedness to Assistant Professor R. W. B. Pearse, D.Sc., for his kind help and valuable suggestions, and to Patna University, India, for the grant of their Birla scholarship.

REFERENCES

FREDRICKSON, W. R., and STANNARD, C. R., 1933, *Phys. Rev.*, **44**, 633.
FREDRICKSON, W. R., and WATSON, W. W., 1927, *Phys. Rev.*, **30**, 429.
GAYDON, A. G., 1946, *Proc. Phys. Soc.*, **58**, 525.
HUNTER, A., and PEARSE, R. W. B., 1936, *J. Sci. Instrum.*, **13**, 403.
JEVONS, W., 1932, *Report on Band Spectra of Diatomic Molecules* (London : Physical Society), p. 55.
KIMURA, M., and UCHIDA, Y., 1932, *Sci. Pap. Inst. Phys. Chem. Res. Tokyo*, **18**, 109.
LOOMIS, F. W., 1928, *Phys. Rev.*, **31**, 323.
LOOMIS, F. W., and NUSBAUM, R. E., 1932, *Phys. Rev.*, **40**, 380.
SINHA, S. P., 1947, *Proc. Phys. Soc.*, **59**, 610; 1948, *Ibid.*, **60**, 436.
WALTER, J. M., and BARRATT, S., 1928, *Proc. Roy. Soc.* A, **119**, 265.
WEIZEL, W., and KULP, M., 1930, *Ann. Phys., Lpz.*, **4**, 971.

On the Equations of Motion of Crystal Dislocations

By F. C. FRANK

H. H. Wills Physical Laboratory, University of Bristol

MS. received 25*th August* 1948, *and in amended form* 25*th November* 1948

ABSTRACT. It is shown that when a Burgers screw dislocation moves with velocity v it suffers a longitudinal contraction by the factor $(1-v^2/c^2)^{\frac{1}{2}}$, where c is the velocity of transverse sound. The total energy of the moving dislocation is given by the formula $E=E_0/(1-v^2/c^2)^{\frac{1}{2}}$, where E_0 is the potential energy of the dislocation at rest. Taylor dislocations behave in a qualitatively similar manner, complicated by the fact that both longitudinal and transverse displacements and sound velocities are involved.

§ 1

FRENKEL and Kontorowa (1938), studying the properties of what is essentially a one-dimensional dislocation model, found equations of motion for the dislocation which can be brought into a form strikingly analogous to those of a particle in special relativity. It has a limiting velocity equal to the characteristic velocity of sound in the (actually dispersive) system, suffers a contraction analogous to that of Lorentz as it approaches that velocity, and the ratio of its energy in motion to its energy at rest likewise depends "relativistically" on velocity. This result (which we actually discovered independently) will be discussed more fully, along with other properties of one-dimensional dislocation models, in papers to be published with Mr. J. H. van der Merwe. It has been noted before (Frank 1948) that in the three-dimensional case of crystal dislocations the kinetic energy of a Burgers "screw" dislocation (Burgers 1939), extrapolated by the approximate formula valid at low velocity up to the velocity of transverse sound waves, is equal to half its potential energy. This is equivalent to the relativistic equation $m_0=E_0/c^2$, where E_0 is rest energy and m_0 rest mass. It is shown below that all the elementary relativistic formulae are applicable to a screw dislocation, and that the behaviour of a Taylor "bridge" (or "edge") dislocation (Taylor 1934) may be described as "relativistic with complications": the limiting velocity is that of longitudinal sound waves, but the velocity of transverse sound waves also plays a part.

§ 2

The displacement function $\mathbf{u}(x, y, z)$ of a resting dislocation according to linear isotropic elastic theory, given by Burgers (1939) for bridge and screw dislocations, is a solution of the three equations $(1_x, 1_y, 1_z)$ of elasto-static equilibrium typified by

$$(\lambda+\mu)\frac{\partial}{\partial x}\left(\frac{\partial u_x}{\partial x}+\frac{\partial u_y}{\partial y}+\frac{\partial u_z}{\partial z}\right)+\mu\left(\frac{\partial^2}{\partial x^2}+\frac{\partial^2}{\partial y^2}+\frac{\partial^2}{\partial z^2}\right)u_x=0. \quad \ldots\ldots(1_x)$$

Dislocations in motion must be represented by solutions of the three equations of elasto-dynamic equilibrium (wave equations) typified by

$$(\lambda+\mu)\frac{\partial}{\partial x}\left(\frac{\partial u_x}{\partial x}+\frac{\partial u_y}{\partial y}+\frac{\partial u_z}{\partial z}\right)+\mu\left(\frac{\partial^2}{\partial x^2}+\frac{\partial^2}{\partial y^2}+\frac{\partial^2}{\partial z^2}\right)u_x-\rho\frac{\partial^2 u_x}{\partial t^2}=0. \quad \ldots\ldots(2_x)$$

In particular, a dislocation in steady motion with velocity v in the x direction must be represented by a propagational solution of equations (2), a time-independent function of x', y and z where $x' = (x - vt)$. With this substitution, x is replaced by x' and $(\partial^2/\partial t^2)$ is replaced by $v^2(\partial^2/\partial x'^2)$ in equations (2), producing three equations $(3_x, 3_y, 3_z)$ which are equivalent to equations (1) with x replaced by x', except for the operands of $(\partial^2/\partial x'^2)$ which are :

$$\text{in } (3_x): \ (\lambda + 2\mu - v^2\rho)u_x \text{ in place of } (\lambda + 2\mu)u_x,$$

$$\text{in } (3_y): \ (\mu - v^2\rho)u_y \text{ in place of } \mu u_y,$$

$$\text{in } (3_z): \ (\mu - v^2\rho)u_z \text{ in place of } \mu u_z.$$

§ 3

Now one of the solutions of (1) is the screw dislocation along the z-axis, for which (Burgers 1939)

$$u_x = 0, \qquad u_y = 0, \qquad u_z = (b/2\pi)\arctan(y/x), \qquad \ldots\ldots (4)$$

equations (1_x) and (1_y) reducing to $0 = 0$ and (1_z) to $\mu\partial^2 u_z/\partial x^2 + \mu\partial^2 u_z/\partial y^2 = 0$. Likewise for a screw dislocation in motion, equations (3_x) and (3_y) reduce to $0 = 0$ and (3_z) to $(\mu - v^2\rho)\partial^2 u_z/\partial x'^2 + \mu\partial^2 u_z/\partial y^2 = 0$. Hence in this case equations (3) are brought into identical form with equations (1) on introducing

$$x'' = x'/(1 - v^2\rho/\mu)^{\frac{1}{2}} = (x - vt)/(1 - v^2/c^2)^{\frac{1}{2}},$$

where $c_1 = (\mu/\rho)^{\frac{1}{2}}$ is the velocity of transverse sound waves in the material. Hence the displacement function of a screw dislocation in motion is identical with that of a screw dislocation at rest, apart from a "Lorentz contraction".

§ 4

The potential energy of a resting screw dislocation is

$$E_0 = \tfrac{1}{2}\mu \int [(\partial u_z/\partial x)^2 + (\partial u_z/\partial y)^2]\, dx\, dy\, dz = (\mu b^2/4\pi)\ln(r_1/r_0)$$

per unit length in the z direction. r_0, of the order of the interatomic spacing b, represents the boundary within which linear elastic theory is inapplicable, and r_1 the outer boundary of the material. Moderate changes in the size or form of these boundaries are unimportant. Neglect of strain energy in the non-linear elastic region within r_0 is justified when r_1/r_0 is large; but on the evidence of the one-dimensional model it is likely that the results obtained below will remain true in a higher approximation which takes account of this energy. The potential energy E_1 of a moving screw dislocation is given by the same integral, which on writing $dx = (1 - \beta^2)^{\frac{1}{2}}\, dx''$, where $\beta = v/c$, becomes

$$\begin{aligned} E_1 &= \tfrac{1}{2}\mu \int [(\partial u_z/\partial x'')^2/(1 - \beta^2) + (\partial u_z/\partial y)^2](1 - \beta^2)^{\frac{1}{2}}\, dx''\, dy\, dz \\ &= \tfrac{1}{2}E_0/(1 - \beta^2)^{\frac{1}{2}} + \tfrac{1}{2}E_0(1 - \beta^2)^{\frac{1}{2}} = E_0(1 - \tfrac{1}{2}\beta^2)/(1 - \beta^2)^{\frac{1}{2}}, \end{aligned}$$

since $\mathbf{u}$ is the same function of (x'', y, z) as it was formerly of (x, y, z).

The kinetic energy associated with a moving screw dislocation is

$$\begin{aligned} E_2 &= \tfrac{1}{2}\rho \int (\partial u_z/\partial t)^2\, dx\, dy\, dz = \tfrac{1}{2}\rho \int (\partial u_z/\partial x'')^2 [v^2/(1 - \beta^2)](1 - \beta^2)^{\frac{1}{2}}\, dx''\, dy\, dz \\ &= \{v^2/(1 - \beta^2)^{\frac{1}{2}}\}(\rho/\mu)E_0/2 = \tfrac{1}{2}E_0\beta^2/(1 - \beta^2)^{\frac{1}{2}}. \end{aligned}$$

Hence the total energy associated with the moving dislocation is

$$E = E_1 + E_2 = E_0/(1-\beta^2)^{\frac{1}{2}}.$$

For dislocations moving at low velocity we may define an equivalent mass m_0 by equating the energy of motion $E - E_0$ to $\frac{1}{2}m_0v^2$. Then $m_0 = E_0/c^2$.

§ 5

The work done by an applied shear stress σ on the glide plane when the dislocation is translated a distance x is $(\boldsymbol{\sigma} \,.\, \mathbf{b})x$ per unit length of dislocation. This energy goes partly into kinetic energy and partly into setting up oscillations in the crystal. This latter "radiation damping" of the motion of the dislocation should arise from the acceleration of the dislocation, under the influence of the applied stress and in its interactions with irregularities in the lattice, e.g. other dislocations, and also, at high velocity, from the periodic structure of the lattice itself. Formally we may define the force acting on the dislocation, f, as $(\boldsymbol{\sigma} \,.\, \mathbf{b})$ diminished by a frictional force arising from the radiation damping. We expect this correction to be small in a reasonably perfect crystal, provided that the velocities or accelerations are not exceedingly high.

We could identify the energy of a moving dislocation by integrating energy in the material. (It should be noted, however, that $E - E_0$, which might reasonably be called the kinetic energy of the dislocation, is not quite identical with the kinetic energy in the material, which is E_1.) The same cannot be done with momentum, but we can define an equivalent momentum, $p = \int f\,dt$, corresponding to $E - E_0 = \int f\,dx$. Then introducing $v/c = \beta = \sin\phi$ (a substitution which simplifies all the formulae of elementary relativistic mechanics) so that $E = E_0/\cos\phi$, we have $dp/dt = f = dE/dx = (E_0 \sin\phi/\cos^2\phi)\,d\phi/dx = (E_0/c\cos^2\phi)\,d\phi/dt$, and hence $p = \int (E_0/c\cos^2\phi)\,d\phi = (E_0/c)\tan\phi = (E/c^2)v$ and $E^2 = E_0^2 + p^2c^2$ as usual.

A screw dislocation (unlike a bridge dislocation) may move in any plane containing its singular line. The transformations employed above may be performed independently for motions in the x and y directions. Hence p has independent x and y components, i.e., is a vector. E is of course scalar. In view of the "radiation damping" we cannot suppose there is strict conservation of the components of p unless we are able to assign a corresponding equivalent momentum to oscillations in the crystal.

§ 6

The case of the Taylor bridge dislocation is more complicated, since both longitudinal and transverse displacements occur in its motion. If it lies along the z-axis, with displacement vector $\mathbf{b}$ on the x-axis, which must also be its direction of motion, the displacements u_z and all derivatives with respect to z vanish by symmetry. Equations (1) for the dislocation at rest then reduce to

$$(\lambda+2\mu)\partial^2u_x/\partial x^2 + \mu\partial^2u_x/\partial y^2 + (\lambda+\mu)\partial^2u_y/\partial x\,\partial y = 0, \qquad \ldots\ldots(5_x)$$

$$(\lambda+2\mu)\partial^2u_y/\partial y^2 + \mu\partial^2u_y/\partial x^2 + (\lambda+\mu)\partial^2u_x/\partial x\,\partial y = 0. \qquad \ldots\ldots(5_y)$$

The major displacements are u_x, parallel to $\mathbf{b}$, and to a first approximation satisfy (5_x) with the final term neglected. Through the final term of (5_y) the x-displacements give rise to y-displacements which react back upon the x-displacements through the final term of (5_x). This description is appropriate to a solution of (5) by successive approximations.

The solution of the first approximation is

$$u_{x(1)} = (b/2\pi) \arctan [\{(\lambda+2\mu)\mu\}^{\frac{1}{2}}(y/x)]. \quad \ldots\ldots(6_x)$$

The closed solution obtained by Burgers (1939) is

$$u_x = (b/2\pi)[\theta + \{(\lambda+\mu)/(\lambda+2\mu)\} \sin\theta \cos\theta], \quad \ldots\ldots(7_x)$$

$$u_y = -(b/2\pi)[\{\mu/(\lambda+2\mu)\} \ln (r/r_0) - \{(\lambda+\mu)/(\lambda+2\mu)\} \sin^2\theta], \quad \ldots\ldots(7_y)$$

where $\tan\theta = y/x$ and $r = (x^2+y^2)^{\frac{1}{2}}$.

The difference between $u_{x(1)}$ and u_x as given by (7) is small, being at the worst $0{\cdot}014v$ (when $\theta = \pi/3$) in the case $\lambda = \mu$ (Poisson's ratio $\sigma = \frac{1}{4}$). Thus the first approximation is a not unsatisfactory one.

Equations (3) for the bridge dislocation in motion become

$$(\lambda+2\mu-v^2\rho)\partial^2 u_x/\partial x'^2 + \mu\partial^2 u_x/\partial y^2 + (\lambda+\mu)\partial^2 u_y/\partial x'\partial y = 0, \quad \ldots\ldots(8_x)$$

$$(\lambda+2\mu)\partial^2 u_y/\partial y^2 + (\mu-v^2\rho)\partial^2 u_y/\partial x'^2 + (\lambda+\mu)\partial^2 u_x/\partial x'\partial y = 0. \quad \ldots\ldots(8_y)$$

To the same first approximation as we have just discussed, taking the first two terms of (8_x) the problem reduces "relativistically" to the static problem on substituting $x'' = x'/(1-v^2/c^2)^{\frac{1}{2}}$ where $c_1^2 = \{(\lambda+2\mu)/\rho\}^{\frac{1}{2}}$, the speed of longitudinal sound waves.

Note added in amendment 24th November 1948.—Further incomplete treatment of the problem (which originally followed here) can be omitted, as a complete solution has now been obtained, and will shortly be published, by Mr. J. D. Eshelby. From his treatment it appears that the requisite differential equations can be satisfied both by an irrotational and a distortional dislocation with displacement vectors in the direction of travel, or by any combination of the two. Both suffer "Lorentz contraction", with limiting velocities equal to the velocities of longitudinal and transverse sound waves respectively. Either motion alone can only be maintained if a force, normal to the direction of motion, is applied at the centre of the dislocation, with counteracting forces on the remote surfaces. These forces do no work, but there is no means of applying the force at the centre. This force vanishes when the irrotational and distortional dislocations are combined in appropriate proportions (dependent on the velocity). This, therefore, gives the only physically important solution. The force at the centre cannot be made to vanish for a dislocation travelling faster than transverse sound.

ACKNOWLEDGMENTS

The author wishes to thank Mr. J. D. Eshelby for the above information; he wishes also to thank Mr. F. R. N. Nabarro and Mr. G. Wyllie for valuable critical discussion.

REFERENCES

Burgers, J. M., 1939, *Proc. Kon. Ned. Akad. v. Wet.*, **42**, 293.

Frank, F. C., 1948, *Report of a Conference on Strength of Solids* (London : Physical Society), p. 48.

Frenkel, J., and Kontorowa, T., 1938, *Phys. Z. Sowjet*, **13**, 1.

Taylor, G. I., 1934, *Proc. Roy. Soc.* A, **145**, 362.

LETTERS TO THE EDITOR

The Resistivity of Thin Metallic Films

Various formulae have been suggested from time to time to account for the variation of the resistivity of thin metallic films with the thickness of the film. The simplest of these is an empirical expression due to Planck (1914):

$$\rho = \rho_\infty(1 + A/D)$$

where ρ is the resistivity and D the thickness of the film, and ρ_∞ the resistivity of the bulk metal; A is an unspecified constant. This formula accounted satisfactorily for his own experimental results and for Pogány's classical work on the resistivities and optical constants of thin films (1916).

When the thickness of the film is a small multiple or submultiple of the length of the mean free path of the electrons the number of electronic collisions is going to be increased. The Figure illustrates the shortening of the mean free path l and the corresponding increase

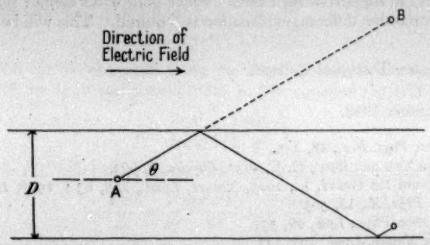

in the collisions. AB represents the mean free path in the bulk metal, and, in this case, the number of collisions will be $\nu(1 + kl/D)$ where k is a numerical factor. As a rough first approximation the latter may be said to be equal to $4/\pi$ since $2/\pi$ is the mean of the possible values of $\sin\theta$, and there are two surfaces. When D is larger than l, k will have a different (smaller) value, which can be calculated by suitable averaging. Substituting the above value for the frequency of collision between the atoms and electrons in Drude's classical formula it follows that

$$\sigma = \frac{Ne^2}{2m\nu(1 + kl/D)} \quad \text{or} \quad \sigma = \frac{\sigma_\infty}{1 + 4l/\pi D} \qquad \ldots\ldots (1)$$

where σ is the conductivity of the film, D its thickness, σ_∞ the conductivity of the bulk metal, N the number of free electrons per cm^3, and e and m the electronic mass and charge respectively. From (1) we obtain

$$\rho = \rho_\infty(1 + 4l/\pi D) \qquad \ldots\ldots (2)$$

which can be identified with Planck's empirical formula mentioned above.

Considering small temperature changes at about room temperature it is assumed that ρ_∞ and l experience appreciable, but D negligible, variations. Then (2) can be written

$$\rho = {}_0\rho_\infty(\alpha T + a)(1 + 4l_0/\pi D\gamma T). \qquad \ldots\ldots (3)$$

α is the normal temperature coefficient of resistivity, γ the coefficient of the mean free path, a that part of the resistivity which does not depend on the temperature; the suffix $(_0)$ refers to values at 0° C. but T is measured on the absolute scale.

When (3) is differentiated with respect to T an expression is obtained for the effective temperature coefficient α':

$$\alpha'=\alpha-\frac{1}{T}\left(\frac{1}{1+\pi D\gamma T/4l_0}\right) \qquad \ldots\ldots(4)$$

It is readily seen that α' is zero when

$$1/\alpha=T(1+\pi D\gamma T/4l_0), \qquad \ldots\ldots(5)$$

and for correspondingly smaller thicknesses or lower temperatures α' will be negative. In general, α' is less than α.

It follows that when l_0 is large the thickness D for which $\alpha'=0$ will be large for given values of γ and T. There is evidence suggesting that the mean free path of the electrons in bismuth is exceptionally long. It is thus to be expected that comparatively thick bismuth films will exhibit a negative temperature coefficient (Tulley 1946). In addition, it follows from (5) that the thicker the film the lower the temperature at which $\alpha'=0$ (Curtiss 1921). It is not suggested that expression (3) has a general applicability at lower temperatures, indeed, it is known that the resistivity varies at temperatures lower than 0° c. with a higher power of T than unity. It is none the less interesting to note that the results of van Itterbeek and De Greve (1945, 1946) on the resistivity of nickel films at comparatively low temperatures are in good agreement with the above expressions. The temperature coefficient of resistivity varies with the thickness, and the minima of resistivity vary with the thickness and the temperature as predicted. These authors quote the results of De Haas and Van den Berg (1937) on gold wires in support of their own. Since gold wires cannot really be compared with thin films a somewhat different explanation is required. This will be dealt with in the near future.

South-West Essex Technical College, R. A. Weale.
London E.17.
November 1948.

Curtiss, L. F., 1921, *Phys. Rev.*, **18**, 255.
De Haas, W. J., and Van den Berg, G. J., 1937, *Physica*, **4**, 663.
van Itterbeek, A., and De Greve, L., 1945, *Nature, Lond.*, **156**, 63; 1946, *Ibid.*, **158**, 100.
Planck, W., 1914, *Phys. Z.*, **15**, 563.
Pogány, B., 1916, *Ann. Phys., Lpz.*, **49**, 531.
Tulley, T J., 1946, *Nature, Lond.*, **157**, 372.

Note on the Slowing Down of Mesons

Fermi, Teller and Weisskopf (1947), and Fermi and Teller (1947), have given a formula for the rate of loss of energy of slow mesons passing through a metal, the metal being treated as a degenerate electron gas. The formula is (Fermi and Teller, equation (15))

$$\frac{dW}{dt}=\frac{2}{3\pi}\frac{\boldsymbol{m}^2\boldsymbol{e}^4V^2}{\hbar^3}\ln\frac{137v_0}{\boldsymbol{c}} \qquad \ldots\ldots(1)$$

where $\boldsymbol{m}$, $\boldsymbol{e}$ are the mass and charge of an electron, V the velocity of the meson, W its energy and v_0 the maximum velocity of the electrons which form the degenerate Fermi gas in the metal. The formula is derived for the case when* $V\ll v_0$. Some doubt has been thrown on the validity of this result (cf. for example Fröhlich 1948); the purpose of this note is to confirm the result by showing that it is identical with that obtained in a problem on the electrical resistance of alloys, for which the application of the same methods has given results in agreement with experiment.

If the effect of the lattice field is neglected, the calculations required to obtain the following two quantities are identical: (*a*) The rate dW/dt of loss of energy by a heavy charged particle moving with velocity V through the gas. (*b*) The rate of loss of energy of an electron gas moving with velocity V past a stationary charged particle (e.g. a proton). The second problem is the same as that of finding the residual resistance of a metal containing

* For a treatment of the effect of free electrons when $V>v_0$ see Kramers (1947).

dissolved hydrogen. For suppose that the resistance of a metal containing xN stationary protons per unit volume is $x\rho$; N is here the number of metal atoms per unit volume. Then the rate of loss of energy per unit volume, if a current of density j is flowing, is

$$x\rho j^2. \qquad \ldots\ldots (2)$$

If the metal is monovalent and thus contains N electrons per unit volume, we may set $j=NeV$, so that (2) becomes $x\rho N^2e^2V^2$. The rate of loss of energy due to a single stationary charged particle, which can be equated to dW/dt, is given by

$$dW/dt=\rho Ne^2V^2. \qquad \ldots\ldots (3)$$

The resistance ρ due to any type of foreign atom can be calculated by the method originally due to Nordheim (1931) (cf. also Mott and Jones 1936, p. 289). We may write

$$\rho=mv_0A/e^2, \qquad \ldots\ldots (4)$$

where A is the area defined by

$$A=\int I(\theta)(1-\cos\theta)\,d\omega. \qquad \ldots\ldots (5)$$

$I(\theta)d\omega$ is here the cross-section for scattering of an electron having velocity v_0 by a foreign atom into the solid angle $d\omega$. This can be calculated if the field round the foreign atom is known; in Mott and Jones (1936), p. 97, a screened Coulomb field of potential

$$U(r)=\pm(e^2/r)\exp(-qr) \qquad \ldots\ldots (6)$$

is taken, and q obtained by using the Thomas-Fermi method to find the density of the electron gas round a proton. One finds

$$q=(4me^2/\hbar^2)(3N/\pi)^{\frac{1}{3}}. \qquad \ldots\ldots (7)$$

With this field $I(\theta)$ can be obtained, using the Born approximation; one finds (using the value given for $I(\theta)$ by Mott and Jones (1936), p. 294, equation (86))* from (4), (5), (6), (7)

$$\rho=\frac{2\pi e^2}{mv_0^3}\ln\left(\frac{\pi\hbar v_0}{e^2}\right).$$

Substituting in (2), using the equation $mv=(3\pi)^{\frac{1}{3}}\pi\hbar/N^{\frac{1}{3}}$, we obtain the formula

$$\frac{dW}{dt}=\frac{2}{3\pi}\frac{m^2e^4V^2}{\hbar^2}\ln\left(\frac{\pi\hbar v_0}{e^2}\right)$$

which differs from that of Fermi and Teller only in the π in the logarithm. Since the Born approximation is strictly valid only if $\hbar v_0\gg e^2$, the change is unimportant.

No experimental results are known for the increase of resistance due to hydrogen in monovalent metals, to which alone this analysis should be applicable; but the theory agrees well with experiment when applied to calculate the increase of resistance due to the addition of 1% of Ni, Zn, Ga, Ge or As to copper (Mott and Jones 1936, p. 293). The resistance is found experimentally to increase in the ratio of the numbers 1, 1, 4, 9, 16 for these metals. This can be explained (Mott and Jones 1936, p. 292) quantitatively on the above theory, taking a field round each foreign atom of potential $(ze^2/r)\exp(-qr)$, where z takes the values -1, 1, 2, 3 etc. It thus appears that, for example, a zinc atom replacing a copper atom behaves like an additional charge e, and the residual resistance is that due to a screened charge.

H. H. Wills Physical Laboratory,
University of Bristol.
23rd November, 1948.

N. F. Mott.

Fermi, E., and Teller, E., 1947, *Phys. Rev.*, **72**, 399.
Fermi, E., Teller, E., and Weisskopf, V., 1947, *Phys. Rev.*, **71**, 314.
Fröhlich, H., 1948, *Nature, Lond.*, **162**, 450.
Kramers, H. A., 1947, *Physica*, **13**, 401.
Mott, N. F., and Jones, H., 1936, *Theory of the Properties of Metals and Alloys* (Oxford: Clarendon Press).
Nordheim, L., 1931, *Ann Phys., Lpz.*, **9**, 641.

* In this equation we have put $y\ll 1$, since only under these conditions is the Born approximation valid.

REVIEWS OF BOOKS

Preparation and Characteristics of Solid Luminescent Materials, by G. R. FONDA and F. SEITZ (Editors). Pp. xv + 459. (New York: John Wiley, 1948.) 30*s*.

This book comprises twenty-nine papers together with associated discussions which formed the subject matter of a Symposium on Luminescence held at Cornell University in October 1946. It is concerned with recent researches on specific aspects of luminescence in synthesized phosphors, such as sulphides, silicates and tungstates. The papers presented at the Conference have been arranged in five main groups, while a further group contains the final discussions of the Conference.

In the first group of papers a general survey of phosphors, their characteristics and methods of preparation is made. The next group contains four papers which deal with two important aspects of recent research on the storage of energy in phosphors. These aspects are the mechanisms of phosphorescence and thermoluminescence, both of which arise from the thermal ejection of trapped electrons, and the processes involved in the infra-red stimulation of phosphors. The third group of papers is devoted to factors affecting the fluorescence characteristics of phosphors, such as phosphor constitution, nature and intensity of exciting radiation and the phosphor temperature. The next six papers deal in more detail with the storage of energy in phosphors and its release by thermal or optical ejection of trapped electrons.

The last group of papers covers miscellaneous aspects of luminescence, such as photochemical action in phosphors, the function of manganese as a luminescence activator in different solids and the correlation of the structures of different classes of materials. In the last section of the book the present theoretical problems of luminescence and possible future approaches to their solution are discussed. In particular, the need for using luminescent solids in the form of single crystals in experimental studies is emphasized.

This book is not intended to be a comprehensive, up-to-date text-book on luminescence. Its value lies in its accounts of the results of recent studies having a rather specialized nature and in the discussions which may have more general significance. These discussions would probably have been even more valuable if they had been based on abstracts of the papers circulated previous to the Conference. It might also have been better to reduce the number of papers and to include and expand those in which a marked contribution to the knowledge of luminescence processes was evident.

However, there is included in the book an account of studies showing the renewed interest in the release of stored energy in phosphors by infra-red radiation. Quenching and stimulation processes in phosphors due to infra-red irradiation were popular subjects for early workers in luminescence. Although they are intimately connected with trapped electrons, the latest studies show that there is little correlation between the thermal and optical ejection of these electrons. The confusion of ideas with respect to the effects of infra-red radiation in phosphors shown in the appropriate papers serves to indicate the present inadequacy of the theory developed for the interpretation of other processes, such as phosphorescence and thermoluminescence.

Although the book will be of great value to those engaged in research on luminescence, the lack of clarity in some of the individual papers will make it difficult reading for others having a secondary interest in the subject.

G. F. J. GARLICK.

CONTENTS FOR SECTION B

PAGE

Dr. H. A. Dell. An Investigation of the Physical Properties of Thin Films used in the Reduction of Surface Reflection 81
Mr. L. R. Griffin. An Extended Theory of the Reflection Echelon Grating . 93
Mr. E. Colin Cherry. The Duality between Interlinked Electric and Magnetic Circuits and the Formation of Transformer Equivalent Circuits 101
Mr. K. W. Hillier and Dr. H. Kolsky. An investigation of the Dynamic Elastic Properties of some High Polymers 111
Dr. G. D. Yarnold and Mr. B. J. Mason. A Theory of the Angle of Contact . 121
Dr. G. D. Yarnold and Mr. B. J. Mason. The Angle of Contact between Water and Wax 125
Mr. J. M. M. Pinkerton. The Absorption of Ultrasonic Waves in Liquids and its Relation to Molecular Constitution 129
Letters to the Editor:
Dr. R. Street and Mr. J. C. Woolley. A Note on Magnetic Viscosity in Alnico 141
Reviews of Books 142
Contents for Section A 147
Abstracts for Section A 147

ABSTRACTS FOR SECTION B

An Investigation of the Physical Properties of Thin Films used in the Reduction of Surface Reflection, by H. A. Dell.

ABSTRACT. A simple mathematical treatment of reflection from thin films is extended to cover the properties of films likely to be met with in practice. In particular, reflection from multible films of more than one substance is considered, and the reflection of polarized light from simple films. A photometer used for testing these results is described, and the different types of cryolite films found are enumerated.

Evidence is given suggesting that polished or aged cryolite films behave as if they consisted of a lower stratum of cryolite surmounted by a secondary layer of higher refractive index. Some of the properties of this layer are described.

An Extended Theory of the Reflection Echelon Grating, by L. R. Griffin.

ABSTRACT. The single reflection echelon grating has the disadvantage that it is impossible to interpret the fringe pattern without further information about the correct order allocation. The present methods of obtaining this information are briefly reviewed; they are progressively less useful as the wavelength decreases into the ultra-violet. The properties of the grating are investigated theoretically when the light is incident at relatively large angles in two special cases, and the performance of the instrument in these positions compared with that of its normal use. It is shown that the required order allocation could be obtained using a single reflection echelon grating by measuring the fractional order separation with the grating in two positions. This would considerably increase the value of the instrument.

The Duality between Interlinked Electric and Magnetic Circuits and the Formation of Transformer Equivalent Circuits, by E. Colin Cherry.

ABSTRACT. When making calculations on a circuit, containing both electric impedances and transformers, it is frequently desirable to consider the transformers removed and the constraints they impose replaced by a rearrangement of the impedances connected to their terminals. Such "equivalent circuits" may not always be found; the rules are here established for their formation, and also for checking, by inspection, whether the transformer

constraints are removable in this way in any particular case. It is shown that the equivalent electric circuit of a transformer, having any arrangement of magnetic paths, is derivable from its magnetic circuit by application of the topological principle of duality. This cannot be done if the magnetic circuit is non-planar, as in the case of a transformer possessing four or more winding with leakage couplings; a physically realizable circuit does not then exist.

Under certain conditions the principle may be applied in reverse and the impedances in a given electric circuit may be coupled together by a suitable transformer, so that the various current and voltage constraints are unaltered.

An Investigation of the Dynamic Elastic Properties of Some High Polymers, by K. W. HILLIER and H. KOLSKY.

ABSTRACT. An apparatus for the investigation of the transmission of sound along filaments at frequencies between 1,000 and 6,000 cycles per second is described, both for unstrained specimen and whilst they are being elongated at a constant rate of increase of strain. Measurements of the dynamic elasticity and damping factors of filaments of polythene, neoprene and nylon have been obtained, and the correlation of these results with the molecular rearrangements which take place during stretching is discussed.

A Theory of the Angle of Contact, by G. D. YARNOLD and B. J. MASON.

ABSTRACT. It does not appear to be possible to give a quantitative account of the angle of contact of a continuous liquid in terms of cohesional forces. By using Young's energy relation and making allowance for the effects of adsorbed films on the surface of the solid, expressions are derived for the advancing and receding angles, and a general explanation of the hysteresis of the angle of contact is put forward.

The Angle of Contact Between Water and Wax, by G. D. YARNOLD and B. J. MASON.

ABSTRACT. The effects (*a*) of the velocity of the liquid surface, and (*b*) of the time of immersion, on the angle of contact between clean surfaces of water and wax have been investigated by dynamical method. It is clear that Ablett's measurements are vitiated by the fact that the time of immersion is disregarded. The term "equilibrium angle of contact" appears to be meaningless.

The Absorption of Ultrasonic Waves in Liquids and its Relation to Molecular Constitution, by J. M. M. PINKERTON.

ABSTRACT. Measurements of the absorption of ultrasonic waves in water and ethyl alcohol were made by the pulse method, and are more accurate than those made by other methods. The absorption coefficient α in water was found to vary as the square of the frequency ν over a wide range of temperatures. The measurements in water were made at frequencies between 7·5 and 67·5 Mc/s. and temperatures between 0 and 95° c. The absorption decreased with increasing temperature by a factor of 8 between freezing and boiling points. The observed absorption was about three times that calculated from Stokes' formula and this ratio was nearly independent of temperature. In ethyl alcohol measurements were made at 52·4 Mc/s., and at temperatures between $-50°$ and $+60°$ c. The absorption decreased by a factor 3 in this range and observed values were about twice those given by Stokes' formula. Values of (α/ν^2) at 25° c. are $22{\cdot}0\times10^{-17}$ sec^2/cm. for water and $50{\cdot}5\times10^{-17}$ sec^2/cm. for ethyl alcohol.

Published values of the absorption coefficients of a wide range of pure liquids and of some mixtures are reviewed, and a classification proposed. The experimental results suggests that the absorption in associated liquids is due to a different mechanism from that in non-associated liquids. In the latter the absorption is probably due to the same phenomenon as in gases: a slow exchange of energy between different degrees of freedom. The relaxation frequencies must be above 200 Mc/s. for most liquids. A simple theory is given to explain the observed variation of the absorption with concentration in mixtures of non-associated liquids. The semi-quantitative argeement of theory with experiment lends support to the relaxation hypothesis.